

**EUR 3155.e**

EUROPEAN ATOMIC ENERGY COMMUNITY - EURATOM

**LIBRARY COPY**

**FUEL-CLAD CONTACT CONDUCTANCE**

by

J. ARRIGHI, C. MUSTACCHI and S. ZANELLA

1966



**ORGEL Program**

**Joint Nuclear Research Center  
Ispra Establishment - Italy**

**Physical Chemistry**

## LEGAL NOTICE

This document was prepared under the sponsorship of the Commission of the European Atomic Energy Community (EURATOM).

Neither the EURATOM Commission, its contractors nor any person acting on their behalf :

Make any warranty or representation, express or implied, with respect to the accuracy, completeness, or usefulness of the information contained in this document, or that the use of any information, apparatus, method, or process disclosed in this document may not infringe privately owned rights; or

Assume any liability with respect to the use of, or for damages resulting from the use of any information, apparatus, method or process disclosed in this document.

This report is on sale at the addresses listed on cover page 4

|                          |          |          |            |           |
|--------------------------|----------|----------|------------|-----------|
| at the price of FF 16,50 | FB 165,— | DM 13,20 | Lit. 2 060 | Fl. 11,95 |
|--------------------------|----------|----------|------------|-----------|

**When ordering, please quote the EUR number and the title, which are indicated on the cover of each report.**

Printed by Guyot, s.a.  
Brussels, October 1966

This document was reproduced on the basis of the best available copy.

**EUR 3155.e**

EUROPEAN ATOMIC ENERGY COMMUNITY - EURATOM

**FUEL-CLAD CONTACT CONDUCTANCE**

by

J. ARRIGHI, C. MUSTACCHI and S. ZANELLA

1966



**ORGEL Program**

**Joint Nuclear Research Center  
Ispra Establishment - Italy**

**Physical Chemistry**

## CONTENTS

|  |     |
|--|-----|
| List of figures . . . . .  | 3   |
| List of symbols . . . . .  | 5   |
| 1 — SCOPE . . . . .  | 7   |
| 2 — THEORETICAL . . . . .  | 8   |
| 2.1 General . . . . .  | 8   |
| 2.2 Previous knowledge . . . . .   | 10  |
| 2.3 Suggested model . . . . .  | 14  |
| 3 — EXPERIMENTAL . . . . .   | 17  |
| 3.1 Experimental apparatus . . . . .                                       | 17  |
| 3.2 Surface preparation . . . . .  | 20  |
| 3.3 Measurement of the surface finish . . . . .                            | 24  |
| 3.4 Experimental data . . . . .  | 26  |
| 4 — FLUID CONDUCTANCE . . . . .  | 33  |
| 5 — CYLINDRICAL CONTACT . . . . .  | 36  |
| 5.1 Simplified Theory . . . . .  | 38  |
| 5.2 Complete Theory . . . . .  | 42  |
| 5.3 Plastic clad . . . . .   | 51  |
| 5.4 Out-of-pile experiments . . . . .                                      | 54  |
| 5.5 In-pile experiments . . . . .  | 56  |
| 5.6 Post-irradiation examination . . . . .                                 | 66  |
| References . . . . .   | 76  |
| Appendix I = Measurement of S.A.P. Hardness . . . . .                      | 78  |
| Appendix II = Number of contact points . . . . .                           | 82  |
| Appendix III = Data on the in-pile experiments . . . . .                   | 90  |
| Appendix IV — Physical constants used in the sample Computations . . . . . | 115 |

### SUMMARY

An investigation was made of clad-pellet contact conductance for reactor fuel elements. Standard plane geometry correlations were shown to be unreliable whereas suitable cylindrical geometry measurements both in- and out-of-pile were accounted for by theoretical and experimental analysis. Both the gas conduction and the metal-to-metal conduction components were studied using as parameters the elastic and plastic properties of the materials in contact, contact pressure, surface finish and nature of the fluid in the gap.

Particular care was given to the case of Uranium Monocarbide and Sintered Aluminium Powder as pellet and clad.

= LIST OF FIGURES =

---

- 1 - Uranium Moco-carbide - SAP Conductance. Comparison of correlations
- 2 - Armco Iron-SAP Conductance. Comparison of Correlations.
- 3 - Test Assembly
- 4 - Specimen Assembly
- 5 - Parallel Ridge Surfaces
- 6 - Pyramidal Asperity Test/Plane
- 7 - Double Pyramidal Test
- 8 - Amplified Surface Profile
- 9 - Typical Temperature Profiles
- 10 - Results of Typical Run
- 11 - Microhardness of 7% S.A.P. VS Load
- 12 - S.A.P. - Armco Iron contact conductance in Air (Plane tests)
- 13 - Thermal Resistance of UC-SAP (Simplified Theory)
- 14 - Thermal Resistance of UC-SAP, Fission Gas Filled (Reactor Shut Down)
- 15 - Thermal Resistance UC-SAP, Fission Gas Filled (Flux  $10^{13}$  to  $10^{14}$ , Swelling 0 to 1%)
- 16 - Thermal Resistance UC-SAP, He-Filled (Reactor Shut Down)
- 17 - Thermal Resistance UC-SAP, He-Filled (Flux  $10^{13}$  to  $10^{14}$ , Swelling 0 to 1%)
- 18 - Thermal Resistance UC-Zircaloy 2, Fiss. Gas Filled
- 19 - Thermal Resistance UC-SS, Fiss. Gas Filled
- 20 - Thermal Resistance UC-SS, He Filled
- 21 - Thermal Resistance UC-MAGNOX, Fiss. Gas Filled

- 22 - Thermal Resistance  $UO_2$  - ZIRCALOY 2, Fiss. Gas Filled
- 23 - Thermal Resistance  $UO_2$  - S.S., Fiss. Gas Filled
- 24 - Thermal Resistance UC-SAP (Fiss. gas-450°) - Plastic Clad
- 25 - Thermal Resistance (He - 450 °C) - Plastic Clad
- 26 - Out-of-Pile Cylindrical contact
- 27 - UC Central Temperature VS. Irradiation time Rig 1
- 28 - " " " " Rig 2
- 29 - Thermal Resistance " " Rig 1
- 29a - " " " " " "
- 30 - " " " " Rig 2
- 31 - Pellet Radial Cracks
- 32 - Volume Increase for Arc-Cast UC
- 33 - Co-60 Activities Measured in S.S. Capsules from Rig 1 and Rig 2
- 34 - Ru-106, CS-137, Ce-144 Activities Measured in Samples from Rig 1
- 35 - U-235 and PU-239 Fission Measured in Samples from Rig 1
- 36 - U-235 and PU-239 Fissions Measured in Samples from Rig 2
- 37 - Thermal Flux VS. Irradiation Time Rig 2
- 38 - 4% SAP Hardness Vs. Temperature
- 39 - 7% " " " "
- 40 - Density of Contact spots Vs. Pressure
- 41 - " " " " "
- 42 - " " " " "
- 43 - Sketch of Irradiation Rig
- 44 - Arrangement of the specimen can
- 45 - Difference between SAP Temperature and Heavy Water Temperature Vs. Thermal Power.
- 46 - Difference between Leak Detector and Heavy Water Temperature Vs. Leak Detector Power.

LIST OF SYMBOLS

- a - radius of the contact spot, cm  
C - cold assembly clearance pellet-clad, cm  
C<sub>o</sub> - enrichment of fuel/natural U enrichment  
C' - operating assembly clearance pellet-clad, cm  
D - diameter of curvature of ridge, cm  
d - density of fuel  
E - Young's modulus, kg/cm<sup>2</sup>  
F - Thermal flux through pellet-sheath, W/cm<sup>2</sup>  
G<sub>o</sub> - nominal radial clearance UC-SAP, cm  
G<sub>1</sub> - hot radial clearance UC-SAP, cm  
H - contact hardness, kg/cm<sup>2</sup>  
H<sub>1</sub> - apparent "patch" hardness, kg/cm<sup>2</sup>  
K - harmonic mean conductivity of the two solids in contact, W/cm°C

$$K = \frac{2K_1K_2}{K_1+K_2}$$

- K<sub>1</sub> and K<sub>2</sub> - Thermal conductivity of two solids, W/cm°C  
K<sub>3</sub> - Xenon thermal conductivity, W/cm°C  
K<sub>f</sub> - fluid thermal conductivity, W/cm°C  
K<sub>p</sub> - fuel conductivity, W/cm°C  
L - fluid mean free path, cm  
M - Atomic or molecular mass, gr  
N - density of "contact patches", cm<sup>-2</sup>  
n - number of contact spots per unit surface, cm<sup>-2</sup>  
P - apparent pressure on contacting surfaces, kg/cm<sup>2</sup>  
P<sub>f</sub> - fluid pressure, atm.  
R - mean square roughness of contacting surfaces, cm

$$R = \left[ \frac{R_1^2 + R_2^2}{2} \right]^{1/2}$$

- R<sub>1</sub> and R<sub>2</sub> - arithmetic mean roughness heights, cm  
R<sub>t</sub> - average roughness amplitude (about four times R<sub>1</sub>), cm  
Res - UC-SAP contact or gap thermal resistance, cm<sup>2</sup>°C/W

- $r_0$  - pellet radius, cm
- $r_3$  - SS container inner radius, cm
- $e$  - fractional swelling of fuel pellet
- $S$  - SS container thickness, cm
- $t$  - clad thickness, cm
- $T$  - mean contact temperature, °C
- $\bar{T}$  - average clad temperature, °C
- $\bar{T}_C$  - pellet centre temperature, °C
- $T_s$  - pellet surface temperature, °C
- $\Delta T_1$  - gap temperature drop, °C
- $\Delta T_p$  - pellet center-to-surface temperature drop, °C
- $U$  - UC-SAP contact or gap thermal conductance,  $W/cm^2 \cdot ^\circ C$
- $u$  - solid-solid contact conductance,  $W/cm^2 \cdot ^\circ C$
- $u_f$  - fluid conductance,  $W/cm^2$
- $u_t$  - total conductance,  $W/cm^2 \cdot ^\circ C$
- $\alpha$  - fluid-wall accommodation coefficient
- $\alpha_c$  - clad thermal expansion coefficient  $^\circ C^{-1}$
- $\alpha_p$  - pellet " " " "  $^\circ C^{-1}$
- $\beta$  - SAP-heavy water temperature drop, (Cr-Al mV)
- $\delta$  - mean distance between contact planes, cm
- $\epsilon_0$  - radial strain of UC pellet surface
- $\epsilon_1$  - radial strain of SAP inner surface
- $\phi$  - Thermal neutron flux,  $n/cm^2 \text{ sec}$
- $\lambda$  - wavelength of surface microroughness, cm
- $\nu$  - Poisson's modulus

## 1. Scope

Contact heat transfer between solid surfaces is a major operating factor in such systems as bearings, switching contacts and reactor fuel element claddings. In some instances it may become a controlling design parameter.

Study and comparison of the published correlations showed an uncertainty of at least one order of magnitude when faced with the problem of actually assessing a value to a thermal contact conductance.

A three year research program was therefore carried out, involving on one hand a study of possible refinements of the available theories and on the other hand a direct experimental study, inclusive of separate determination of such parameters as surface hardness, geometry, mechanical finish, fluid atmosphere.

A final set of experiments bearing directly on the problem on hand, i.e. the thermal distribution in a SAP-clad UC element was carried out under irradiation in the proper geometry to simulate an actual reactor fuel in operation.

The correlations obtained in the present study are thought to enable the designer to assess a contact conductance value within  $\pm 30\%$  with a confidence level in excess of 90%.

---

Manuscript received on August 16, 1966.

## 2. Theoretical

### 2.1. General

In most cases, real contact between two surfaces is limited to a minor fraction of the total apparent contact area.

The resistance to heat conduction will therefore be due to the combined effect of the constriction of flux lines through the real contact points and to the distribution of these contact points on the surfaces.

An analytical solution of the Laplace problem relative to two semi-infinite bodies connected through a circle of radius  $a$  is known. The resistance is  $1/2 ak$ .

If the semi-spaces are connected by a number of such circles, and if the rest of the boundary transfers heat by conduction and radiation through the fluid, no closed-form analytical solution exists. This constitutes one of the difficulties of even the simplest model. Further, another difficulty concerns the estimate of the number of actual contact spots per unit surface  $n$  and the radii of such spots when the bodies are loaded in a given manner.

At any rate, a basis for any theoretical model involves two relations, derived as follows.

The actual pressure on the surface of a single contact point is equal to the contact hardness, an ill-defined property into which we shall go later (Appendix I), yielding the relation:

$$n \cdot \pi a^2 \cdot H = P \quad (1)$$

The conductance will be the sum of the parallel conductances of the fluid and the solid spots

$$u = K_f/\delta + n \cdot 2aK \cdot \eta \quad (2)$$

where the apparent mean fluid thickness  $\delta$  is a function of surface accommodation effects and geometry whereas the factor  $\psi$  corrects the solid conductance for the interaction of several contact spots.

Besides the problem of correctly estimating  $\delta$ ,  $H$  and  $\psi$ , which is often an open question, relations (1) and (2) constitute a set of two equations in three unknowns,  $u$ ,  $n$  and  $a$ .

The choice of a third relation which makes the system defined constitutes the difference between the theories proposed by different authors.

2.2. Previous knowledge

Cetinkale and Fishenden ref. (2) give the factor  $\psi$  of eq. (2) as

$$\psi = \frac{\tilde{\pi}}{2 \tan^{-1} \left\{ \frac{1}{a \sqrt{\tilde{\pi}} n} \sqrt{1 - \frac{K_f}{u\delta}} - 1 \right\}} \quad (3)$$

which is readily verified to approach unity when the radius and the density of contact points is small.

The third relation, experimentally determined in ref. (2) can be reduced in this case to

$$n = 3.5 \times 10^{-8} \frac{(\lambda_1 + \lambda_2)^3}{a^5} \quad (4)$$

Combining (1), (2), (3) and (4) we obtain the required conductance correlation

$$u = \frac{K_f}{\delta} + \frac{206 K}{\lambda_1 + \lambda_2} \frac{\left[ \frac{P}{H} \right]^{4/3}}{\tan^{-1} \left\{ \sqrt{\frac{1 - K_f/u\delta}{P/H}} - 1 \right\}} \quad (5)$$

Laming Ref (4) studies the case of surfaces endowed with parallel ridges, which have therefore a constant number of contact spots and arrives to the following:

$$\psi = \frac{1}{1 - 1.41 \left[ \frac{P}{H} \frac{1}{1 - K_f/u\delta} \right]^{1/2}} \quad (6)$$

where

$$n = \frac{1}{\lambda_1 \lambda_2} \quad (7)$$

However, he explains the discrepancies between his theory and measurements by allowing for a variable contact hardness empirically estimated as:

$$H = \frac{1.8 \times 10^4}{(\lambda_1 \lambda_2)^{1/2} P^{1/2}} \quad (8)$$

independent of the nature of the solid involved (aluminum, brass, steel). Combining (1), (2), (6), (7) and (8), Laming's correlation can be expressed as:

$$u = \frac{K_f}{\delta} + \frac{.00842 P^{3/4} K}{(\lambda_1 \lambda_2)^{1/4} \left[ 1 - \frac{.0105 P^{3/4} (\lambda_1 \lambda_2)}{\sqrt{1 - K_f/u\delta}} \right]^{1/4}} \quad (9)$$

Ross and Stoute ref. (6), following a model of Boeschoten and Van der Held ref. (7) and modifying an empirical correlation by Ascoli and Germagnoli ref. (8), assume a pressure-independent radius of contact points given by

$$a = .5 R^{1/2} \quad (10)$$

whereas  $\xi$  is taken as unity, for moderate pressures.

Combining (1), (2) and (10) and rounding off constants

$$u = \frac{K_f}{\delta} + \frac{K P}{.5R^{1/2} H} \quad (11)$$

Fenech and Rohsenow ref. (9) discount the possibility of giving a general correlation between  $n$  and  $a$ . They suggest a graphical determination to be made on the recorded surface profile to obtain  $n$  versus pressure.

However their results point out to a  $p^{-7}$  dependence of  $n$ . Their formula can be simplified, in the case of surface roughnesses of the same order, to

$$u = \frac{K_f}{\delta} + \frac{2.13 K \sqrt{n} (P/H)^{1/2}}{(1-P/H)(1-K_f/K) \left[ \frac{4.26 \sqrt{n} \delta}{(P/H)^{1/2}} + 1 \right]} \quad (12)$$

It is to be noticed that the datum  $\delta$  appears in (12) even in the case  $K_f = 0$ . In order to compare solid-solid conductances estimated by means of the different formulas, we shall use two assumptions which will give an estimate of  $\delta$  and  $n$  to use in (12).

The "mean distance between surfaces" will vary between a value of the order of the sum of the amplitudes of the surface rugosities for zero pressure, to a value zero, when the pressure will equal the hardness.

Although a  $P^{1/2}$  dependence of  $\delta$  is likely to give a better description of the physical situation, for the purpose of comparing (12) to the other expressions, we shall assume a linearity, within a limited range, of  $\delta$  vs.  $P$ . On the other hand, the amplitude of surface rugosities is well approximated by 4 times the arithmetic mean  $R$ . We shall use therefore an expression

$$\delta \cong 8 R \left(1 - \frac{P}{H}\right) \quad (12a)$$

As to  $n$ , assuming  $n = \alpha P^{-7}$  and supposing that when the pressure is half the hardness we attain the maximum number of contact points, i.e.  $1/\lambda^2$ , it will be:

$$\frac{1}{\lambda^2} = \alpha \left(\frac{P}{2}\right)^{-7}$$

and

$$n = \frac{2.7}{\lambda^2} \left(\frac{P}{H}\right)^{.7} \quad (12b)$$

Inserting (12a) and (12b) into (12) we obtain the approximate expression:

$$u = \frac{2.715 K \left(\frac{P}{H}\right)^{.85}}{\lambda \left(1 - \frac{P}{H}\right) \left[ \frac{43.4 (1-P/H) R}{\lambda (P/H)^{0.15}} + 1 \right]} \quad (12c)$$

Kragel'skii and Demkin ref. (10) studied the effect of work hardening and surface waviness on the true contact area, but the exponent of pressure in their correlations has an uncertainty of one order of magnitude. However, they attained the important conclusion that linearity between area of contact and load does not proof the existence of a fully plastic contact.

Having briefly reviewed the main available correlations, let us now compare them by applying them to a concrete example.

Assuming a SAP-UC contact with  $R_1 = R_2 = 5$  microns,  $K_f \ll K$ ,  $\lambda_1 = \lambda_2 = 300$  microns,  $K = .384$  W/cm°C,  $H = 2,856$  Kg/cm<sup>2</sup>, figure 1 shows the contact conductances to be expected by means of the different correlations.

Plots obtained with our model, described in paragraph 2.3, span a range of  $D = 50$  to  $400$  cm and  $N = 3$  cm<sup>-2</sup>.

The estimates based on the different correlations span a full order of magnitude, lowering the confidence level to an unacceptable value to the designer.

### 2.3. Suggested model

Our out-of-pile set of measurements had originally the scope of selecting and refining the existing correlations. However, with equal surface finish and the same materials, our experiments, reported further on, showed a large scatter of results, ranging anywhere from curve (1) to curve (2) of fig. 1. It was therefore apparent that more parameters than those used so far ought to be introduced into a correlation to explain such an erratic behaviour.

The most obvious difference between two supposedly "equal" contacts, as mentioned above, was the existence of lumping zones with high contact point density, due to waviness of surfaces, a fact which was already pointed out in ref. (10) where the matter was however not quantitatively accounted for.

As shown in ref. (11), the density of contact spots on a single patch is well correlated by

$$n = \frac{P}{H_1} \times \frac{.06}{R_t^2} \left(\frac{H_1}{H}\right)^{.825} \quad (13)$$

Combining (1), (2) and (13) we have

$$u = 2 \sqrt{\frac{.06}{\pi}} \left\{ K \frac{P}{R_t} \frac{1}{H^{.9125} H_1^{.0875}} \right. \quad (14)$$

If, on the other hand the constriction resistances of the patches and of the a-spots is taken into account, the following is obtained, ref. (11)

$$u = \frac{\sqrt{\hat{\pi}} K \left( \frac{P}{H_1} \right)^{1/2}}{R_t \tan^{-1} \left[ \left( \frac{H}{H_1} \right)^{1/2} - 1 \right] + \tan^{-1} \left[ \left( \frac{H_1}{P} \right)^{1/2} - 1 \right]} \cdot \frac{\sqrt{.06} \left( \frac{H_1}{H} \right) \cdot .9125 \left( \frac{P}{H_1} \right)^{1/2}}{N^{1/2}} \quad (15)$$

The factor  $\xi$  in formula (14) is derived by comparing (14) with (7.8) of ref. (11):

$$\xi = \frac{\hat{\pi}}{2 \tan^{-1} \left[ \left( \frac{H}{H_1} \right)^{1/2} - 1 \right]} \quad (16)$$

We considered in this derivation  $H_1$  as the macroscopic hardness of the patch. It is in fact an average pressure on the patch, which for the case of a load on the patch lower than the yield strength of the softer material, will be given by the Hertz law

$$H_1 = .662 E^{2/3} \left( \frac{P}{ND^2} \right)^{1/3} \quad (17)$$

Figure 2 shows a plot of the metal to metal conductance in the case of SAP-Armco iron,  $R_1=R_2=5 \mu\text{m}$ ,  $\lambda_1 = \lambda_2=300 \mu\text{m}$ ,  $K=.797 \text{ W/cm}^\circ\text{C}$  and  $H=2,856 \text{ kg/cm}^2$ . Our curves (5) and (6) are plotted with  $N=3$  and  $D$  from 50 to 400 cm.

Fig. 1 and 2 make it obvious that for the case of a nominally "plane" contact, no correlation can be expected to hold if the parameters  $D$  and  $N$  do not appear in the geometrical description of the surface.

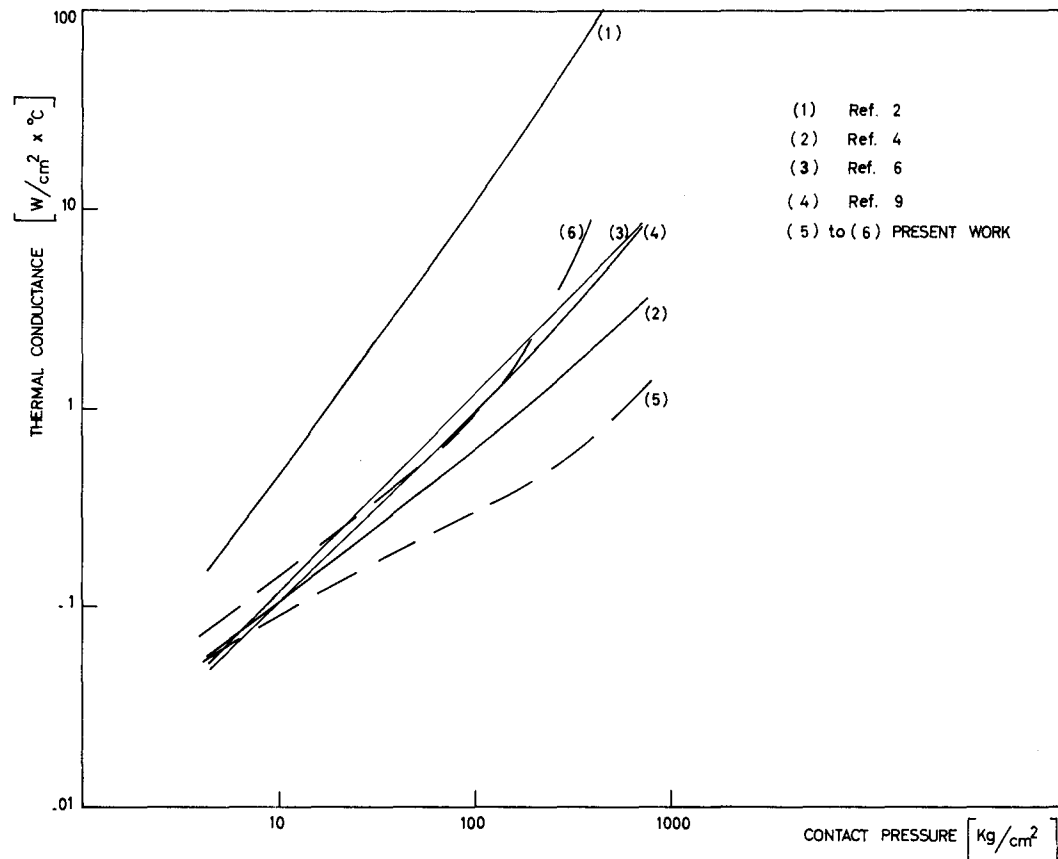


FIG. 1  
URANIUM MONOCARBIDE - SAP CONDUCTANCE  
COMPARISON OF CORRELATIONS

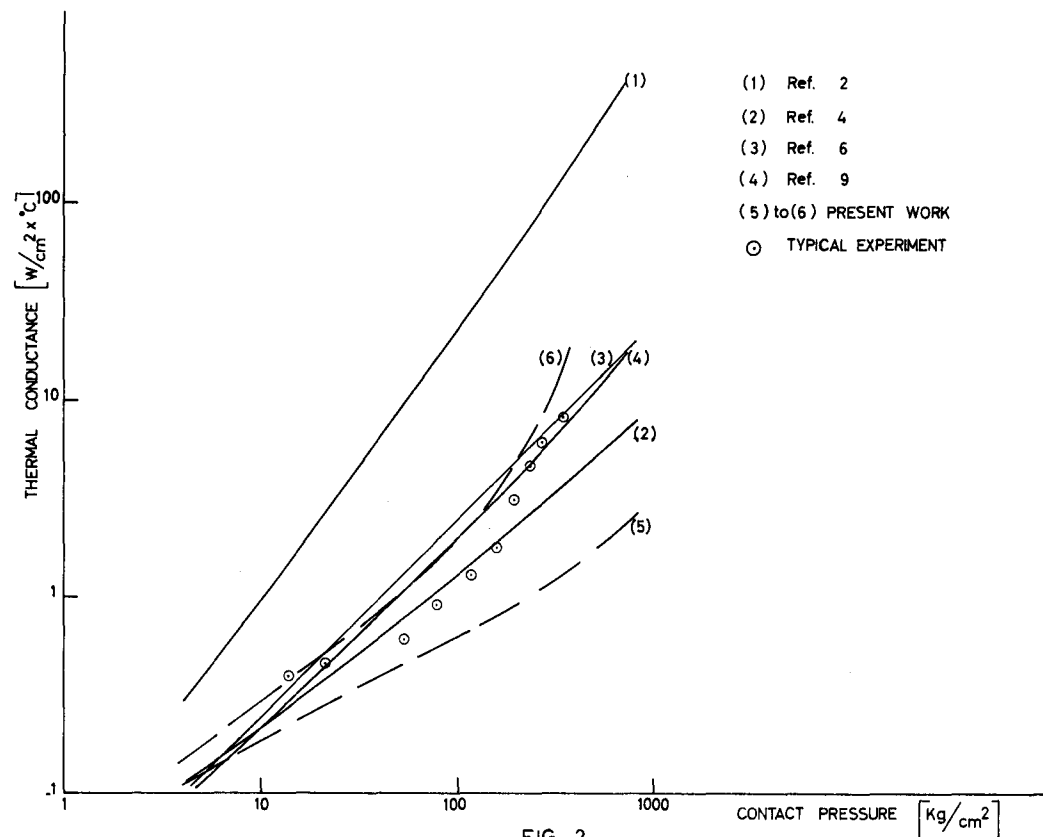


FIG. 2  
ARMCO IRON - SAP CONDUCTANCE  
COMPARISON OF CORRELATIONS

### 3. Experimental

=====

#### 3.1. Experimental apparatus

The test assembly consisted in a press, a coil heater placed vertically on top of the test samples and a cooled S.S. plate. (see Fig. 3).

The press was made by a lever loaded with lead bricks at different positions to increase the pressure gradually. A strain gauge head measured the applied loads. An Armco cylinder transmitted both pressure and heat flux to the specimens.

The maximum total load on the test section was 500 kg, the minimum, 4 kg (weight of the measurement head and the Armco cylinder).

A nichrome heater rated 1 KW was coiled in a cylindrical refractory brick and enclosed in a S.S. box to constitute the heater. The power input to this heater was about 200 Watt in most runs.

The cooling system consisted into two cylindrical boxes. The larger one was located under the specimen support whereas a smaller cooled box prevented the heating of the pressure gauge-head.

The cooling rate was regulated by varying the water flow through the lower cooler.

Ten Chromel-Alumel thermocouples were inserted in holes (0.8 - 1 mm dia.) up to the center of the Armco and S.A.P. cylinders, (see fig.4). All thermocouples were connected through a switch to a recorder and to a precision bridge. Temperatures drops across contactes were derived by extrapolation of the temperature profiles.

A 12.8 mm. dia S.A.P. sample was pressed between two Arceo cylinders and yielded, for each pressure, a high and a low temperature contact.

Contacting surfaces were prepared by various means as described later and roughnesses were measured with a surface analyzer before each test.

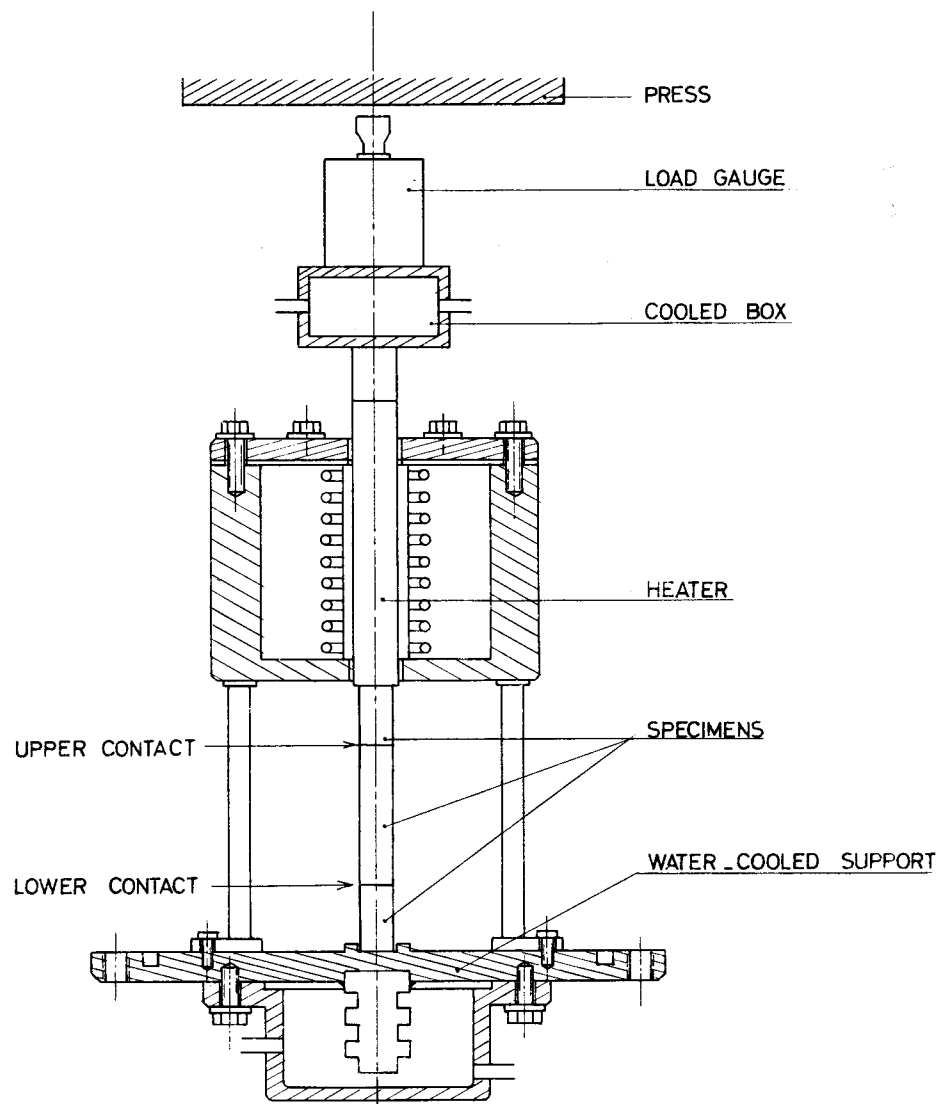


FIG. 3  
TEST ASSEMBLY

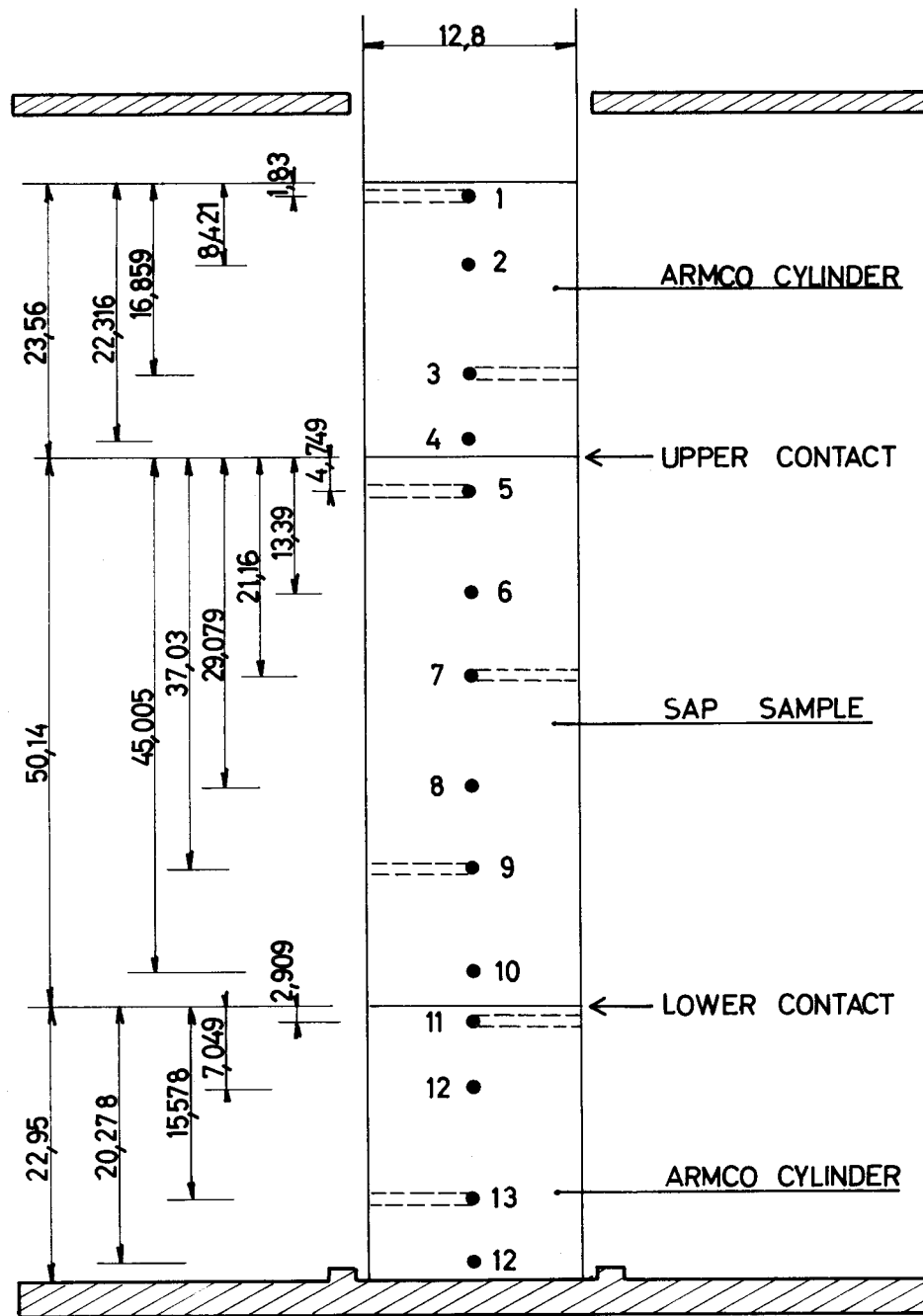


FIG. 4  
SPECIMEN ASSEMBLY AND THERMOCOUPLE POSITIONS

### 3.2. Surface preparation

12.8 mm dia, bars of S.A.P. and Armco iron were cut with different lengths and the specimens were clamped inside a large diameter (6 cm) S.S. cylinder before polishing, to obtain as large a radius of curvature of the polished sample as possible.

The required surface finish was obtained in two stages. The specimen surface was ground gradually using different abrasive papers in a turning machine and the surface finish recorded was approximately  $R_t=1-2 \mu\text{m}$  at the end of the first stage.

The specimen was then transferred to an automatic polishing table using diamond paste. The surface finish recorded was  $R_t=0.1-0.5 \mu\text{m}$ .

Rugosities were then generated on the surface as parallel ridges, pyramids and stochastic scratches.

Couples of samples with parallel ridges were assembled with the respective ridges orthogonal to each other to determine by visual inspection the number and the area of the contact points after the runs. Fig. 5 shows two typical surfaces after a run.

A number of runs were carried out with pyramidal asperities pressing on optically flat planes (see fig. 6) and pyramids against pyramids (fig. 7) Profilograph records however showed that the pyramidal asperities had a very irregular vertex since the machining operation had generated small craters on top of the pyramids and the actual contact was made on the perimeters of such craters. For this reason the machined surfaces were lightly polished before each run.

A third series of samples were hand-roughened with different abrasive papers to obtain stochastic finishes which were shown by the surface analyzer to have values of  $R_t$  between  $1 \mu\text{m}$  and  $40 \mu\text{m}$ .

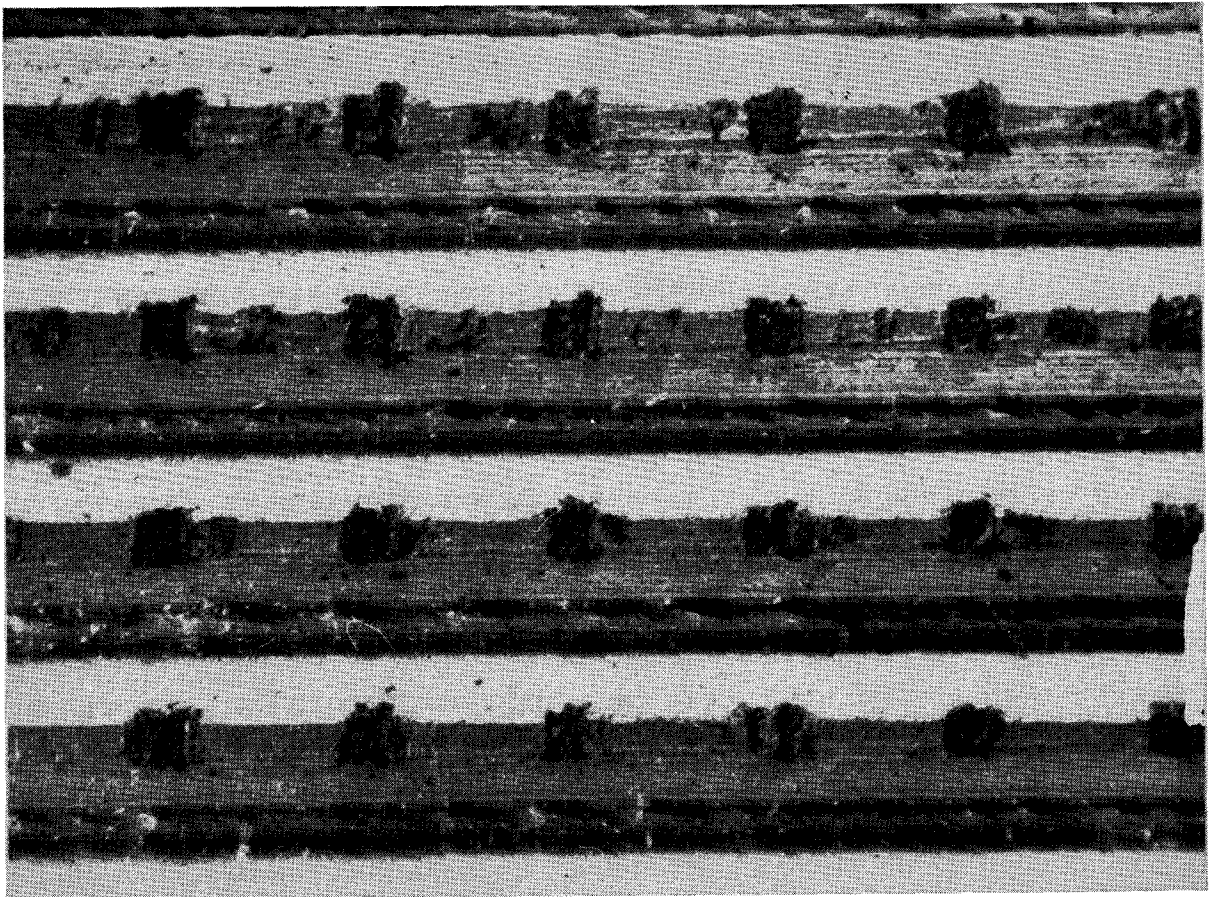
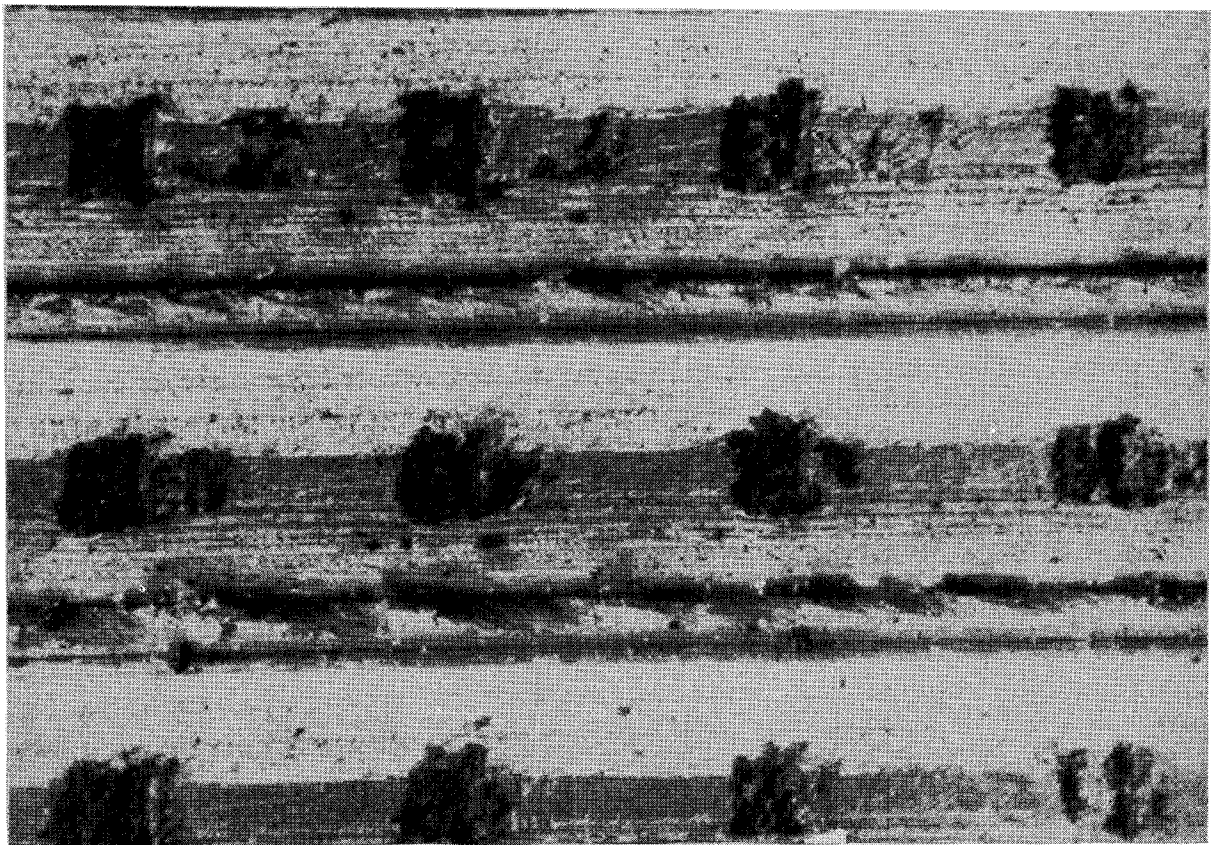


FIG. 5 PARALLEL RIDGE SURFACES 100 x



150 x

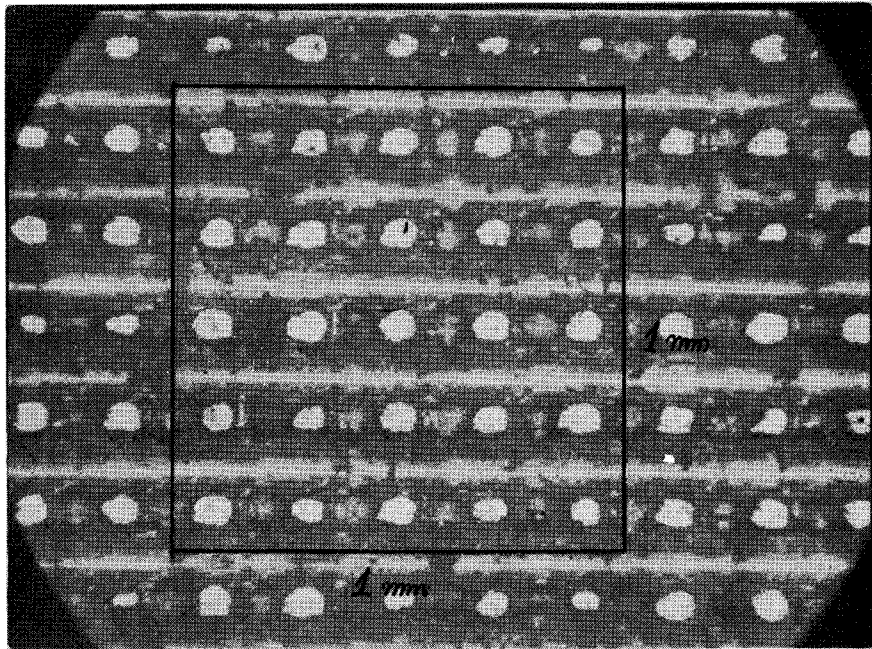


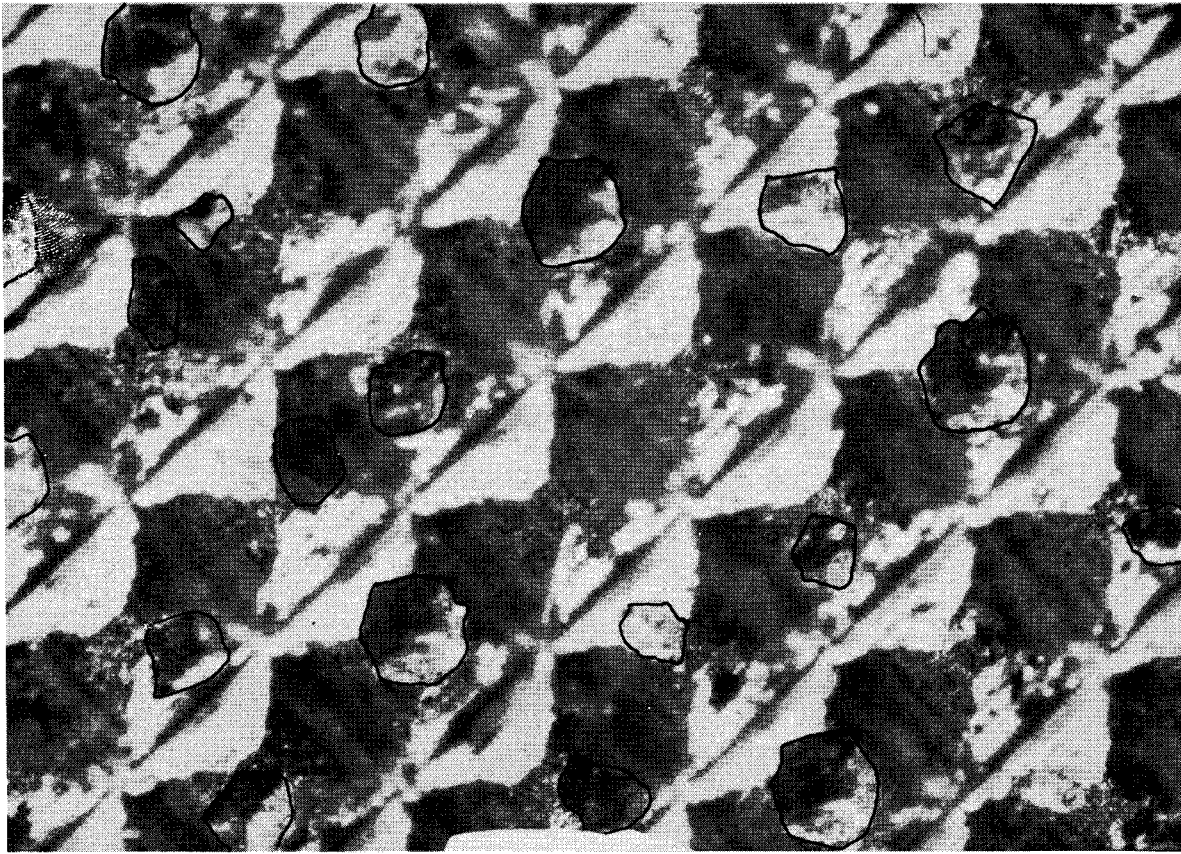
FIG. 6

PYRAMIDAL ASPERITY TEST PLANE

2.42 mm

S = 4.06 mm<sup>2</sup>

1.679



400 x

2.42 mm

S = 4.06 mm<sup>2</sup>

1.679 mm

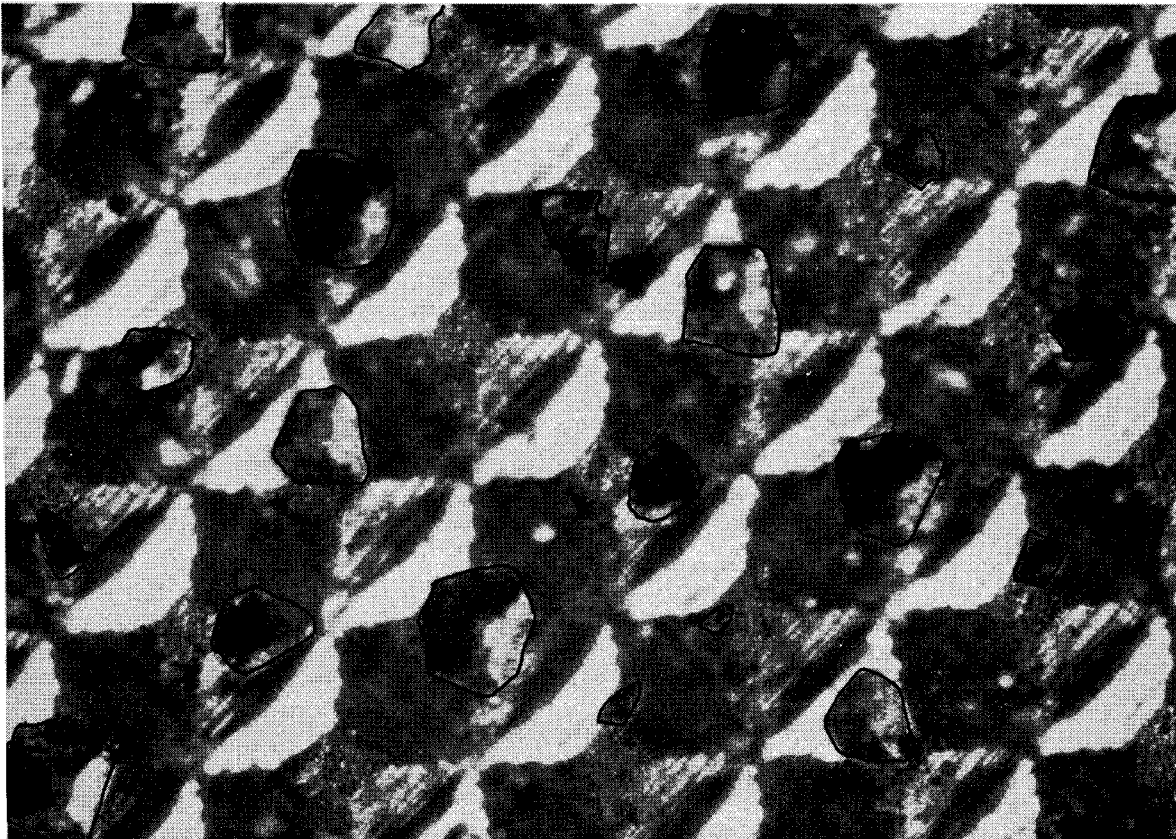


FIG. 7 DOUBLE PYRAMIDAL TEST

400x

### 3.3. Measurement of the surface finish

The surface finish was characterized by means of a Förster mod. 5815 surface analyzer endowed with a variable reluctance exploring stylus, modulating a carrier frequency, passing a wideband amplifier, a series of integrating operational amplifiers and a recorder.

Referring to fig. 8, several mean roughnesses were determined, defined as follows:

$$R_a \text{ (center-line-average)} = \frac{1}{B-A} \int_A^B |f(x)| dx$$

$$R_t = \text{Average of (Max } f(x) - \text{Min } f(x) \text{ )}$$

$$R_g = \text{(Root-Mean square)} = \sqrt{\frac{1}{B-A} \int_A^B [f(x)]^2 dx}$$

The stylus would explore a length of about 1 cm on the sample. Curvatures with wavelengths longer than 7 mm would fall out of the pass-band of the system.

Typical values for  $R_a$ , and  $R_t$  of a series of samples are reported hereafter and show that our runs spanned a range of  $R_t$  from about 1 to 30  $\mu\text{m}$ .

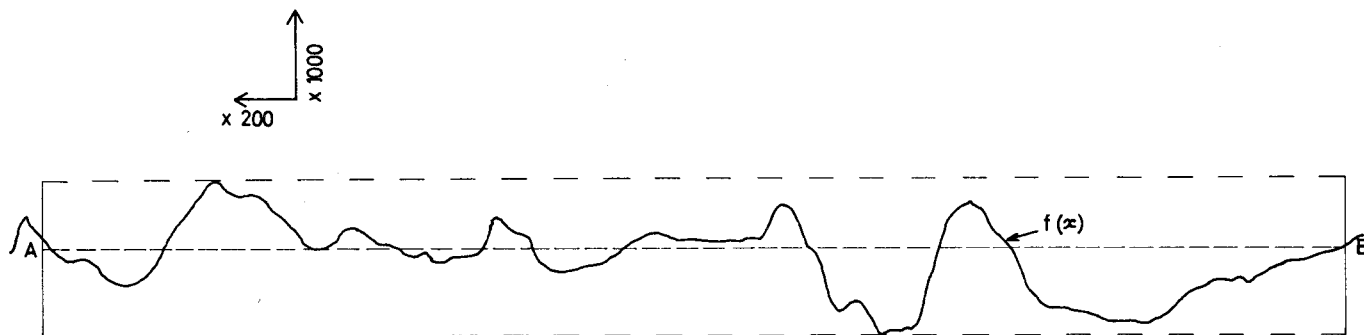


FIG. 8

AMPLIFIED SURFACE PROFILE

SPECIMEN ROUGHNESS

| TEST N° | UPPER CONTACT |                          |             |                          | LOWER CONTACT |                          |             |                          |
|---------|---------------|--------------------------|-------------|--------------------------|---------------|--------------------------|-------------|--------------------------|
|         | ARMCO         |                          | SAP 7 %     |                          | SAP 7 %       |                          | ARMCO       |                          |
|         | Ra( $\mu$ )   | R <sub>z</sub> ( $\mu$ ) | Ra( $\mu$ ) | R <sub>z</sub> ( $\mu$ ) | Ra( $\mu$ )   | R <sub>z</sub> ( $\mu$ ) | Ra( $\mu$ ) | R <sub>z</sub> ( $\mu$ ) |
| 29      | 2.05          | 13                       | 3.8         | 13                       | 4.5           | 20                       | 1.95        | 14                       |
| 30      | 0.60          | 4.5                      | 7           | 30                       | 0.15          | 0.56                     | 0.56        | 3.2                      |
| 31      | 0.60          | 4.5                      | 0.85        | 6.5                      | 0.40          | 2.50                     | 0.56        | 3.2                      |
| 32      | 5.42          | 24                       | 6.42        | 25                       | 1             | 5.5                      | 5.02        | 28                       |
| 33      | 6             | 24                       | 1.4         | 8.5                      | 6.4           | 40                       | 7.15        | 30                       |
| 34      | 0.94          | 5.5                      | 1.25        | 9.5                      | 4.25          | 26                       | 0.15        | 1.5                      |
| 35      | 0.27          | 1.8                      | 0.22        | 11.9                     | 3.2           | 19                       | 0.95        | 4.9                      |
| 36      | 2.6           | 15                       | 1.7         | 8                        | 1.9           | 12                       | 2.6         | 18                       |
| 37      | 3.5           | 18                       | 4.1         | 22                       | 4             | 18                       | 3.7         | 18                       |
| 38      | 0.75          | 4                        | 1.8         | 12.5                     | 1.6           | 3.9                      | 2.75        | 14.5                     |
| 39      | 1.5           | 7.5                      | 0.45        | 4.5                      | 2.3           | 13                       | 1.2         | 7.3                      |
| 40      | 2.7           | 17                       | 0.53        | 4.9                      | 2.17          | 12.5                     | 4.37        | 22                       |
| 41      | 1.1           | 6.3                      | 2.2         | 17                       | 2.87          | 16.75                    | 3.55        | 24                       |

### 3.4. Experimental data

In each run the load was increased stepwise from 18 kg to 450 kg and temperature readings were taken at each step.

Contact thermal conductance is:

$$u = \frac{Q}{\Delta T^*} \quad (18)$$

where  $Q$  is the heat flux through the specimen.

$\Delta T^*$  is the extrapolated temperature discontinuity at the contact. Heat flux through the contact is:

$$Q = \frac{K_1 \Delta T_1}{l_1} \quad (19)$$

where  $K_1$ ,  $\Delta T_1$  and  $l_1$  are respectively the thermal conductivity, the temperature drop and length of the Armco specimen.

Substituting Eq (18) into Eq (19) we obtain the thermal contact conductance (Watt/cm<sup>2</sup> °C)

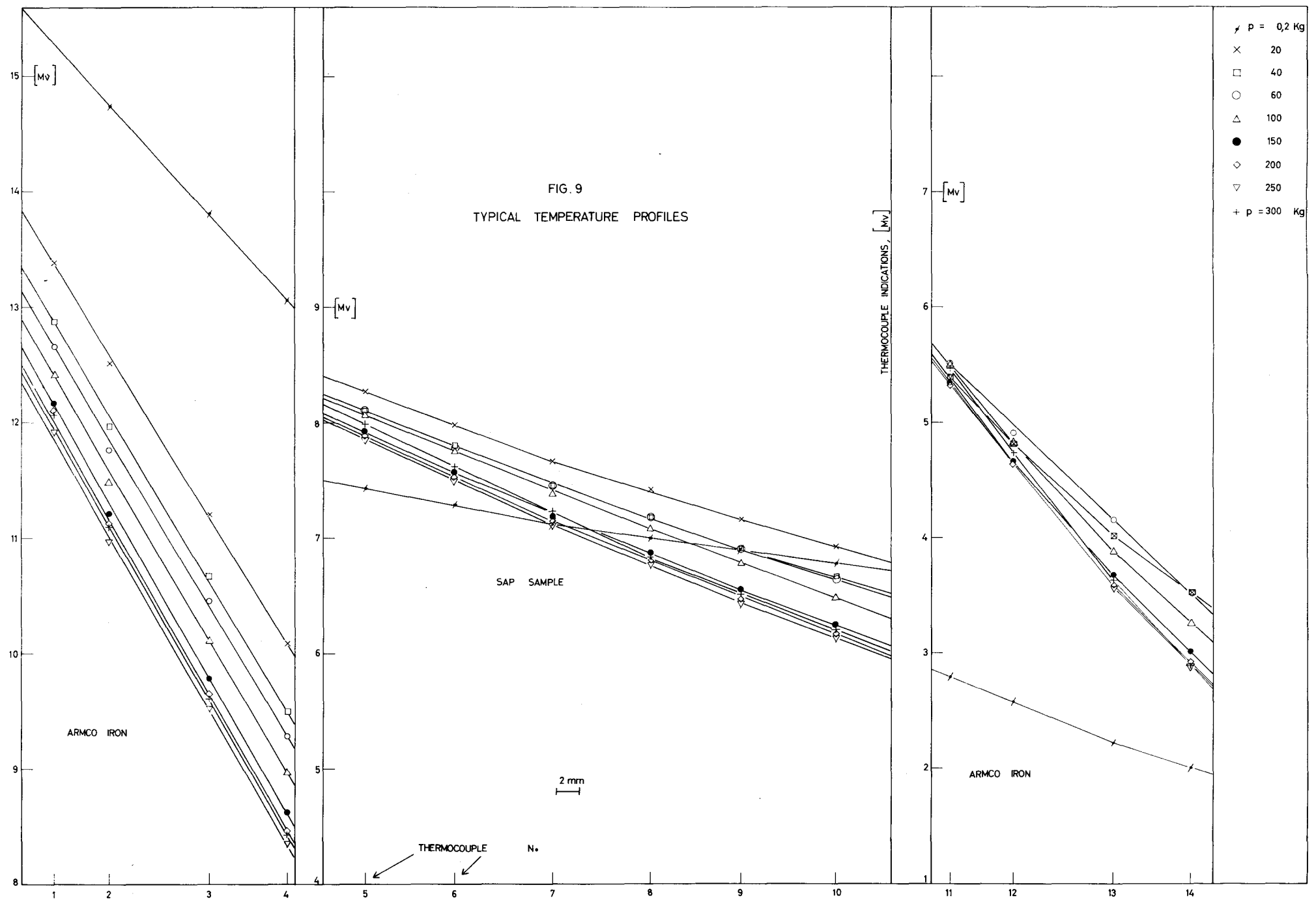
$$u = \frac{K_1 \Delta T_1}{l_1 \Delta T^*} \quad (20)$$

We show hereafter in detail the data measured during a typical run (test n° 26). This specific test was one of the series where a parallel-ridge surface was pressed against another parallel-ridge surface, at right angles.

|                            | Upper contact |        | Lower contact |       |
|----------------------------|---------------|--------|---------------|-------|
|                            | Armco         | SAP 7% | SAP 7%        | Armco |
| wavelength (microns)       | 806           | 1200   | 1195          | 800   |
| mean width of the peaks "  | 146           | 120    | 119           | 200   |
| mean depth of the valleys" | 450           | 600    | 600           | 450   |

Thermocouple readings are plotted and extrapolated in fig. 9 to obtain the experimental  $\Delta T^*$ .

Thermal conductance calculations for each value of the pressure are tabulated below.



TEST N° 26 ( UPPER CONTACT )

| F<br>(kg) | P<br>(kg/cm <sup>2</sup> ) | ARMCO<br>(mV) |       | $\Delta T$<br>ARMCO<br>(mV) | $\bar{T}$<br>ARMCO<br>(mV) | $\bar{T}$<br>ARMCO<br>(°C) | K ARMCO<br>(Watt/cm°C) | T<br>SAP<br>(mV) | $\Delta T$<br>CONTACT<br>(mV) | $\Delta T$<br>CONTACT<br>x<br>1 | $\Delta T$<br>ARMCO<br>x<br>K | U<br>(Watt/cm <sup>2</sup> °C) |
|-----------|----------------------------|---------------|-------|-----------------------------|----------------------------|----------------------------|------------------------|------------------|-------------------------------|---------------------------------|-------------------------------|--------------------------------|
|           |                            | upper         | lower |                             |                            |                            |                        |                  |                               |                                 |                               |                                |
| 0.2       | 0.156                      | 15.58         | 12.98 | 2.60                        | 14.28                      | 350                        | 0.518                  | 7.50             | 5.48                          | 12.80                           | 1.35                          | 0.105                          |
| 20        | 15.6                       | 13.83         | 9.97  | 3.86                        | 11.90                      | 292                        | 0.552                  | 8.41             | 1.56                          | 3.66                            | 2.13                          | 0.583                          |
| 40        | 31.3                       | 13.34         | 9.37  | 3.97                        | 11.35                      | 279                        | 0.560                  | 8.25             | 1.12                          | 2.63                            | 2.22                          | 0.845                          |
| 60        | 46.8                       | 13.13         | 9.16  | 3.97                        | 11.14                      | 274                        | 0.563                  | 8.25             | 0.91                          | 2.14                            | 2.23                          | 1.04                           |
| 100       | 78                         | 12.89         | 8.84  | 4.05                        | 10.86                      | 267                        | 0.567                  | 8.21             | 0.63                          | 1.48                            | 2.3                           | 1.55                           |
| 150       | 117                        | 12.65         | 8.48  | 4.17                        | 10.56                      | 260                        | 0.571                  | 8.08             | 0.40                          | 0.94                            | 2.38                          | 2.53                           |
| 200       | 156                        | 12.50         | 8.34  | 4.16                        | 10.42                      | 257                        | 0.573                  | 8.05             | 0.29                          | 0.68                            | 2.38                          | 3.50                           |
| 250       | 195                        | 12.33         | 8.21  | 4.12                        | 10.27                      | 253                        | 0.575                  | 8.02             | 0.19                          | 0.446                           | 2.36                          | 5.30                           |
| 300       | 234                        | 12.44         | 8.30  | 4.14                        | 10.37                      | 256                        | 0.573                  | 8.16             | 0.14                          | 0.329                           | 2.37                          | 7.20                           |

TEST N° 26 ( LOWER CONTACT )

|     |       |      |      |      |      |     |       |      |      |       |      |        |
|-----|-------|------|------|------|------|-----|-------|------|------|-------|------|--------|
| 0.2 | 0.156 | 2.86 | 1.95 | 0.91 | 2.40 | 59  | 0.705 | 6.72 | 3.86 | 9.22  | 0.64 | 0.0695 |
| 20  | 15.6  | 5.52 | 3.39 | 2.13 | 4.45 | 108 | 0.665 | 6.79 | 1.27 | 3.03  | 1.42 | 0.468  |
| 40  | 31.3  | 5.55 | 3.39 | 2.16 | 4.47 | 109 | 0.664 | 6.52 | 0.97 | 2.32  | 1.43 | 0.617  |
| 60  | 46.8  | 5.66 | 3.33 | 2.33 | 4.49 | 109 | 0.664 | 6.48 | 0.82 | 1.96  | 1.55 | 0.792  |
| 100 | 78    | 5.69 | 3.10 | 2.59 | 4.39 | 107 | 0.666 | 6.30 | 0.61 | 1.46  | 1.72 | 1.18   |
| 150 | 117   | 5.53 | 2.82 | 2.71 | 4.17 | 102 | 0.670 | 6.06 | 0.53 | 1.27  | 1.82 | 1.43   |
| 200 | 156   | 5.56 | 2.74 | 2.82 | 4.15 | 101 | 0.671 | 5.97 | 0.41 | 0.98  | 1.89 | 1.93   |
| 250 | 195   | 5.60 | 2.71 | 2.89 | 4.15 | 101 | 0.671 | 5.95 | 0.35 | 0.836 | 1.94 | 2.32   |
| 300 | 234   | 5.67 | 2.69 | 2.98 | 4.18 | 102 | 0.670 | 6.02 | 0.55 | 0.836 | 2.00 | 2.40   |

Experimental conductances given by Eq. (20) are plotted in fig. 10 vs. applied pressures. Substituting in Eq. 9 the harmonic mean conductivities 0.875W/cm°C and 0.995W/cm°C and the measured wavelengths, the contact conductances, for the upper and the lower contacts are given by

$$u = \frac{0.0237 P^{3/4}}{1-0.00328 P^{3/4}} \quad \text{and} \quad u = \frac{0.0254 P^{3/4}}{1-0.00328 P^{3/4}}$$

$u$  (Watt/cm<sup>2</sup>°C) being the contact conductance of the solids.

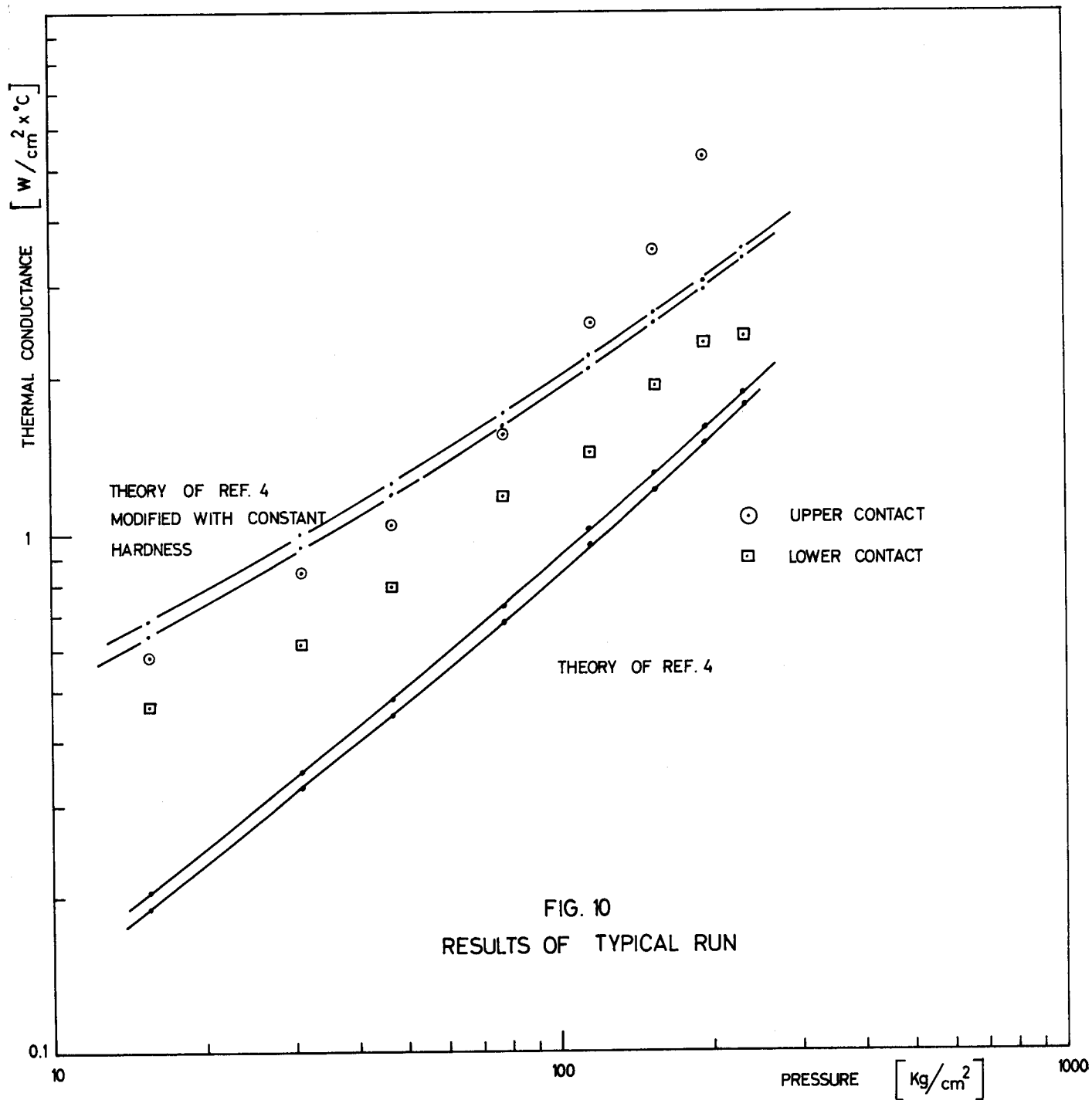
These correlations plotted in fig. 10 appear to yield results lower than the observed experimental conductances. One must notice that the Laming correlations are based upon the assumption that the microhardness decreases linearly with the square root of the applied load, an assumption which was not confirmed by our observations, which, on the contrary, pointed out to a constant microhardness, at a given temperature. Infact, fig. 11 shows a hardness plot vs. applied load with no apparent variation.

Ref. (4) does not actually carry out microindentation tests, but deduces an "apparent" hardness from the observed values of metal-metal conductance. Being there no real evidence of such a variation, we also plotted in fig. 10 a conductance derived as in Ref. (4) but under the assumption of a constant microhardness:

$$U_{\text{upper}} = \frac{0.1495 P^{1/2}}{1-0.021 P^{1/2}} \quad \text{and} \quad U_{\text{lower}} = \frac{0.16 P^{1/2}}{1-0.0198 P^{1/2}}$$

which fit the experimental results no worse than the correlations based on the assumption of a variable  $H$ .

Test N° 26 is carried out in air and fluid conductances are neglected because they are one order of magnitude lower than solid-solid conductances, since the fluid thickness is very large. All experimental contact conductances obtained with surfaces endowed with stochastic surface finish are shown in fig. 12.



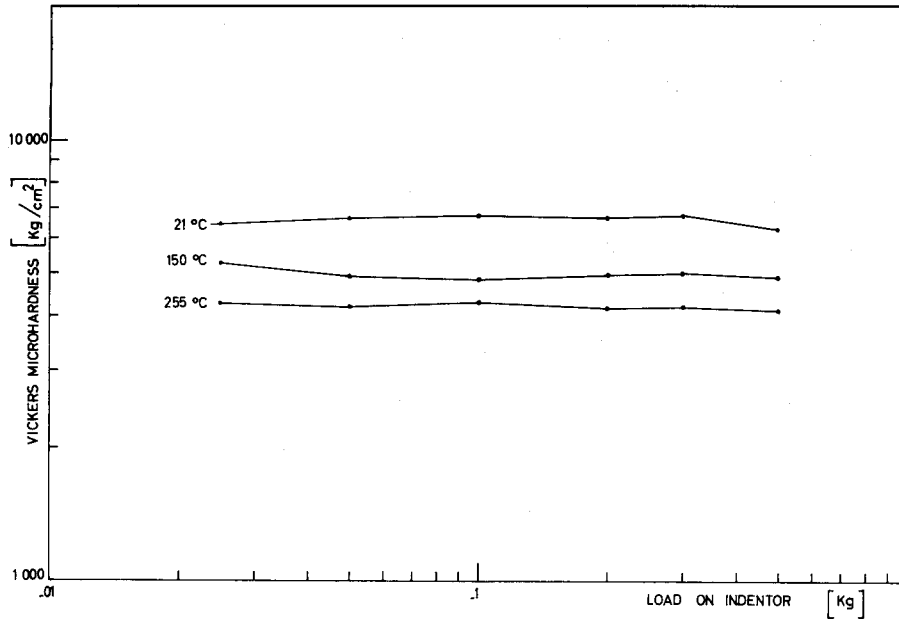
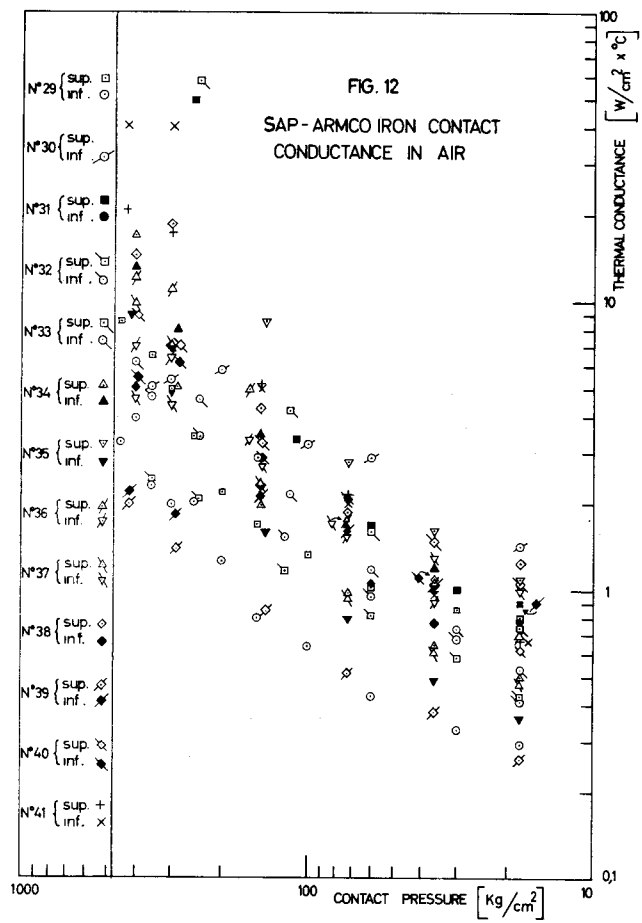


FIG. 11  
MICROHARDNESS OF 7% SAP VS LOAD



#### 4. Fluid conductance

In any contact, beside the solid-solid contact conductance, there is a parallel conductance due to the fluid enclosed between the contact spots. We have so far accounted for such a conductance by:

$$u_f = \frac{K_f}{\delta}$$

We shall hereafter discuss the most appropriate values to be used for both  $K_f$  and  $\delta$ .

If the distances involved are much larger than the mean free path of the fluid molecules,  $K_f$  will be the classical gas conductivity. If this is not so, one must take into account the accommodation effects of the fluid on the solid surfaces either by using formula (2) ref. (12) or by increasing the geometrical distances involved by extrapolation widths, reported in appendix II ref. (12) :

$$u_f = \frac{1}{\frac{\delta_{-2L}}{K_f} + \frac{T^{1/2}(1/\alpha_1 + 1/\alpha_2)M^{1/2}}{7.36 \times 10^5 P_f}} \quad (21)$$

For fission gases at 1 atm pressure, such extrapolation widths are of the order of 0.5  $\mu\text{m}$  on each side of the gap, suggesting an additional width of 1  $\mu\text{m}$  to be added to the actual geometrical wall distance.

In the great majority of our tests and in practically all situations concerning a fuel pellet-sheath contact, the voids involved are much larger than the

1  $\mu\text{m}$  above mentioned so that it is reasonable to lump the extrapolation width into an "effective fluid thickness"  $\delta$  experimentally determined.

By extrapolation to zero solid-solid contact pressure, we obtained in about 30 runs, values for  $\delta$ , which we correlated against  $\sum R_t$ . The results, tabulated hereafter, where B is the ratio  $\delta/\sum R_t$  are to be found at the end of this paragraph.

The arithmetic mean B was found to be 0.74 with a mean square deviation 0.58. Discarding all values of F which fall beyond the mean square deviation, one finds.

$B = 0.67 \pm 0.5$  with a confidence level of 90%

It is therefore recommended, for design purposes, to use

$$u_f = \frac{K_f}{2/3 \sum R_t} \quad (22)$$

which is in line with experimental evidence of ref. (4) and, although it may be affected of a large uncertainty, is infact often negligible whenever a moderate solid-solid contact is present.

| TRST<br>No | $\Sigma R$<br>( $\mu$ ) | $U_f$<br>(W/cm <sup>2</sup> °C) | $\delta$<br>( $\mu$ ) | $\bar{E}$     | $\Delta =  0.74 - \bar{E} $ | $\Delta^2$   |
|------------|-------------------------|---------------------------------|-----------------------|---------------|-----------------------------|--------------|
| 29         | 26                      | 0.403                           | 8.7                   | 0.334         | 0.406                       | 0.164        |
|            | 34                      | 0.242                           | 14.5                  | 0.427         | 0.313                       | 0.098        |
| 30         | 34.5                    | 0.304                           | 11.5                  | 0.334         | 0.406                       | 0.164        |
|            | 3.76                    | 0.494                           | 7.08                  | 1.880         | 1.140                       | 1.300        |
| 31         | 11                      | 0.620                           | 5.65                  | 0.514         | 0.226                       | 0.051        |
|            | 5.7                     | 0.248                           | 14.1                  | 2.480         | 1.740                       | 3.040        |
| 32         | 49                      | 0.279                           | 12.5                  | 0.256         | 0.484                       | 0.234        |
|            | 33.4                    | 0.143                           | 24.5                  | 0.735         | 0.005                       | -            |
| 33         | 32.5                    | 0.222                           | 15.8                  | 0.486         | 0.254                       | 0.064        |
|            | 70                      | 0.120                           | 29.2                  | 0.418         | 0.322                       | 0.104        |
| 34         | 15                      | 0.475                           | 7.38                  | 0.492         | 0.248                       | 0.062        |
|            | 27.5                    | 0.229                           | 15.3                  | 0.556         | 0.184                       | 0.034        |
| 35         | 3.75                    | 0.586                           | 6                     | 1.610         | 0.870                       | 0.760        |
|            | 23.9                    | 0.427                           | 8.2                   | 0.343         | 0.397                       | 0.158        |
| 36         | 23                      | 0.305                           | 11.5                  | 0.500         | 0.240                       | 0.057        |
|            | 30                      | 0.158                           | 22.2                  | 0.740         | 0                           | -            |
| 37         | 40                      | 0.242                           | 14.5                  | 0.363         | 0.377                       | 0.142        |
|            | 36                      | 0.258                           | 13.5                  | 0.375         | 0.365                       | 0.133        |
| 38         | 16.5                    | 0.605                           | 5.8                   | 0.351         | 0.389                       | 0.152        |
|            | 18.4                    | 0.325                           | 10.8                  | 0.587         | 0.153                       | 0.023        |
| 39         | 12                      | 0.142                           | 24.7                  | 2.060         | 1.320                       | 1.740        |
|            | 10.3                    | 0.274                           | 12.8                  | 1.240         | 0.500                       | 0.250        |
| 40         | 21.9                    | 0.405                           | 8.65                  | 0.395         | 0.345                       | 0.119        |
|            | 34.5                    | 0.157                           | 22.3                  | 0.646         | 0.094                       | -            |
| 41         | 23.3                    | 0.340                           | 10.3                  | 0.442         | 0.298                       | 0.089        |
|            | 40.75                   | 0.127                           | 27.6                  | 0.678         | 0.062                       | -            |
|            |                         |                                 |                       | <u>19.242</u> |                             | <u>8.938</u> |

### 5. Cylindrical contact

The cylindrical contact typical of a fuel pellet-clad situation is in many respects a more reproducible and geometrically definable system than the plane contact discussed in chapter 2.3.

The main reason is that the ridging of the surfaces into contact is not as important as in a plane contact. As soon as a moderate pressure between fuel and clad is present, the slenderness of the sheath tube is such to match the sheath and pellet surfaces in such a way as to avoid the "patching" effect, reducing the situation to one where the microroughness will be the controlling factor in determining the number of contact spots.

This appears to be true for "thin clads" i.e. metal clads which do not exceed 1 mm thickness. This fact was verified by optical inspections of pellets chemically swelled by oxidation (UC to  $UO_2$ ) in S.A.P. tubes endowed with an original elliptical cross-section.

The solid-solid conductance, in such a case will be given by (ref. 11):

$$U = .434 \frac{K}{R_t} \left(\frac{P}{H}\right)^{.9125} \frac{1}{\tan^{-1} \left[ \left(\frac{H}{P}\right)^{1/2} - 1 \right]} \quad (23)$$

using for  $R_t$  the larger of the two rugosities, which in the cases we observed is that of the centerless ground fuel pellet.

In a series of measurements carried out on the inside of a S.A.P. tube, we found an average  $R_t = 2.4 \mu\text{m}$  whereas fuel pellets had typical  $R_t$ 's of 15 to 20  $\mu\text{m}$ .

In the case of UC-SAP with a 400°C clad temperature,  $R_t = 17 \times 10^{-4} \text{ cm}$ ,  $H = 3,200 \text{ kg/cm}^2$ ,  $K = 0.34$ ,  $\delta = 2/3 \times 20 \times 10^{-4}$  and the total conductance is

$$U = \frac{.055 P^{.9125}}{\tan^{-1} \left[ 56.5 P^{-1/2} - 1 \right]} + \frac{K_f}{13.3 \times 10^{-4}} \quad (24)$$

A natural -U UC pellet of density 13.4 g/cm<sup>3</sup>, exposed to a thermal neutron flux  $\phi$ , will have a heat generation, discounting the effects of gamma heating:

$$2.7 \times 10^{-13} \phi \times 13.4 \times \frac{238}{250} = 3.44 \times 10^{-12} \phi \text{ W/cm}^3$$

The center-to-surface temperature drop in the UC pellet, with  $K = 0.15 \text{ W/cm } ^\circ\text{C}$  and a radius  $r_0$ , will be

$$\Delta T_{uc} = \frac{3.44 \times 10^{-12} \phi r_0^2}{4 \times 0.15} = 5.73 \times 10^{-12} \phi r_0^2 \text{ } ^\circ\text{C}$$

### 5.1. Simplified Theory

The hot radial gap will be given by the cold assembly clearance, decreased by the UC swelling and corrected for the differential expansion of UC and SAP, i.e.

$$C' = C - s r_o + r_o (\bar{T} - 20) \alpha_c - r_o (\bar{T}_c - \frac{1}{3} \Delta T_p - 20) \alpha_p$$

On the other hand,  $\bar{T}_c - \Delta T_{uc} - \bar{T}$  is the gap temperature drop, equal to the heat flux divided by the conductance, i.e.

$$\Delta T_1 = \frac{3.44 \times 10^{-12} \phi \times \tilde{u} r_o^2}{2 \tilde{u} r_o \times u_t} = \frac{172 \times 10^{-12} \phi r_o}{u_t}$$

$$\bar{T}_c = \bar{T} + \Delta T_1 + \Delta T_{uc} = \bar{T} + \frac{1.72 \times 10^{-12} \phi r_o}{u_t} + 5.73 \times 10^{-12} \phi r_o^2$$

whence

$$C' = C + r_o \left[ -s - 2 \times 10^{-4} + 10^{-5} \bar{T} - 10^{-17} \phi r_o \left( \frac{1.72}{u_t} + 3.82 r_o \right) \right] \quad (25)$$

To completely determine the system, one must express P as a function of the pellet-clad operating interference, as in 8.1. and 8.2. (ref. 11).

Of course, to have an actual contact, it must be  $C' < 0$  in eq. 25. The pressure in the case of an interference  $-\frac{C'}{r_o}$  will be (ref. 11)

$$P = \frac{-C'/r_0}{\frac{1}{E_c} \left[ \frac{2r_0^2 + t^2 + 2r_0 t}{t(t + 2r_0)} + \nu_c \right] + \frac{1-\nu_p}{E_p}} \quad (26)$$

For the case UC-SAP

$$\begin{aligned} E_c &= 5 \times 10^5 \text{ kg/cm}^2 && \text{(ref. 11)} \\ E_p &= 2.2 \times 10^6 \text{ "} && \text{(ref. 13)} \\ \nu_c &= 0.4 && \text{(ref. 15)} \\ \nu_p &= 0.3 && \text{(estimated)} \end{aligned}$$

Equation 26, using these values and assuming  $t \ll r_0$  will become:

$$P = -5 \times 10^5 \frac{C't}{r_0^2} \quad (27)$$

Introducing (27) into (24), we obtain, with  $K_f$  for fission gases equal (5 Xe + 1 Kr) estimated to be  $0.97 \times 10^{-4} \text{ W/cm}^2\text{C}$

$$u_t = 0.073 + \frac{8.7 \times 10^3 \left[ \frac{-C't}{r_0^2} \right]^{0.9125}}{\tan^{-1} \left[ 8 \times 10^{-2} \left( -\frac{C't}{r_0^2} \right)^{-0.5} - 1 \right]} \quad (28)$$

with  $C'$  given by (25)

For the case  $T = 400 \text{ }^\circ\text{C}$   $t = 0.1 \text{ cm}$   $r_o = 1.5 \text{ cm}$   
 $\phi = 10^{14} \text{ n/cm}^2 \text{ x sec}$

formulas (25) and (28) become:

$$C' = C - 1.5 s - 7.19 \times 10^{-3} - \frac{3.87 \times 10^{-3}}{u_t}$$

and

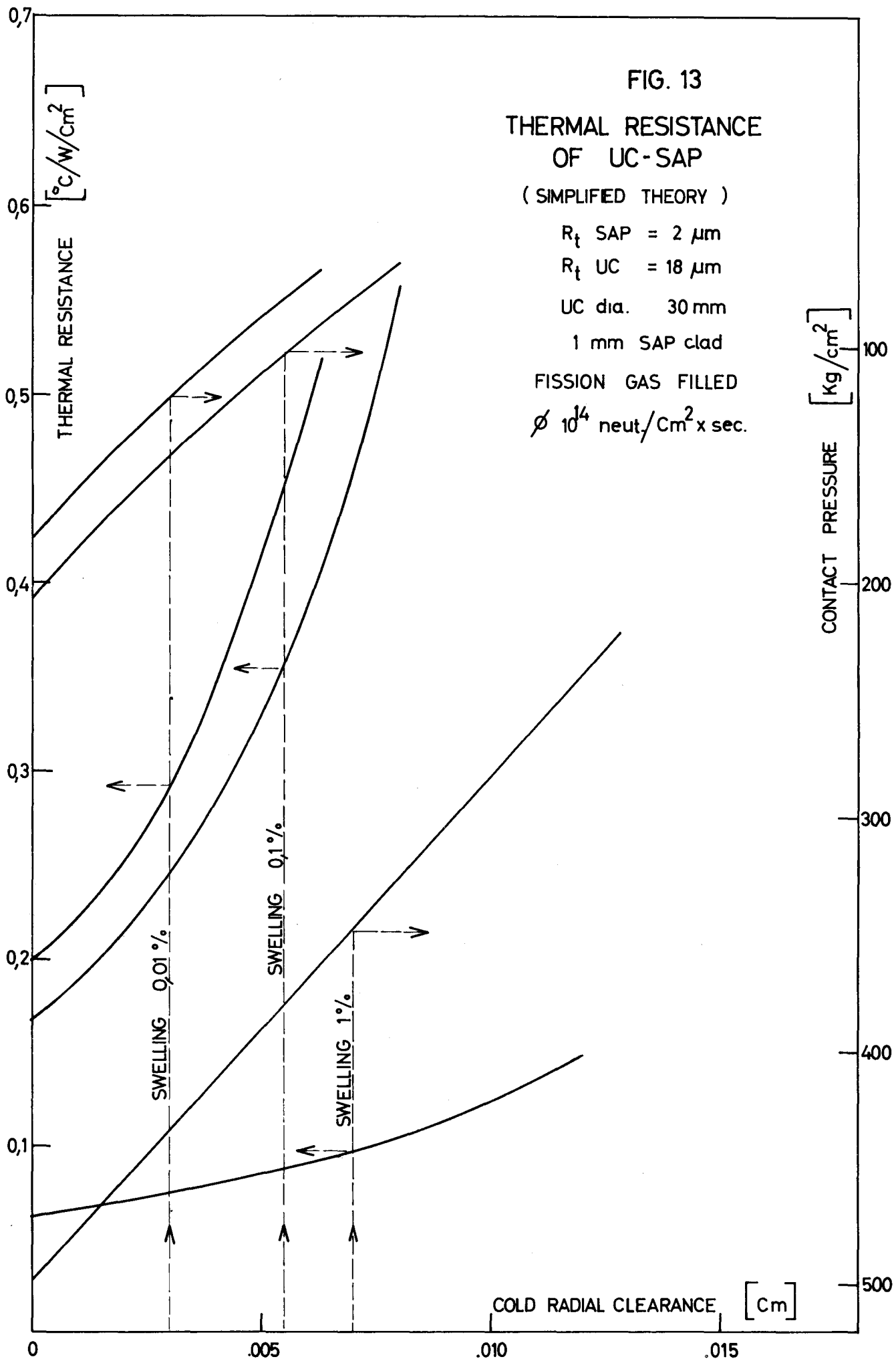
$$u_t = \frac{0.073 + 509 (-C')^{0.9125}}{\tan^{-1} \left[ 0.38(-C')^{-0.5} - 1 \right]} \quad (30)$$

Combining (29) and (30) one can relate  $u_t$  to  $C$  and  $s$  and also obtain the operating contact pressure from (27) i.e.:

$$P = -2.22 \times 10^4 \times C' \quad (31)$$

such expressions being valid, of course, for  $C' < 0$ , that is, for the case of an actual contact between surfaces.

This simplified theory does not account for the strain of the clad due to the fuel-clad interference. It leads to typical results as shown in fig. 13, which are not conservative for design purposes as far as the thermal resistance is concerned. The mechanical stress on the clad will infact yield a lower fuel-clad pressure and therefore a higher thermal resistance, in most practical cases.



### 5.2. Complete theory

This model is closer to the actual physical situation than the former. We shall account for the strains of both fuel and clad due to the effects of the contact pressure.

We have thus

$$\epsilon_p = \text{Strain of fuel pellet} = \alpha_p (T_s - 20) + \frac{\alpha_p \Delta T_p}{2(1 - \nu_p)} - \frac{P r_o}{E_p} (1 - \nu_p)$$

$$\epsilon_c = \text{Strain of clad} = \alpha_c (T - 20) + \frac{r_o}{t} \frac{P}{E_c} \left(1 - \frac{\nu_c}{2}\right)$$

On the other hand, the fuel temperature drop is

$$\Delta T_p = 1.61 \times 10^{-11} \frac{\phi C_o d}{M} \frac{r_o^2}{K_p} \quad (32)$$

The hot operating radial gap is

$$C' = C - s r_o + r_o (\epsilon_c - \epsilon_p)$$

whence, by substitution

$$C' = C - s r_o + r_o \left[ \alpha_c (T - 20) + \frac{r_o}{t} \frac{P}{E_c} \left(1 - \frac{\nu_c}{2}\right) - \alpha_p (T_s - 20) - \frac{1.61 \times 10^{-11} \alpha_p}{2(1 - \nu_p)} \frac{\phi C_o d}{M} \frac{r_o^2}{K_p} + \frac{P r_o}{E_p} (1 - \nu_p) \right] \quad (33)$$

Interference fit and contact pressure will be related by a simplified version of formula of formula (26), i.e.

$$P = \frac{-C'/r_o}{\frac{1}{E_c} \left( \frac{r_o}{t} + \nu_c \right) + \left( \frac{1-\nu_p}{E_p} \right)} \quad (34)$$

and, finally, fuel surface and clad temperature are related by

$$T_s = \bar{T} + 3.215 \times 10^{-11} \frac{\phi C_o d r_o}{M u} \quad (35)$$

where u, the total conductance, is

$$u = \frac{K_f}{2/3 \sum R_t} + \frac{.434 K}{R_t} \left( \frac{P}{H} \right)^{.9125} \frac{1}{\tan^{-1} \left[ \left( \frac{H}{P} \right)^{1/2} - 1 \right]} \quad (36)$$

Substituting in (33) the values of C' and T<sub>s</sub> from (34) and (35) and solving for P, one obtains the value of the fuel-clad contact pressure during operation:

$$P = \frac{-C'/r_o + s - (\bar{T} - 20)(\alpha_c - \alpha_p) + 3.215 \times 10^{-11} \frac{\phi C_o d r_o \alpha_p}{M} \left[ \frac{1}{u} + \frac{r_o}{4K_p(1-\nu_p)} \right]}{\frac{(1-\nu_p)}{E_p} (1+r_o) + \frac{1}{E_c} \left[ \frac{r_o}{t} \left( 2 - \frac{\nu_c}{2} \right) + \nu_c \right]} \quad (37)$$

Equations (36) and (37) determine completely both the contact pressure and the conductance between fuel and clad, once the physical dimensions, physical properties thermal flux and enrichment are known. Of course the clad temperature  $\bar{T}$  must also be specified.

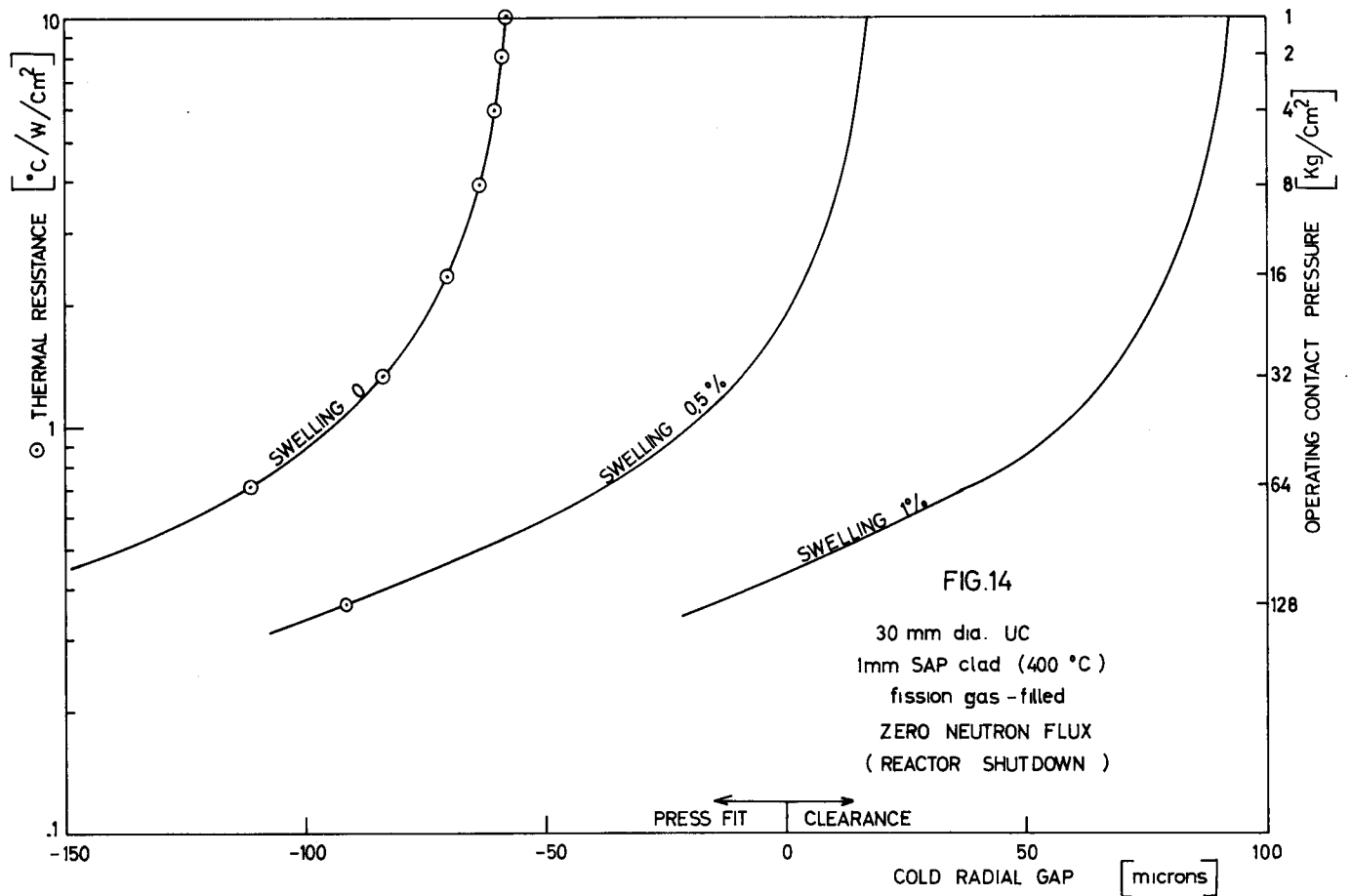
All properties relating to clads, fuels and filling fluids have been left in symbolic form in (36) and (37) for ease of application to any system of materials, such as  $UO_2$ , UC, U metal, clad with Al, Zircaloy, Stainless Steel, Magnox, filled with He, fission gases etc.

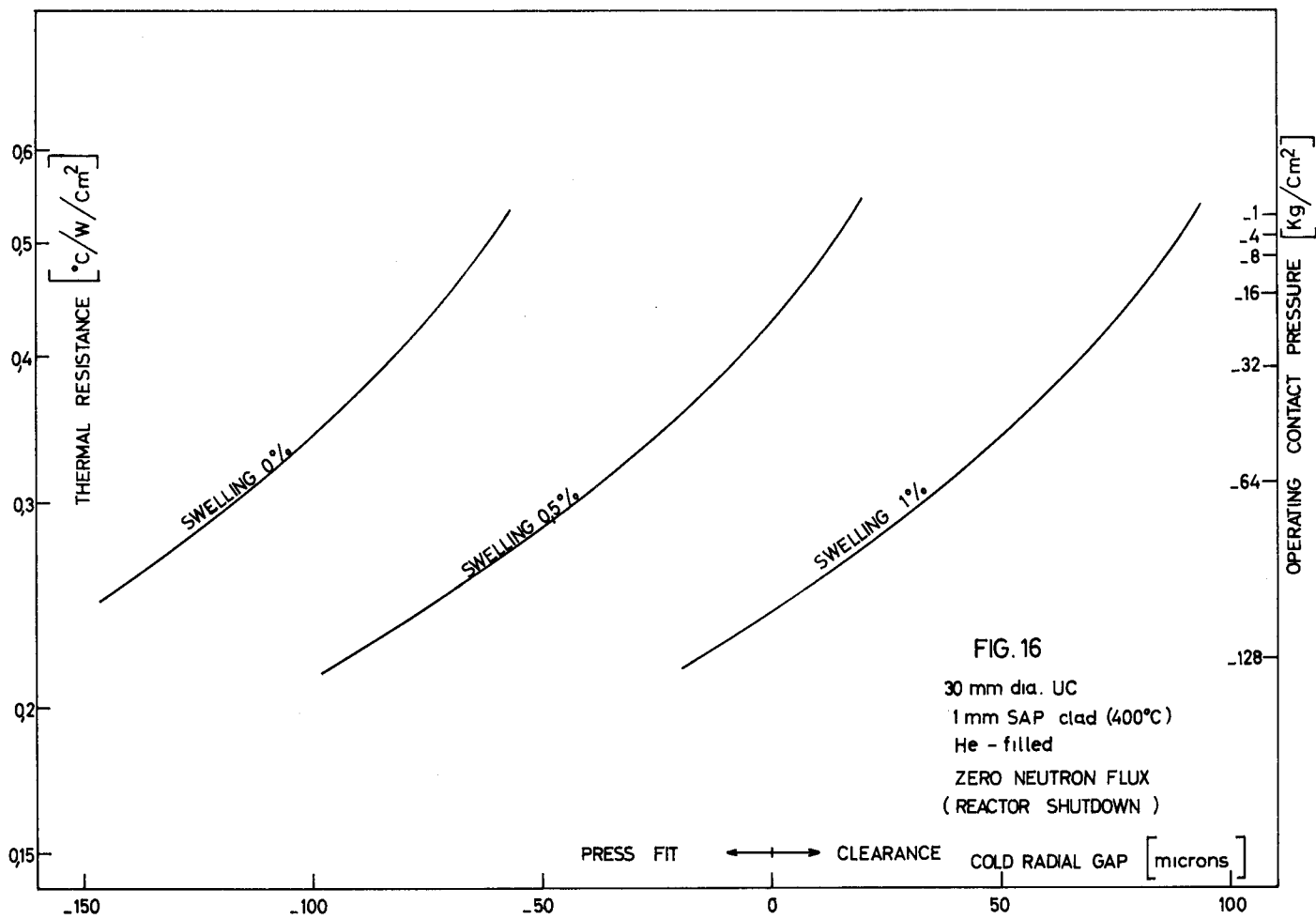
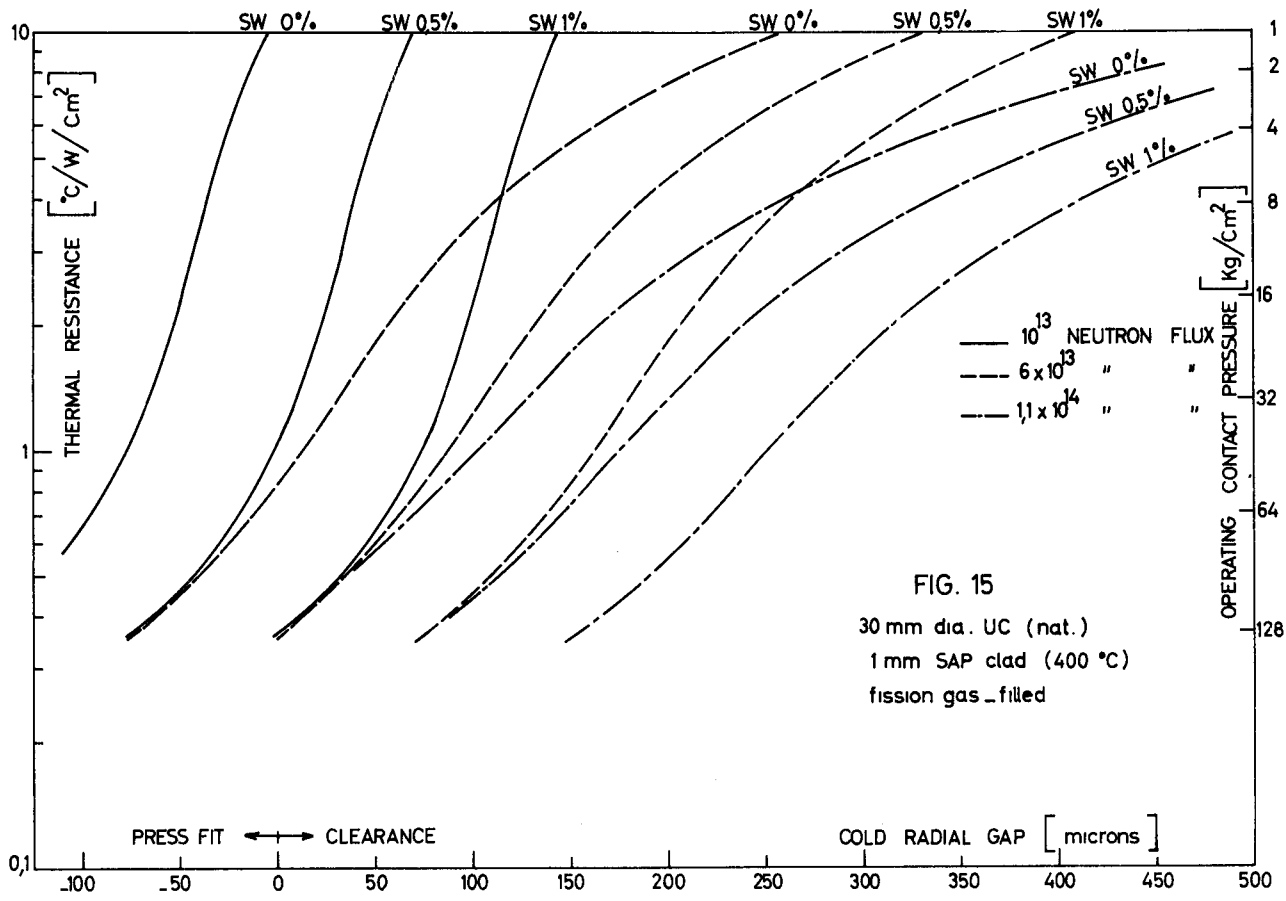
For the purpose of illustrating the application of (36) and (37) to practical situations close of interest to the fuel element designer, a number of computations have been carried out and plotted in fig. (14) to (23). A listing of the computation procedure, in FORTRAN 2 V 3 is shown hereafter, as a help to the fuel element designer. The equivalence of symbols in our text and in the machine program is shown below

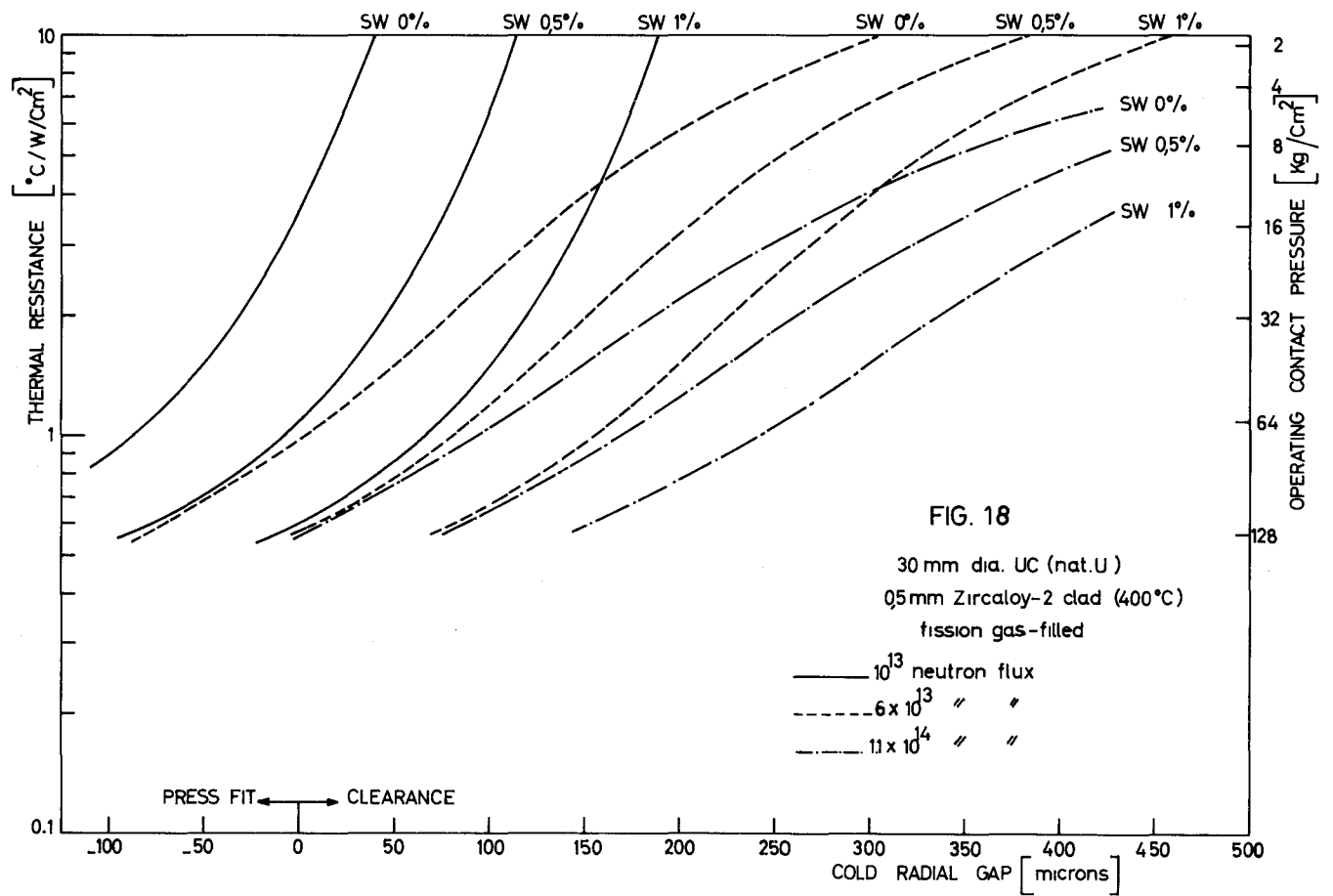
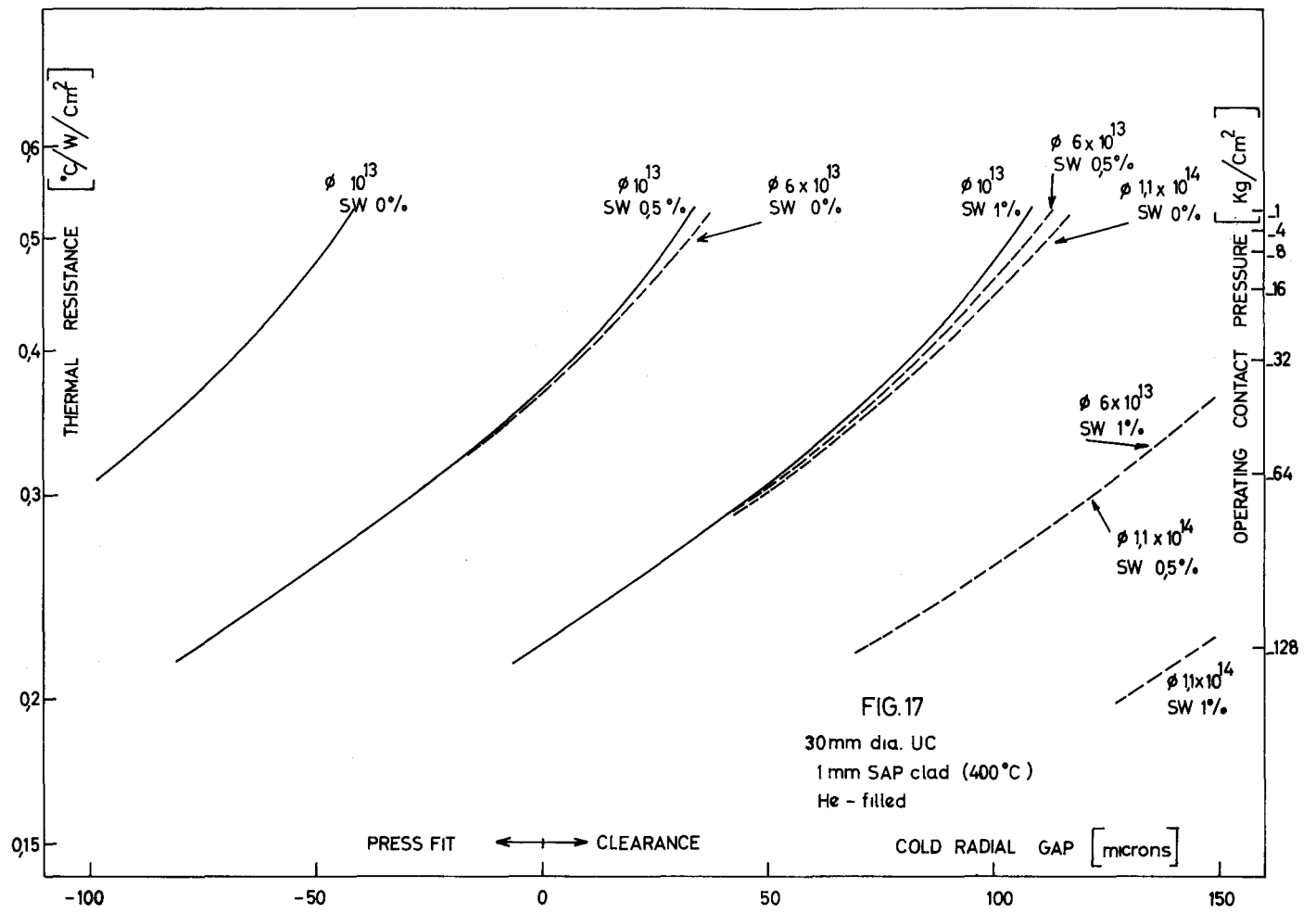
| TEXT  | F2V3   | TEXT       | F2V3   |
|-------|--------|------------|--------|
| c     | C      | $r_o$      | R      |
| $C_o$ | CØ     | $R_t$      | RT     |
| d     | DENS   | $\Sigma R$ | SRT    |
| $E_c$ | EC     | s          | S      |
| $E_p$ | EP     | t          | TT     |
| H     | DURC   | $\bar{T}$  | T      |
| K     | CØAR   | u          | U      |
| $K_c$ | CØNDUC | $\alpha_c$ | ALFAC  |
| $K_f$ | CØNDG  | $\alpha_p$ | ALFAP  |
| $K_p$ | CØNDP  | $\phi$     | FI, FØ |
| M     | PESØ   | $\nu_c$    | XNU    |
| P     | P      | $\nu_p$    |        |

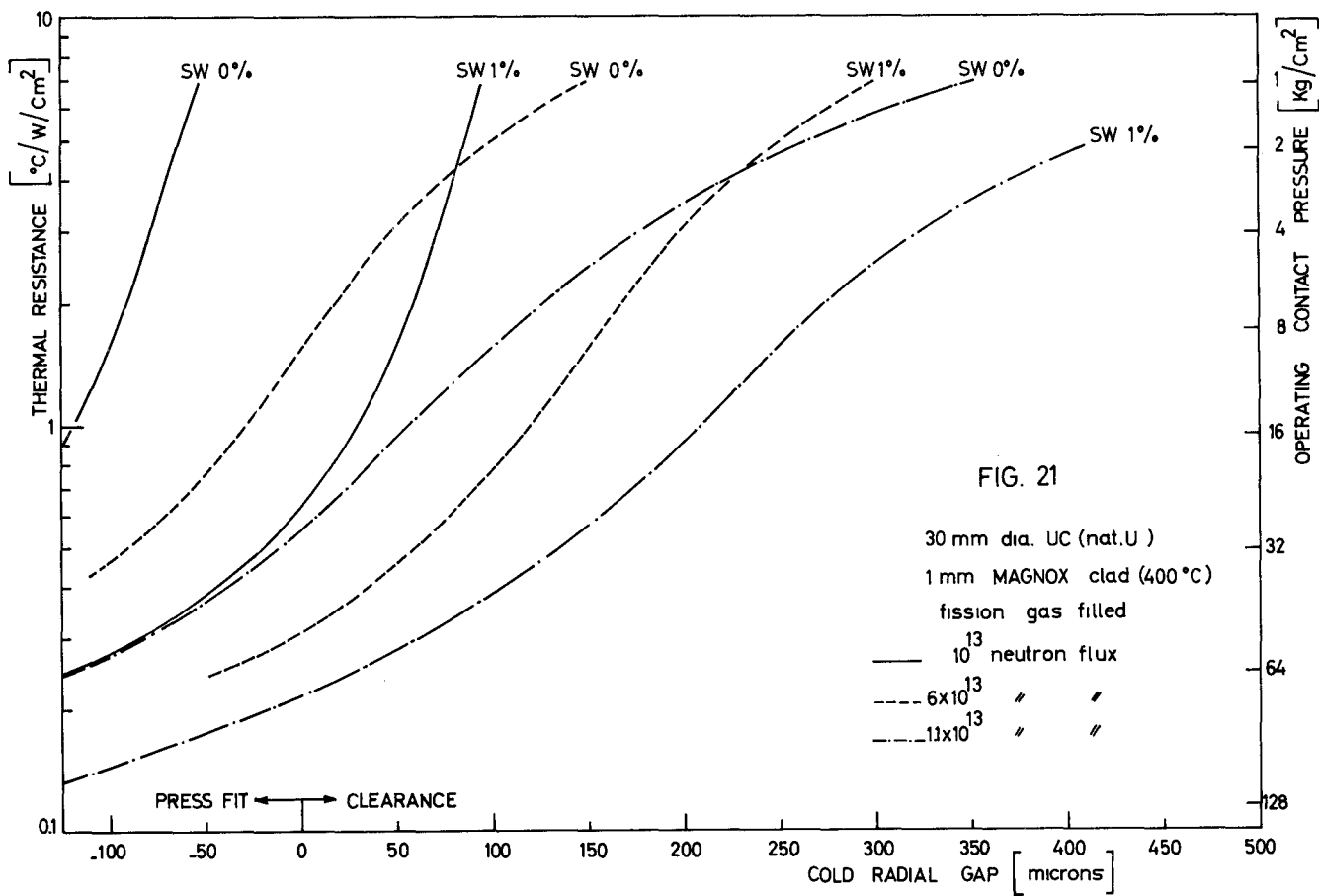
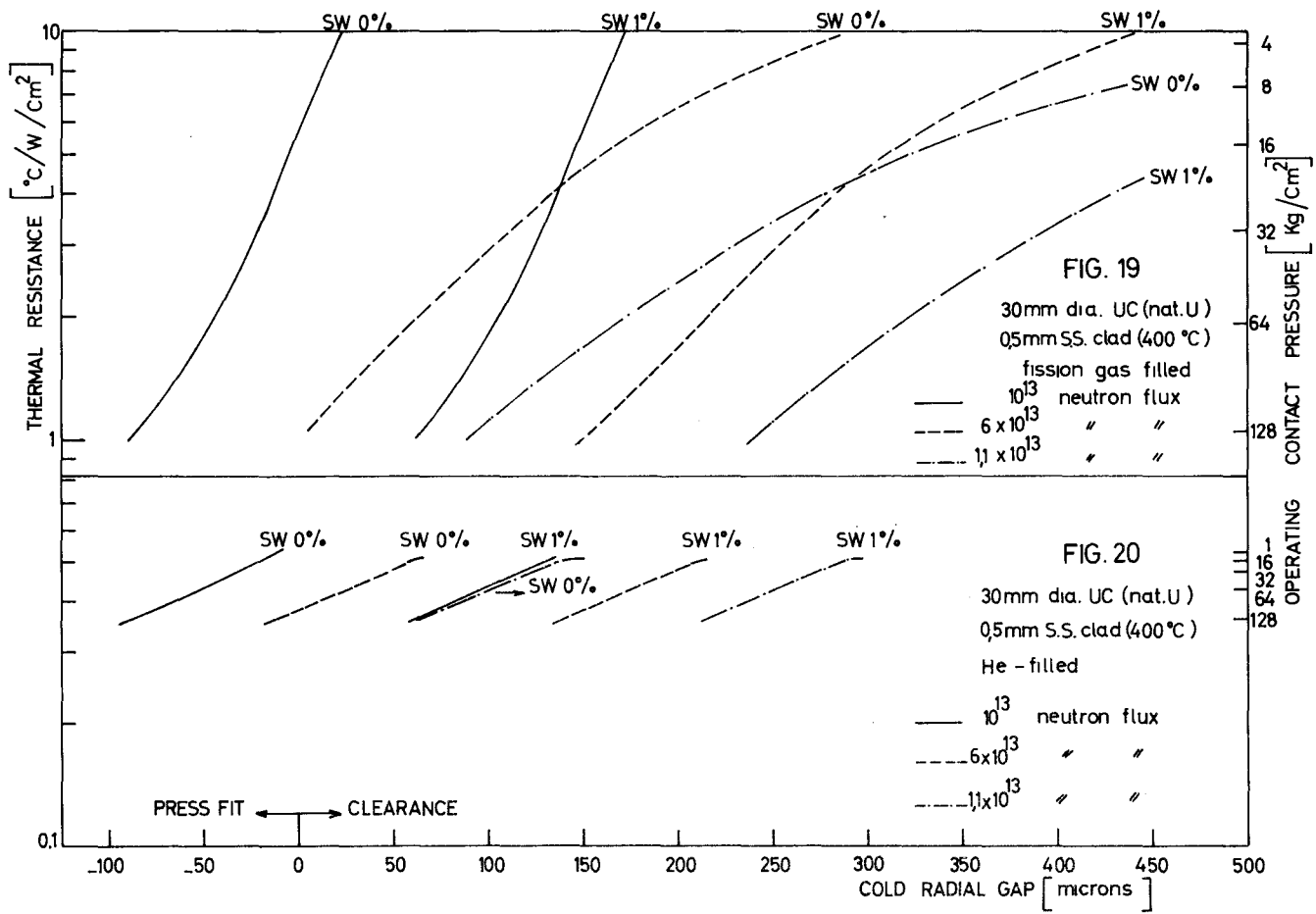


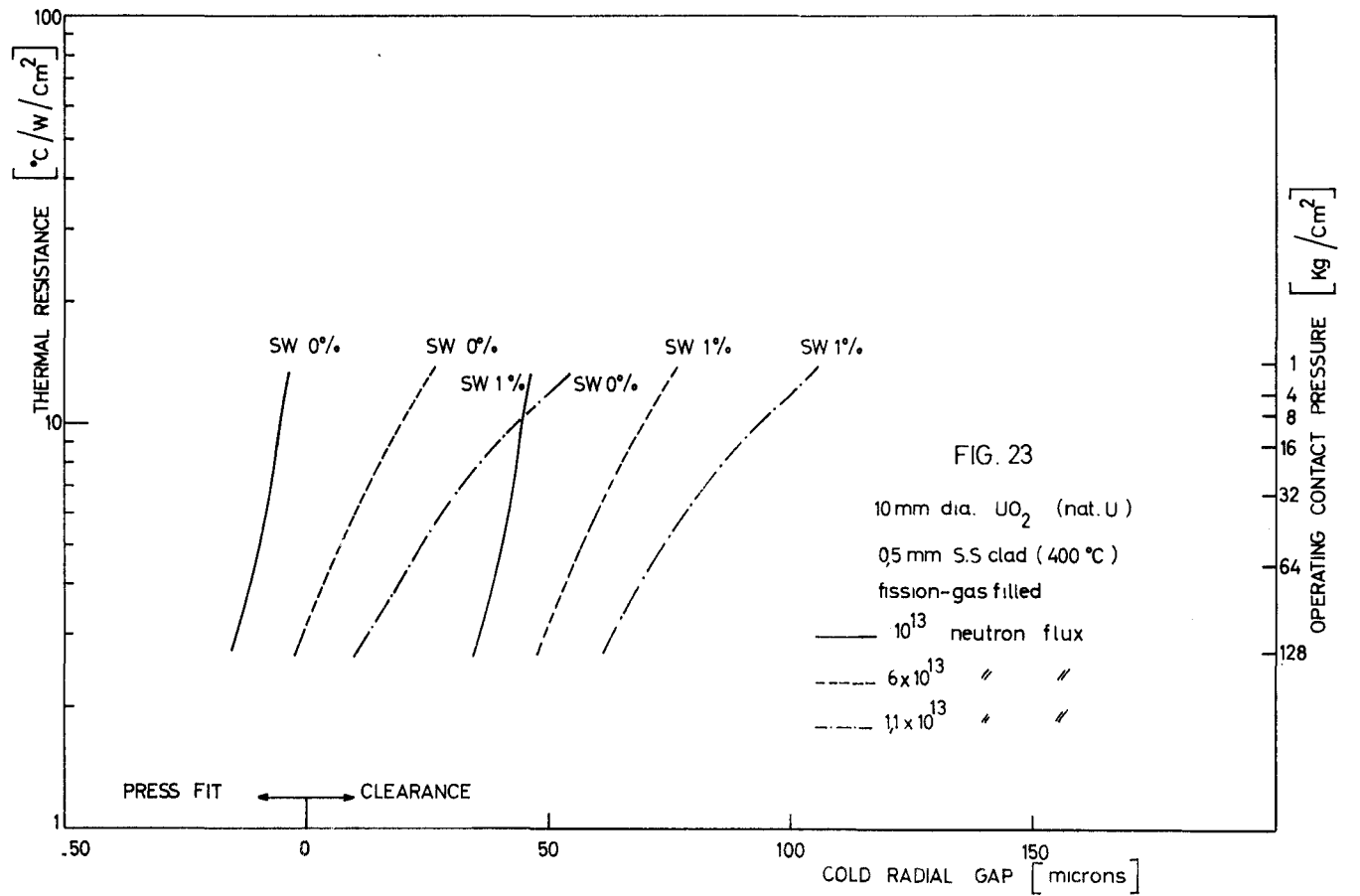
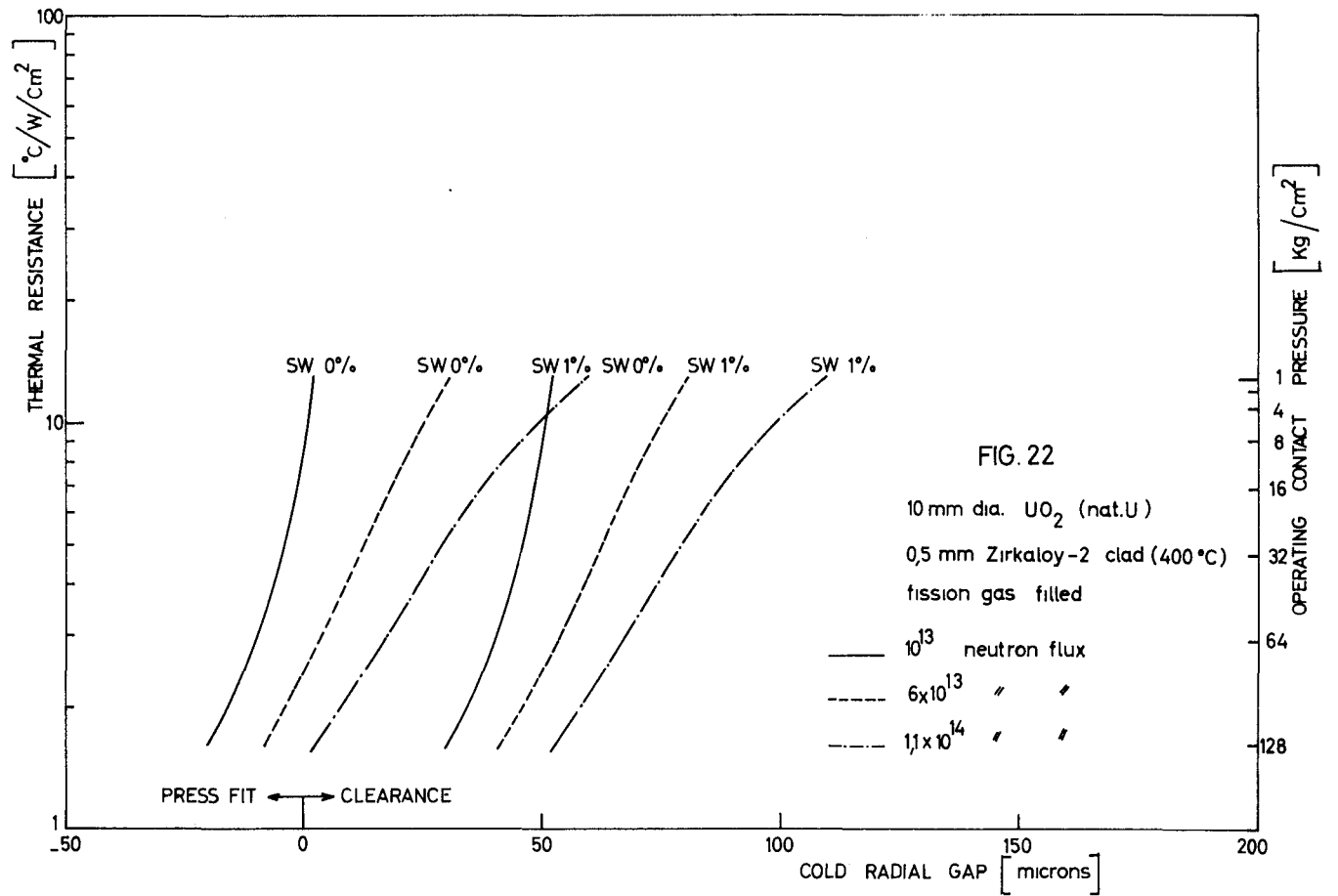
Appendix IV gives the values of the physical constants used in the sample computations and plotted in Fig. (14) to (23). No account has been taken of gamma heating in the fuel and of creep properties of the clad material in such sample computations.











### 5.3. Plastic Clad

Fig. 14 to 23, plotted according to the formulas of chapter 5.2., are reliable only in the range for which relation (34) holds, i.e. as long as the behaviour of the clad can be accounted for by the laws of elasticity.

It is apparent, however that quite often, a contact pressure  $P$  induces a tangential stress in the clad  $\frac{Pxr}{\delta}$  in excess of the elastic limits. In this case one must account for the plastic strain of the clad and modify eq. (37) accordingly.

A plastic deformation of the clad will result in an increase of the inner bore radius and will prevent the contact pressure from increasing beyond certain limits.

The transition from the "elastic" to the "plastic" situation will be controlled by the creep properties of the clad material. We may however study the final thermal situation, which will correspond to a plastically deformed material.

We shall illustrate the above with a concrete case, which will avoid the uncertainty of selecting one or the other description of the strain-stress curves in the plastic state, hardly amenable to generalizations.

With a 7% S.A.P. clad at a temperature of 450°C, it is shown in ref. 11 that the total strain in the plastic region can be approximated by

$$\epsilon = 732 - 752 \exp(-1,120 \epsilon) \quad (38)$$

Subtracting from the total strain the contribution  $\frac{\epsilon}{E_c}$  of the elastic strain, we obtain as a

permanent deformation, with  $\bar{\nu} = Pr_o/t$

$$\epsilon_o = \frac{1}{1,120} \ln \frac{752}{732 - \frac{Pr_o}{t}} - \frac{Pr_o}{t E_c} \quad (39)$$

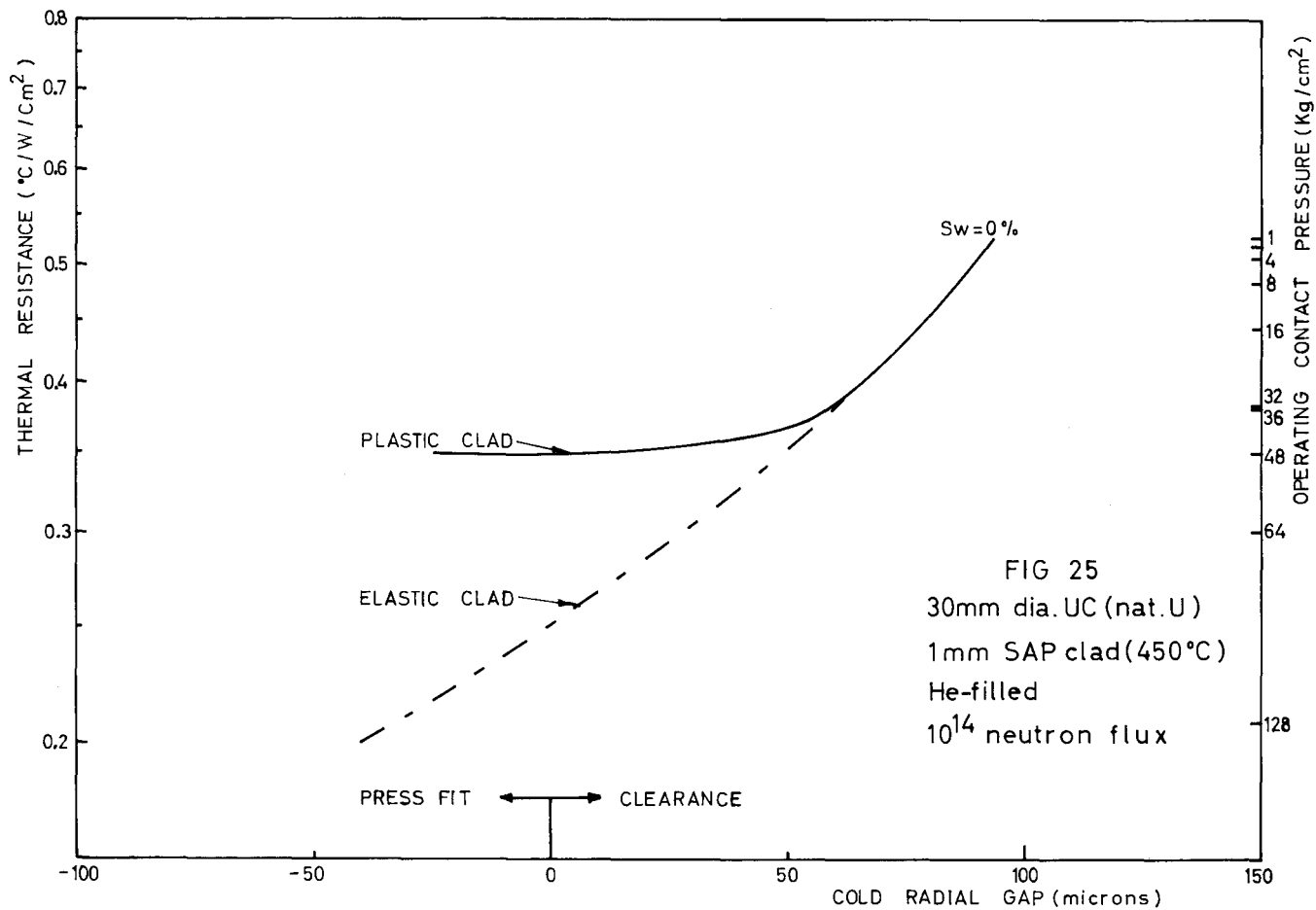
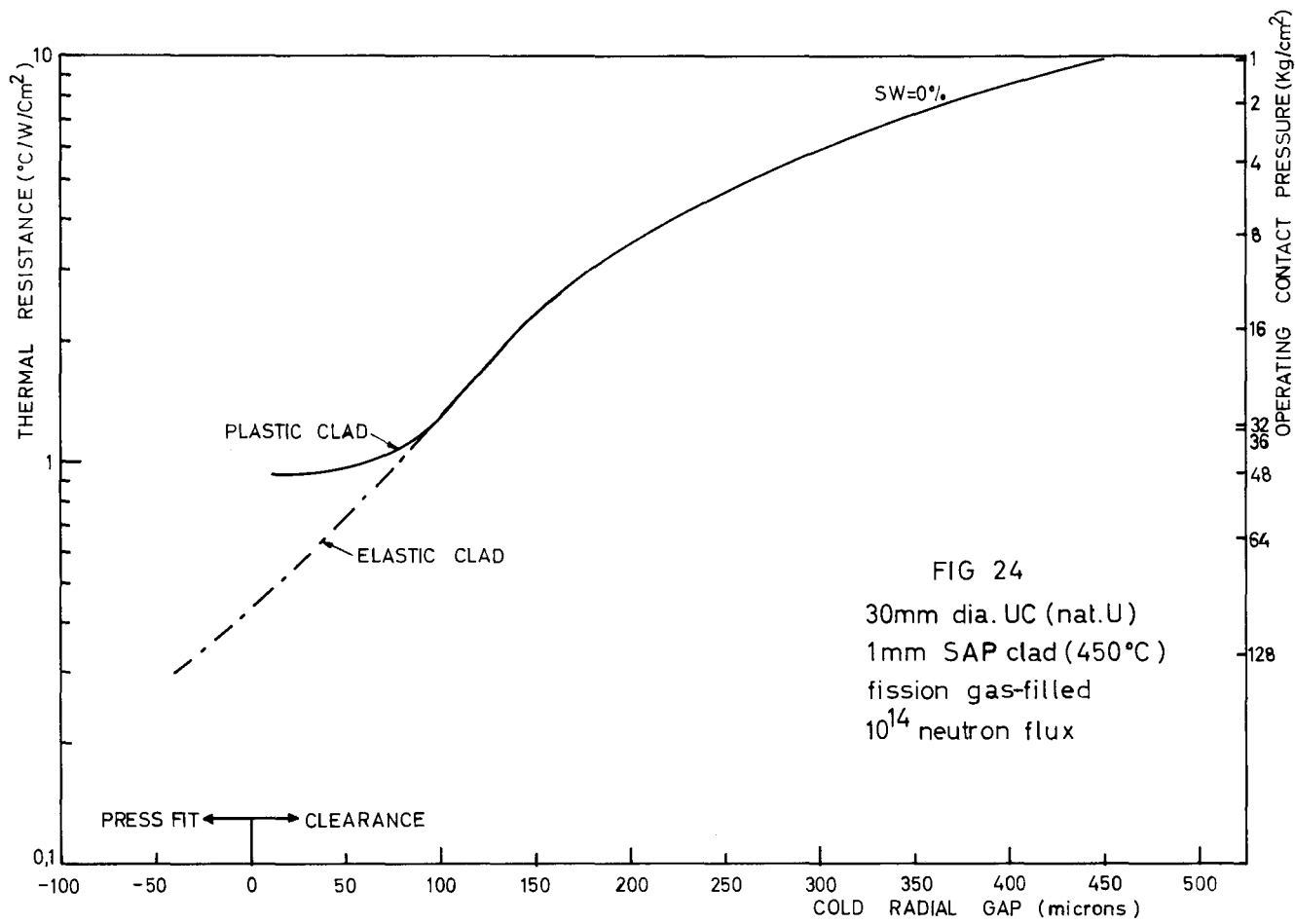
The hot operating gap from eq. (33) must therefore be increased by an amount  $r_o \times \epsilon_o$ , yielding

$$C' = C - sr_o + r_o \left[ \alpha_c (T-20) + \frac{r_o}{t} \frac{P}{E_c} \left(1 - \frac{\nu_c}{2}\right) - \alpha_p (T_s - 20) - \frac{\alpha_p \Delta T_p}{2(1-\nu_p)} + \frac{Pr_o}{E_p} (1-\nu_p) + \frac{1}{1,120} \ln \frac{752}{732 - Pr_o/t} - \frac{Pr_o}{E_c t} \right]$$

which, in combination with (32), (35), (34) and (36) will describe the behaviour of the clad material in the plastic range.

Figs. 24 and 25 show the effect of accounting for the plastic strain of the clad: a small assembly clearance or an interference fit between clad and pellet will eventually lead to a maximum initial operating contact pressure of the order of 50 kg/cm<sup>2</sup> and will prevent the contact resistance from falling below values of 0.95 and 0.35 °C/W/cm<sup>2</sup>, respectively, with fission gases and He in the gaps.

Whereas the values of the thermal resistance in the plastic range are time-independent (left scale of figs. 24 and 25), the operating pressures (right scale) will of course decrease with time, since although the density and area of contact spots may remain the same, the operating pressure will be relieved by the creep of the clad material.



#### 5.4. Out-of-pile experiments

A series of measurements of contact conductance in cylindrical geometry were carried out on metal pellets loosely inserted or shrink fitted into metal clads. A number of metals were chosen for the pellet and the clad, including Aluminium, S.A.P., Armco-iron and Invar, in order to operate with different expansion coefficients.

Surface roughnesses in the range  $R_t=5$  to  $100 \mu\text{m}$  were used and axial heat generation was obtained by means of a W wire. Temperatures of the clad and of two different radial positions in the pellets were monitored.

Tests were made in vacuo, in air and in argon.

Fig. 26 shows a typical test carried out with an SAP pellet 17.86 mm O.D. clad in Invar. Differential thermal expansions were estimated and compared to gaps deduced from temperature discontinuity at the contact gap.

The effect of  $R_t$  on conductance is clearly seen to affect the nominal gap by an amount  $2/3 R_t$ , as previously discussed.

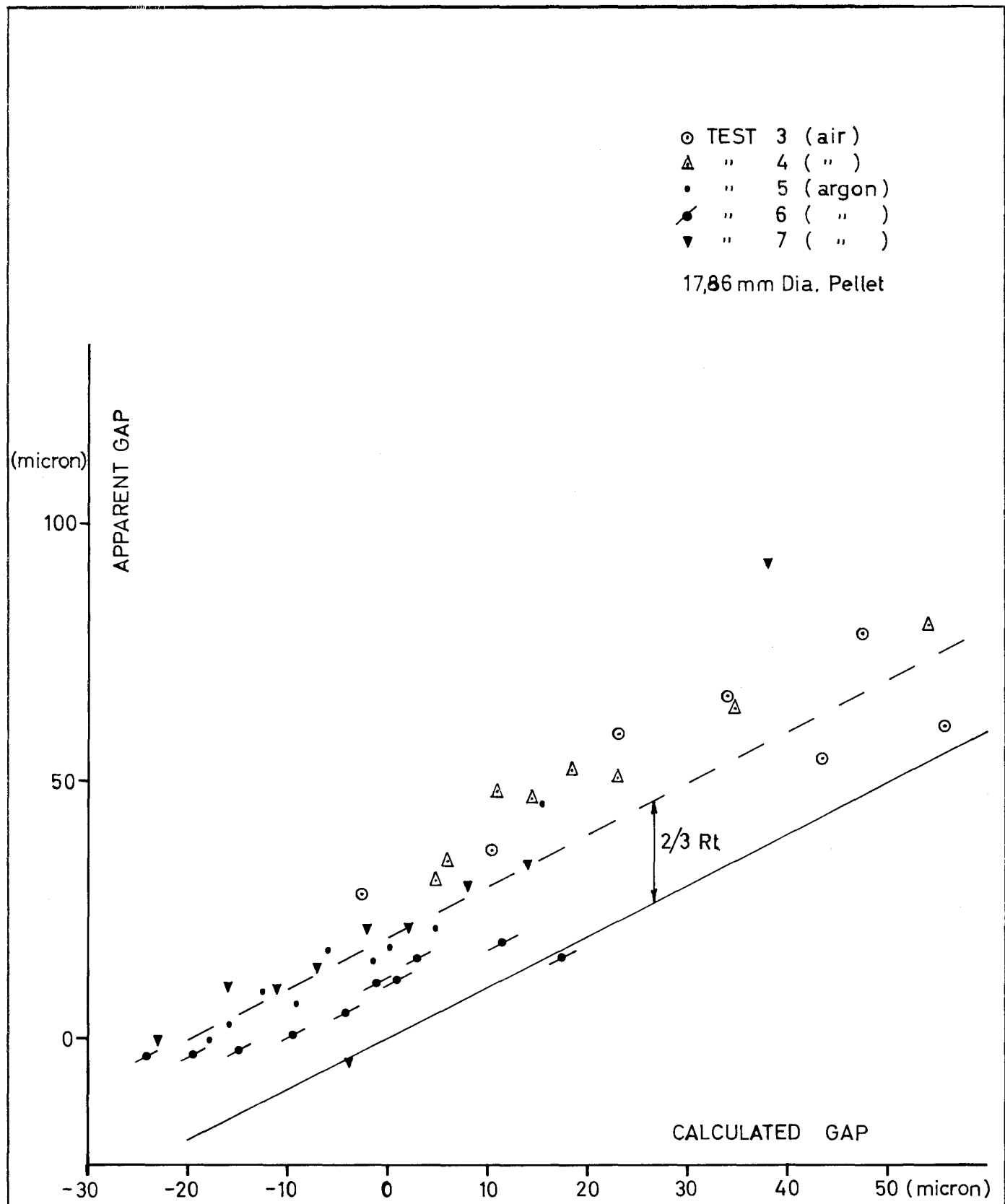


FIG 26

OUT-OF-PILE CYLINDRICAL CONTACT

### 5.5. In-pile experiments

Two rigs were irradiated by the Physical Chemistry Branch of C.C.R. Ispra to measure the fuel-clad contact conductance. Each rig contained three test assemblies made of Uranium Carbide pellets sheathed in sintered aluminium powder (S.A.P.) with a Xenon atmosphere.

The first rig was exposed to a flux of  $4.5 \times 10^{13}$  n/cm<sup>2</sup> sec. maximum (unperturbed) in channel N°9 of the Ispra 1 reactor.

Nominal Cold radial clearances between fuel and sheath were 0.0023, 0.0046, 0.0104 cm in the first three assemblies and 0.0015 cm in the others.

Operating temperature distributions in the fuel and sheath system were measured during irradiation and indicated fuel temperatures lower than theoretically expected.

To reproduce the thermal flux prevailing in an Or-gel reactor, the same rigs were irradiated once again in the central channel at a thermal flux of  $10^{14}$ .

Daily readings of the UC central temperature were plotted as a function of the irradiation time in Figs. 27 and 28.

UC Temperatures dropped some 50, 100, 150 °C in cans A, B, C of rig 1 during the first full power reactor period (about two weeks).

Heat transfer coefficient between sheath and cooling heavy water was assumed to be constant and the neutron flux was therefore assumed to be well enough correlated to the sheath-water temperature drop.

The best fit over several reactor periods gave an expression for the thermal flux (see appendix III)

$$\phi = 0.74 \beta + 0.1 \beta^2$$

Heat generation, temperature distributions and fuel-clad temperature drop were calculated taking into account both the fission heat and the gamma heating.

Gap conductances are given by (App. III)

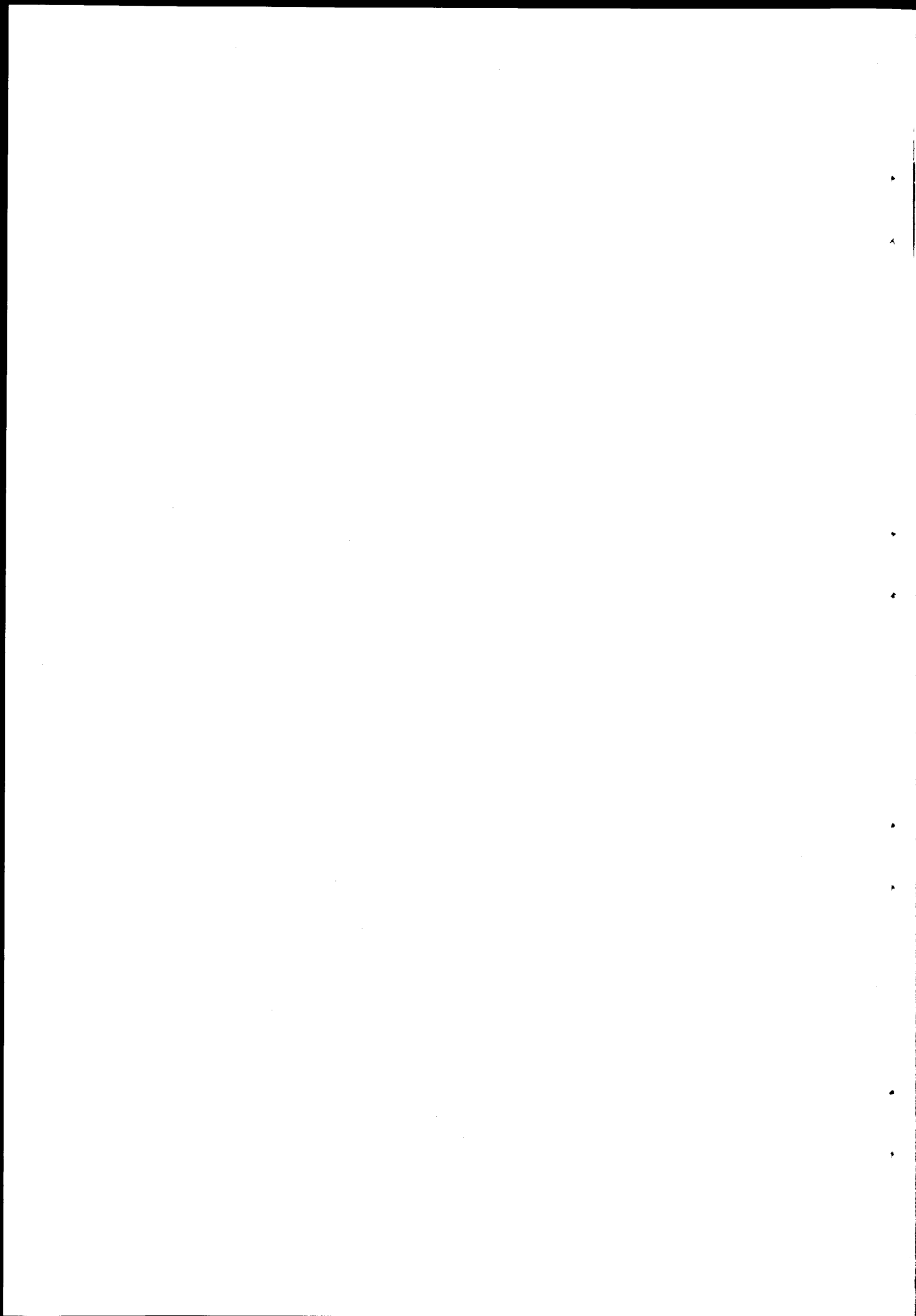
$$U = \frac{F}{\Delta T_1} = \frac{15.5 \phi}{T_c - T - 45.3 \phi}$$

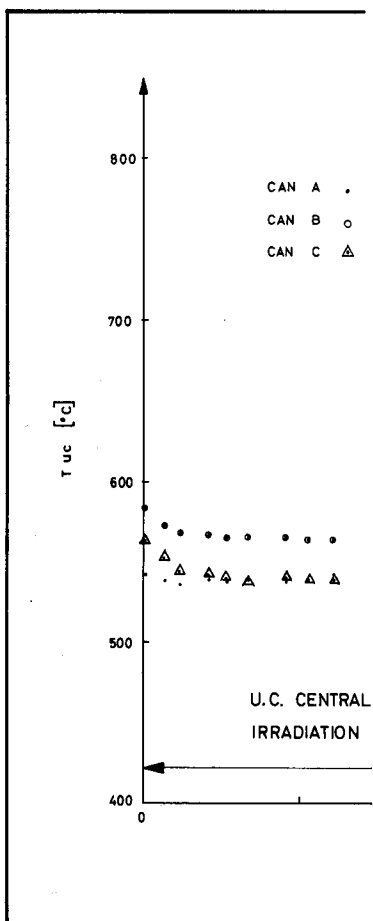
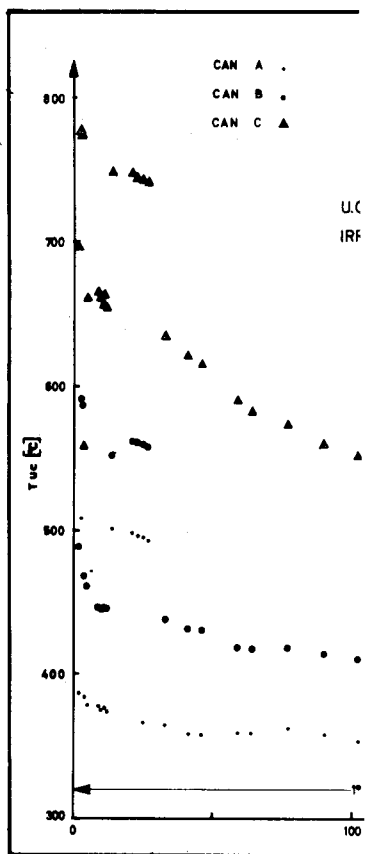
Experimental data are shown plotted in Fig. 29, 29a and 30 as thermal resistance versus irradiation time. It is apparent that the thermal resistance underwent a striking decrease throughout the irradiation.

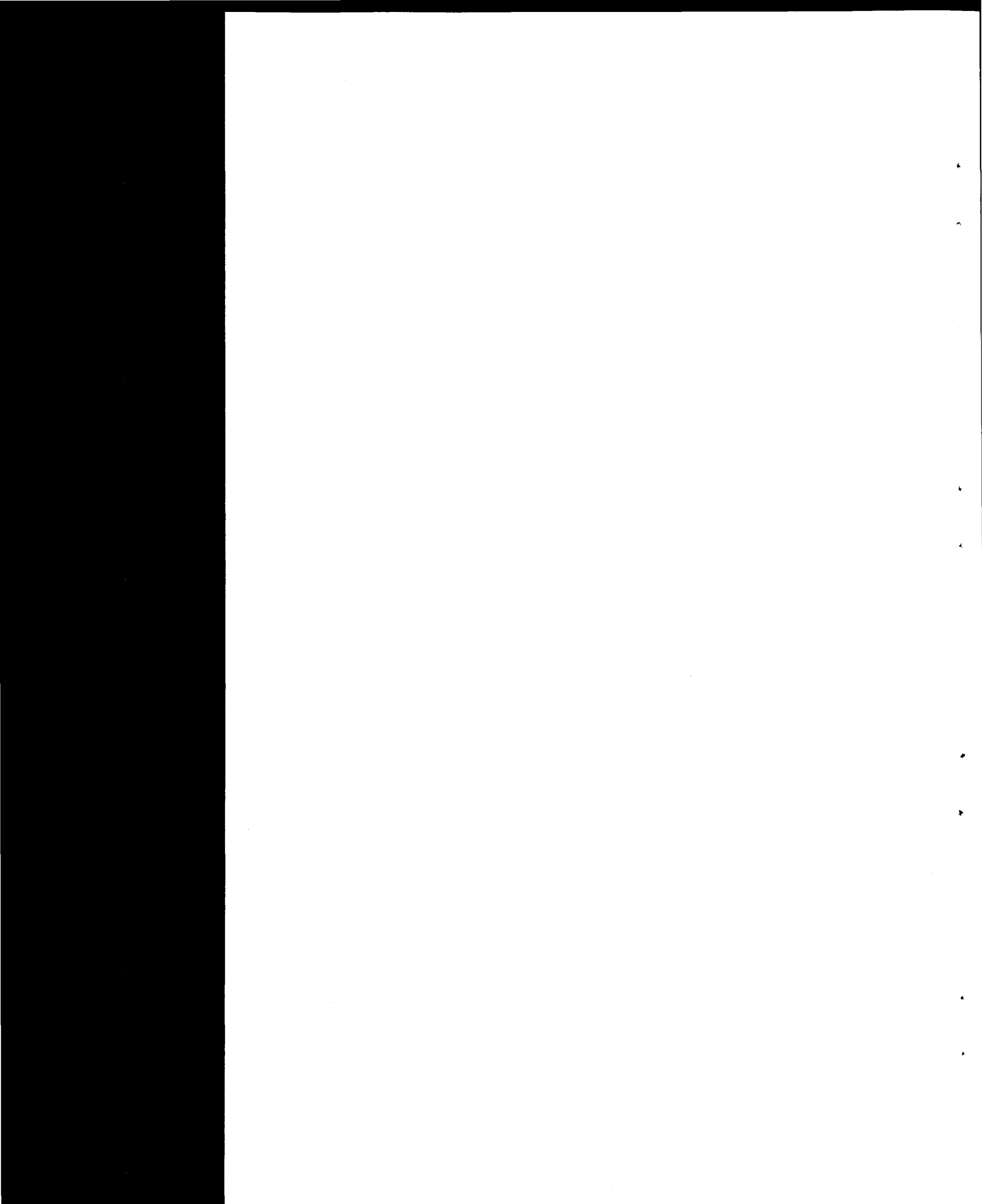
With 0.0023, 0.0046, 0.0104 cm nominal radial gaps in cans A,B,C, of rig N°1 and 0.0015 cm in all three cans of rig. N°2 and since UC and SAP have thermal expansion coefficients of about  $10 \times 10^{-6}/^{\circ}\text{C}$  ref. (13) and  $21.5 \times 10^{-6}/^{\circ}\text{C}$  ref. (14), the operating clearances ought to increase during irradiation.

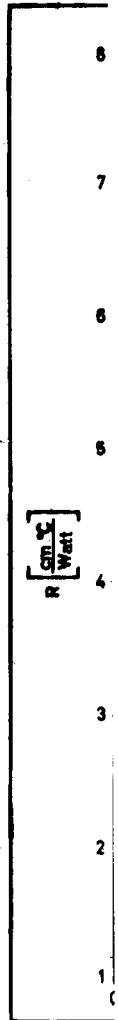
The reasons of the centre temperature decrease can be explained by:

- a) pellet cracks leading to a diametral increase of the pellet,
- b) variation of thermocouple e.m.f. during irradiation,
- c) UC swelling due to fission gases,
- d) chemical transformations in the pellet leading to a "chemical swelling",
- e) creep or rupture of SS container.
- f) Shrinkage of the S.A.P. bore.
- a) Pellet cracks were thought very likely, since examination of the unirradiated pellet stock showed radial cracks caused by relaxation the internal tension generated during cooling after fusion combined with oxidation. A typical picture is shown in Fig. 31.









$R$   
 $\frac{\text{cm}^2 \cdot \text{C}}{\text{Watt}}$

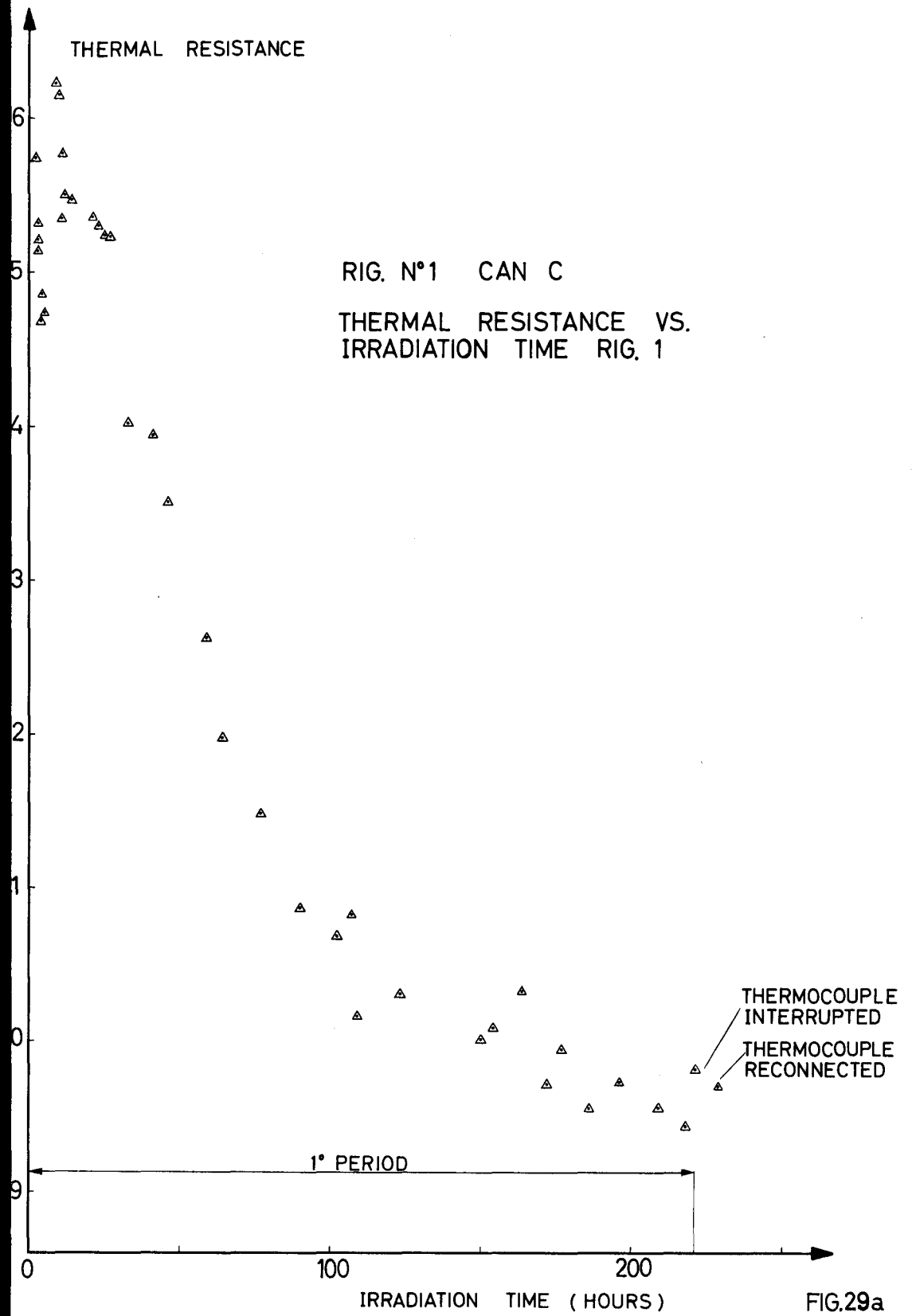


FIG.29a

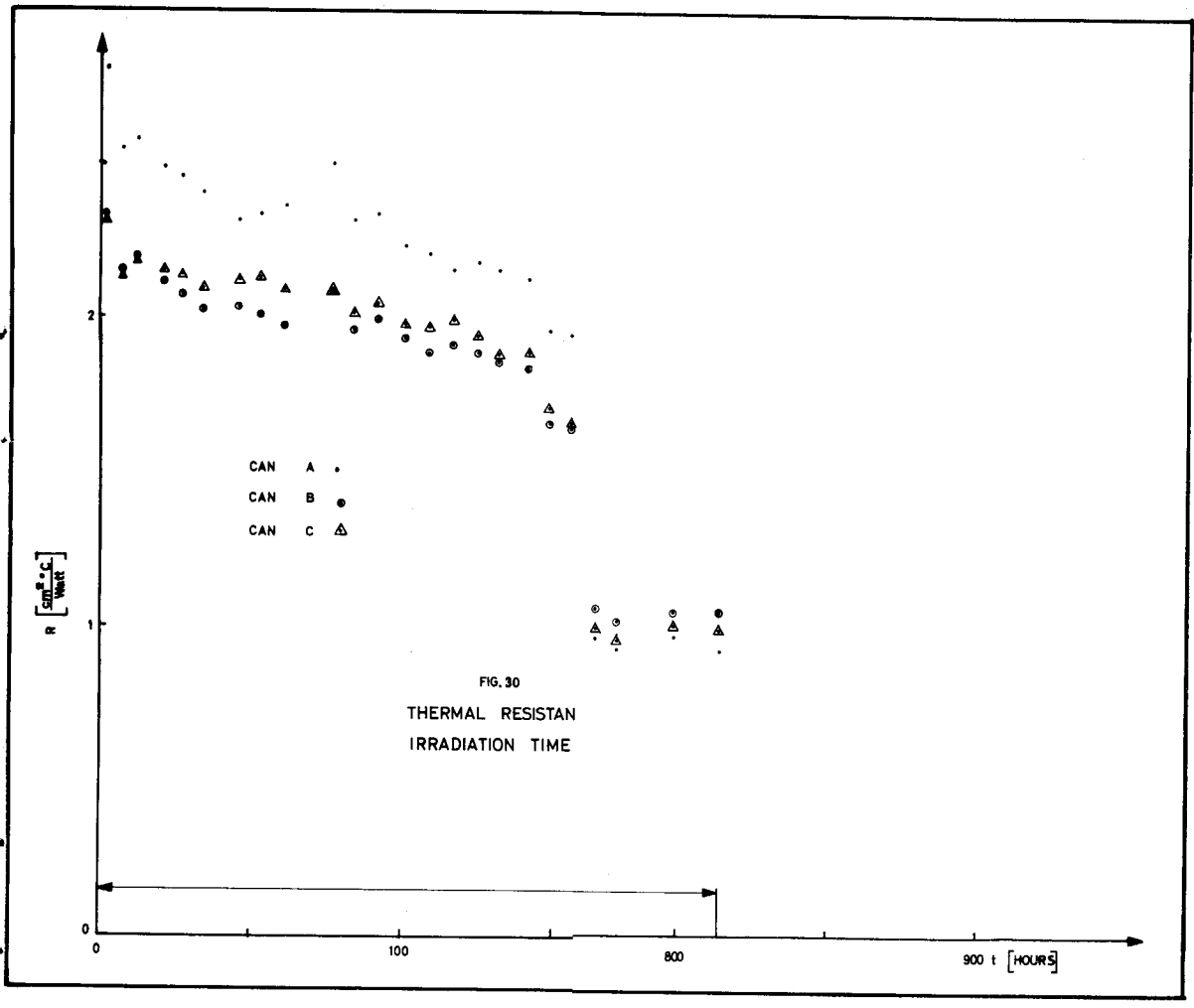




FIG. 31  
PELLET RADIAL CRACKS

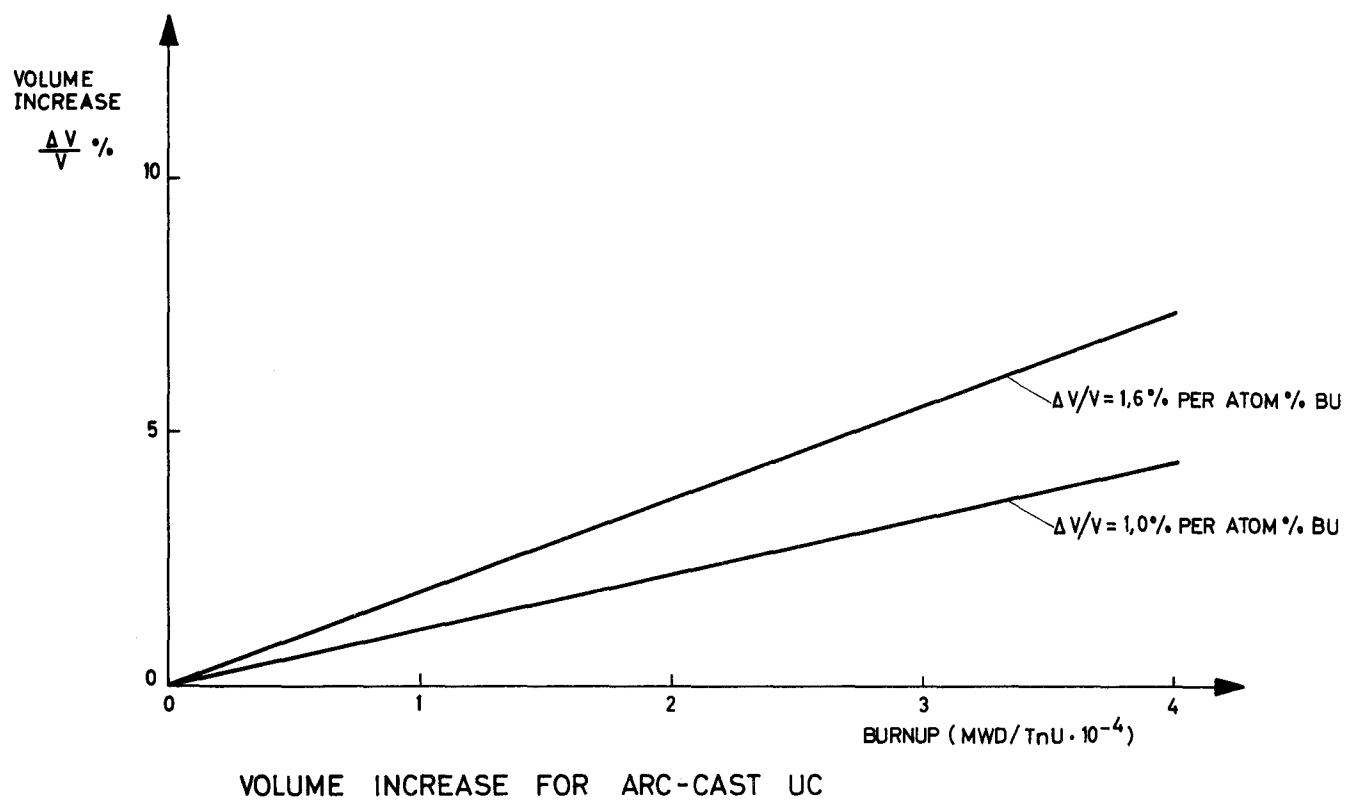


FIG. 32

- b) E.m.f. variations caused by irradiation of Pt-10% RhPt thermocouples to an integrated thermal dose of  $6 \times 10^{19}$  per cycle at approx. 600°C are estimated to be negligible.
- c) Swelling of the UC pellet due to fission gases was unlikely since the operating temperatures and the burnups were too low to have any appreciable effect. Rough Ref. (19) estimated a volume increase from solid fission products for UC of 1.0 to 1.6% per atom% burnup (1 atom% of U burnup is equivalent to 9400 MWD/Ton U) and from Fig. 32 which is plotted for reference, he concluded that swelling is caused by the cumulation of solid fission products if temperatures are lower than 800°C and burnups smaller than 25,000 MWD/Ton U. In our case the temperatures were lower than 800°C and burnups were 580 MWD/Ton U for Rig N° 2 and 725 MWD/Ton U for Rig. N°1. From Fig. 32 the volume increase of UC pellet was estimated to be of the order of 1 to 2%. Therefore swelling due to fission products is negligible.
- d) Presence of a different gas in the initial Xenon charge could have occurred if some Helium infiltrated into the capsules through cracks in the welds. In this case the conductivity of the gas in the gap would gradually increase and the UC pellet temperature decrease. The possibility of gas release from the SAP clad was rejected because temperatures were too low (150°-200°C). However, the possibility remains of an oxidation of UC to  $UO_2$  due to water or oxygen released from the MgO pellets. Interaction of UC and  $UO_2$  during irradiation may have led to a formation of free U and liberation of CO with subsequent swelling.
- e) Creep of the SS capsules at a temperature of approx. 50°C could not occur.
- f) Some shrinkage of the S.A.P. bore by stress relieving under the combined effect of the temperature and radiation could occur.

### 5.6. Post-irradiation examination

The two irradiation rigs were dismantled after a 1- year decay in the hot-cell of the Ispra-1 reactor with the help of the hot-cell operators.

Scope of the examination was:

- 1 - A check on the pellet and the bore diameters to estimate the amount of swelling or creep, if any.
- 2 - A check on the flux by  $\gamma$  activation measurements. The outer appearance of the UC-SAP assemblies in their cans showed no obvious deformation or cracks in the cans. It was impossible to locate the cobalt flux monitors. Therefore a sampling was made of
  - Two S.S. fillings for each can (S.S. contained .026% Co) which were  $\gamma$  counted (fig.33).
  - A few fragments of the UC pellets were thoroughly examined by M. Bresesti of the Nuclear Chemistry service to determine burnups.

The latter examinations yielded beside the shape of the thermal neutron flux (Figs 34, 35 and 36) also the maximum actual value it attained in rig. n° 1 ( $5.29 \times 10^{13}$ ) and n° 2 ( $5.05 \times 10^{13}$ ).

It was shown that during the irradiations a continuous increase of the fission heat generation was due to Pu formation (11% and 7% contribution of Pu, respectively, for rig n° 1 and 2).

Fig. 37, which shows the flux as estimated from temperature indications checks with the above results, and shows a flux increase 20 to 25% at the end of irradiation.

The UC pellets were extracted from their S.A.P. clad by heating the assembly to 300-350°C. The differential thermal expansion of S.A.P. and UC allowed this extraction with no difficulty in most cases. A slight pressure was exerted on the pellet by means of a vacuum-controlled piston extractor. The irradiated pellet diameters were measured in the hot-cell itself by means of a microgauge giving a precision of  $\pm 1 \mu\text{m}$ . The S.A.P. bores were also measured in a plain glove box. The results of these measurements are:

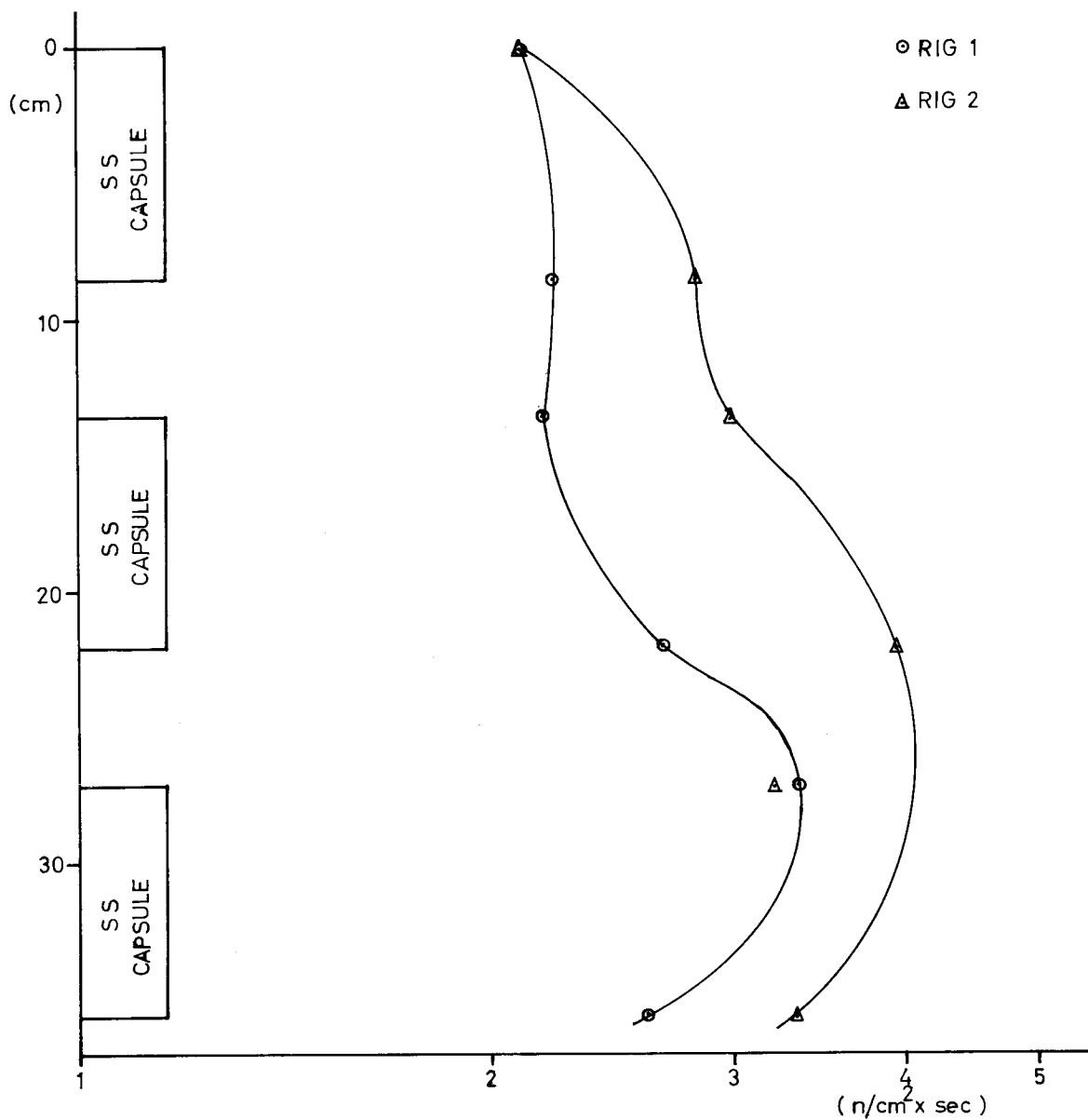


FIG 33

Co-60 ACTIVITIES MEASURED IN S.S. CAPSULES  
 FROM RIG 1 AND RIG 2

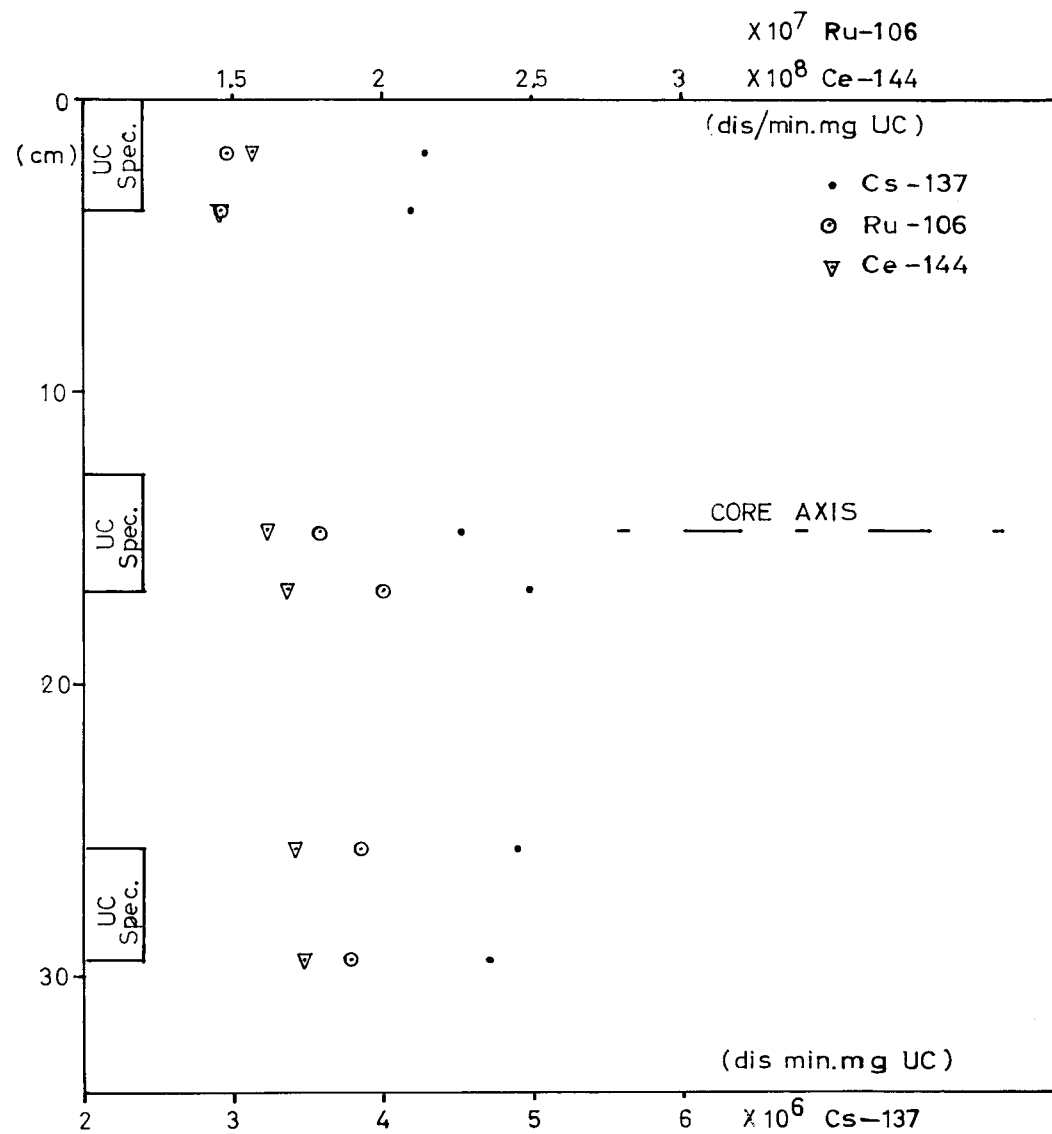


FIG 34

Ru 106, Cs 137, Ce 144 ACTIVITIES MEASURED IN  
 SAMPLES FROM RIG 1

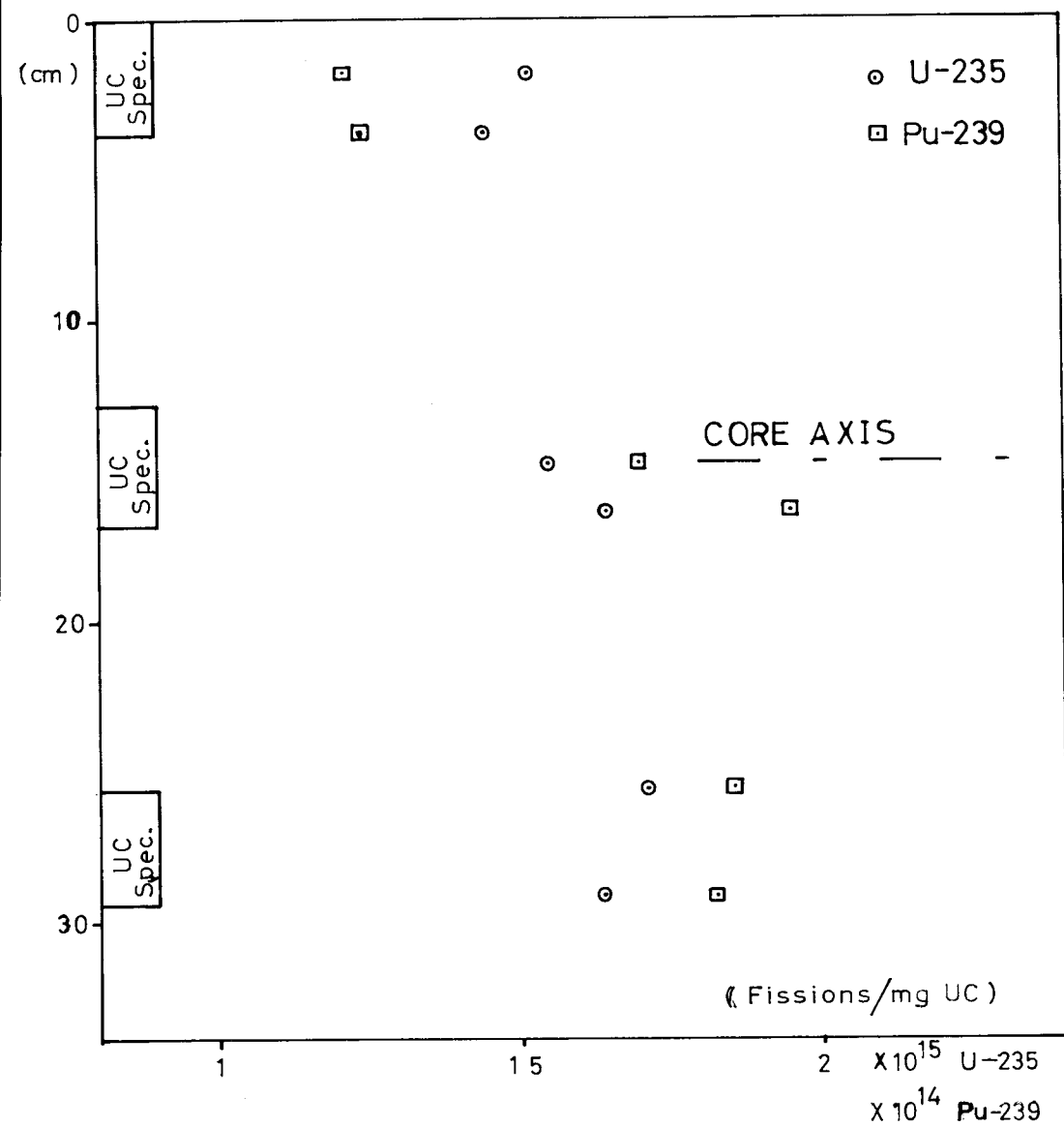


FIG 35

U-235 AND Pu-239 FISSIONS MEASURED IN  
SAMPLES FROM RIG 1

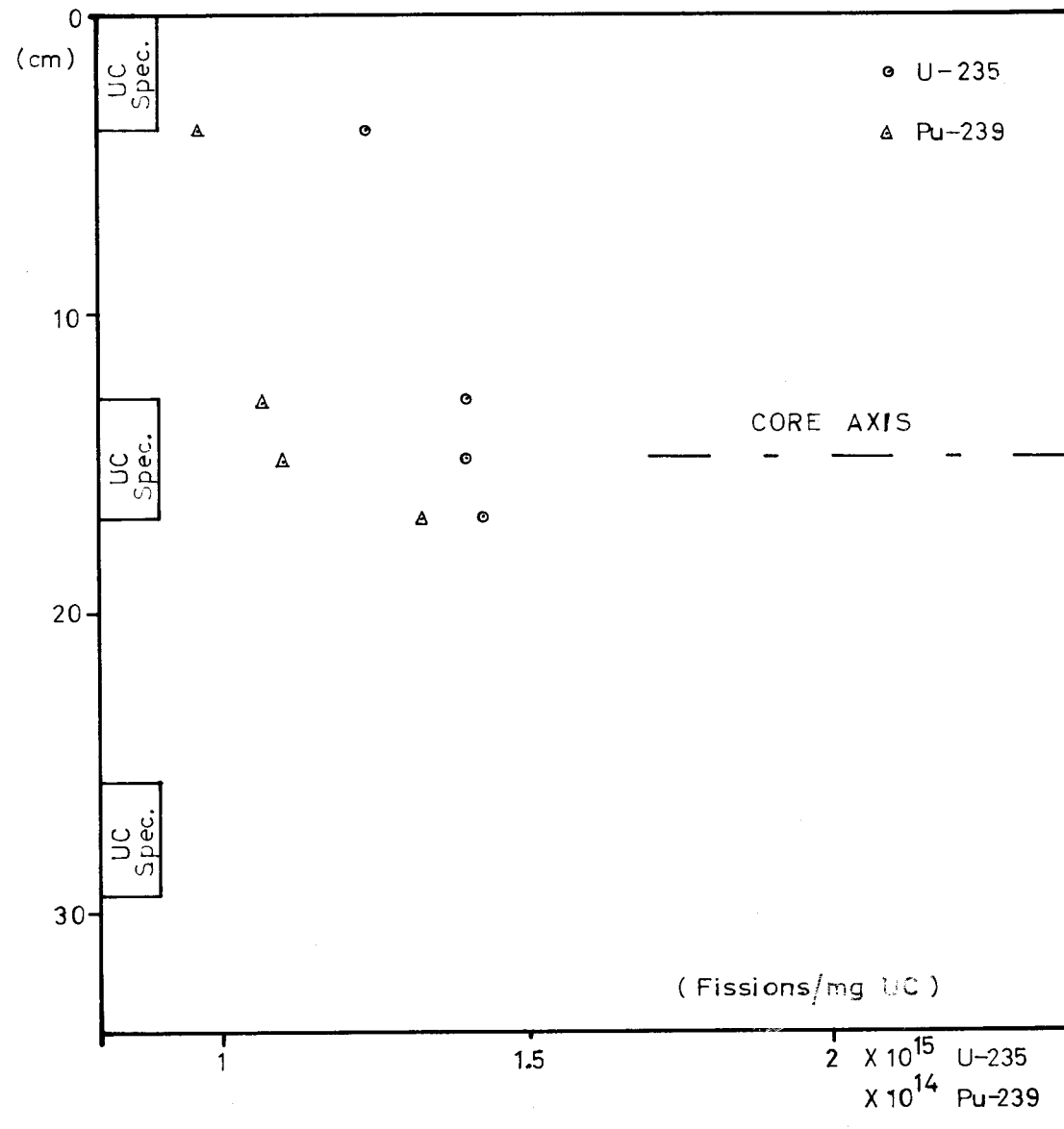
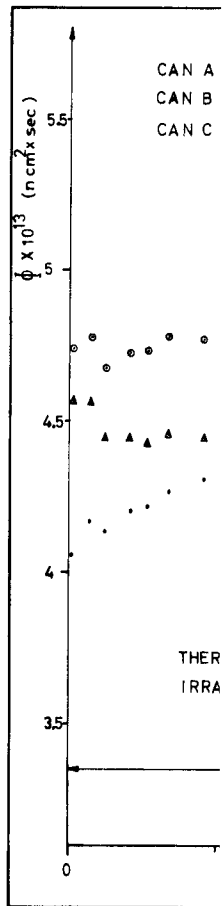
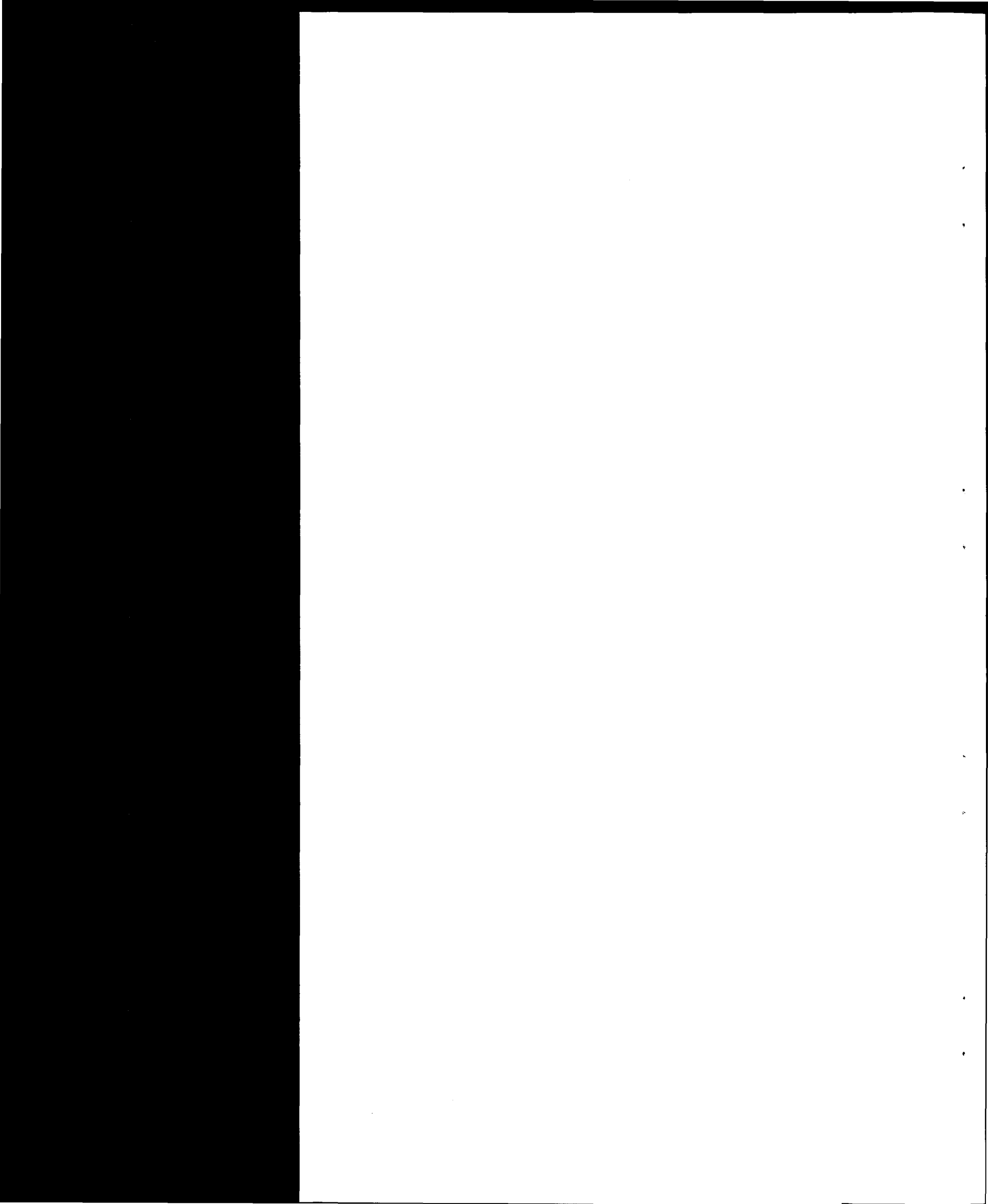


FIG 36

U-235 AND Pu-239 FISSIONS MEASURED IN  
SAMPLES FROM RIG 2





RIG. 1

Nominal (pre-irradiation) measurements

|       | Pellet<br>n° | Max.Diam.<br>cm. | Min.Diam.<br>cm. | Mean Diam.<br>cm. | Mean Bore<br>Diam.cm. | Diametral<br>Clearance<br>cm. |
|-------|--------------|------------------|------------------|-------------------|-----------------------|-------------------------------|
| Can A | 1            | 1.905508         | 1.904797         |                   |                       |                               |
|       |              |                  |                  | 1.905336          | 1.909953              | 0.004622                      |
| Can B | 2            | 1.905635         | 1.905406         |                   |                       |                               |
|       |              |                  |                  | 1.905616          | 1.914842              | 0.009206                      |
| Can C | 3            | 1.906016         | 1.905127         |                   |                       |                               |
|       |              |                  |                  | 1.906092          | 1.926907              | 0.020814                      |
|       | 4            | 1.906168         | 1.905154         |                   |                       |                               |
|       | 5            | 1.906524         | 1.905863         |                   |                       |                               |
|       | 6            | 1.906168         | 1.905813         |                   |                       |                               |

Post-irradiation measurements

|       |   |        |         |                             |         |         |
|-------|---|--------|---------|-----------------------------|---------|---------|
| Can A | 1 |        |         |                             |         |         |
|       | 2 |        | CRACKED |                             |         |         |
| Can B | 3 | 1.9180 | 1.9104  |                             |         |         |
|       |   |        |         | 1.9135 <sup>±</sup> 0.0017  | 1.9103  | -0.0032 |
| Can C | 4 | 1.9159 | 1.9106  |                             |         |         |
|       |   |        |         | 1.91878 <sup>±</sup> 0.0036 | 1.92306 | 0.00428 |
|       | 5 | 1.9339 | 1.9102  |                             |         |         |
|       | 6 | 1.9273 | 1.9186  |                             |         |         |

Swelling of UC was

|       | Diametral<br>Swelling cm.  | Swelling<br>%/° | Max.Irrad.<br>Temperature °C | Burnup<br>MWD/ton U |
|-------|----------------------------|-----------------|------------------------------|---------------------|
| Can B | 0.0079 <sup>±</sup> 0.0017 | 0.415           | 650                          | 725                 |
| Can C | 0.0127 <sup>±</sup> 0.0036 | 0.668           | 800                          | 725                 |

RIG. 2

Nominal (pre-irradiation) measurements

|       | Pellet<br>n° | Max.Diam.<br>cm. | Min.Diam.<br>cm. | Mean Diam.<br>cm. | Mean Bore<br>Diam.<br>cm. | Diametral<br>Clearance<br>cm. |
|-------|--------------|------------------|------------------|-------------------|---------------------------|-------------------------------|
| Can A | 7            | 1.907667         | 1.906778         |                   |                           |                               |
|       |              |                  |                  | 1.906735          | 1.909673                  | 0.002946                      |
|       | 8            | 1.906778         | 1.905711         |                   |                           |                               |
| Can B | 9            | 1.906270         | 1.905609         |                   |                           |                               |
|       |              |                  |                  | 1.906251          | 1.909445                  | 0.003200                      |
|       | 10           | 1.906727         | 1.906397         |                   |                           |                               |
| Can C | 11           | 1.905762         | 1.905508         |                   |                           |                               |
|       | 12           | 1.905127         | 1.904695         | 1.905478          | 1.908454                  | 0.003072                      |
|       | 13           | 1.906016         | 1.905762         |                   |                           |                               |

Post-irradiation measurements

|       |                       |        |        |          |         |          |
|-------|-----------------------|--------|--------|----------|---------|----------|
| Can A | CRACKED               |        |        |          |         |          |
| Can B | 9                     | 1.9248 | 1.9123 |          |         |          |
|       |                       |        |        | 1.917565 | 1.90493 | -0.01263 |
|       | 10                    | 1.9302 | 1.9143 |          |         |          |
| Can C | IMPOSSIBLE TO EXTRACT |        |        |          |         |          |

Swelling of UC was:

|       | Diametral<br>Swelling<br>cm | Swelling<br>% | Max. Irrad.<br>Temperature<br>°C | Burnup<br>MWD/ton U |
|-------|-----------------------------|---------------|----------------------------------|---------------------|
| Can B | 0.0113 <sup>±</sup> 0.0040  | 0.58          | 580                              | 580                 |

A remarkable swelling had taken place. It is very likely that this swelling was due to oxidation during heating for pellet extraction.

S.A.P. bores decreased by 45  $\mu\text{m}$  for can B, 38  $\mu\text{m}$  for can C of rig n°1 and 45  $\mu\text{m}$  of can B of rig 2. Outer diameter of the clad showed decreases of the order of 5  $\mu\text{m}$ . It is however believed that a permanent strain of the S.A.P. could have occurred by stress-relieving even though temperature never exceeded 400°C.

Analysis of the results of the irradiations point out to a few discrepancies:

- 1 - Contact conductance values were too high on the basis of the nominal cold gaps.
- 2 - A sudden increase of conductance was seen when shifting rig n°1 from channel n°9 to the central channel.
- 3 - Contact conductance seemed to increase with time during irradiation.

On the light of the post-irradiation examination, the Causes for the above discrepancies are thought to be:

- 1 - Cold assembly gaps were smaller than specified.
- 2 - The sudden increase of conductance was due to the pellet cracks and bore decrease by stress relaxation.
- 3 - Increase of conductance during irradiation is due to enhanced fission heat generation because of Pu buildup. A more detailed analysis follows:

#### Rig n° 2

Gas conductance was

$$U_{\text{gas}} = Kf/2/3 \sum R_t = 0.1 \text{ W/cm}^2 \times \text{°C}$$

Initial value or  $u_{\text{Tot}}$  is about 0.4  $\text{W/cm}^2 \text{°C}$  (see fig. 30)

Therefore  $U_{\text{natal}} = 0.3 \text{ W/cm}^2 \times \text{°C}$

Using formula 8.5 of ref. 11 with a constriction alleviation factor  $2/\pi$

$$U_{\text{Metal}} = \frac{.434 K}{R_t} \cdot \frac{2}{\pi} \cdot \left(\frac{P}{H}\right) \cdot .9125$$

With  $T_{\text{SAP}} = 200 \text{ }^\circ\text{C}$      $K = .276 \text{ W/cm}^\circ\text{C}$      $R_t = 15 \times 10^{-4} \text{ cm}$   
 $H = 4,700 \text{ kg/cm}^2$      $U_{\text{metal}} = 2.29 \times 10^{-2} P \cdot .9125$

and the contact pressure must have been in the neighborhood of  $1.4 \text{ Kg/cm}^2$ . This low value of the contact pressure shows that the hot gap was closed without an appreciable amount of interference.

Initial clearance (see appendix III) was

$$G_o = G_1 - 1.89 \times 10^{-5} T + 3.4 \times 10^{-4} - 3.02 \times 10^{-4} \phi + 9.53 \times 10^{-6} T_c$$

and with  $T = 200 \text{ }^\circ\text{C}$      $\phi = 5$      $T_c = 550 \text{ }^\circ\text{C}$      $G_o = 3 \mu\text{m}$

The S.A.P. bore must have had a diameter given by:  
 pellet dia + assembly clearance i.e.

$$1.90625 + .0006 \text{ cm} = 1.90685 \text{ cm}$$

which checks with the post-irradiation determination of the S.A.P. bore diameter ( $1.90493 \text{ cm}$ ).

At the end of the irradiation,  $u_{\text{tot}}$  was about  $1 \text{ W/cm}^2\text{C}$ , corresponding to a contact pressure of about  $3.4 \text{ Kg/cm}^2$ . Interference fit must have been about  $0.12 \mu\text{m}$  and therefore  $G_o$  is again estimated at  $3 \mu\text{m}$ .

Rig n° 1

Gas conductance is again  $0.1 \text{ W/cm}^2\text{C}$ . Conductance data at the beginning of irradiation are (see fig. 29 and 29a)

|              | <u>U<sub>total</sub></u> | <u>U<sub>metal</sub></u> |
|--------------|--------------------------|--------------------------|
| <u>can A</u> | 0.172                    | 0.07                     |
| <u>can B</u> | 0.149                    | 0.05                     |
| <u>can C</u> | 0.0625                   | -                        |

Cans A and B had therefore contact without interference fit at operating conditions.

Estimating  $G_o$  as before, with  $\bar{T} = 125 \text{ }^\circ\text{C}$ ,  $\phi = 2 \times 10^{13}$ ,  $T_c = 390^\circ\text{C}$  in can A and  $490^\circ$  in can C we obtain

$$G_o \text{ can A} = 11 \mu\text{m}$$

$$G_o \text{ can B} = 20.5 \mu\text{m}$$

whereas for can C the apparent hot gap was:

$$K_{\text{gas}}/U_{\text{total}} = 17.6 \mu\text{m}$$

The portion of gap due to the effect of surface roughness ( $\frac{2}{3} \sum R_t$ ) was  $10 \mu\text{m}$ . Then, The actual radial hot clearance was  $7.6 \mu\text{m}$ .

With  $\bar{T} = 125 \text{ }^\circ\text{C}$ ,  $\phi = 2$ ,  $T_c = 700 \text{ }^\circ\text{C}$  we estimate

$$G_o \text{ can C} = 48 \mu\text{m}$$

At the end of the irradiation, thermal data were:

|              | <u>U<sub>total</sub></u> | <u>U<sub>metal</sub></u> |
|--------------|--------------------------|--------------------------|
| <u>Can A</u> | 0.25                     | 0.15                     |
| <u>Can B</u> | 0.20                     | 0.10                     |
| <u>Can C</u> | 0.105                    | -                        |

which show that the cold gap in cas A and B went practically unchanged whereas the cold gap in can C is estimated to be  $40 \mu\text{m}$ , with a decrease of abt.  $8 \mu\text{m}$ .

When using in our formulas the derived above, observed conductances during irradiation check quite well with those that were actually observed.

References

- 1) R. Holm - Electrical contacts  
Almquist and Wiksells, Stockholm 1946
- 2) T.N. Cetinkale and M.Fishenden - Thermal conductance of Metal Surfaces in Contact.  
International Conference on Heat Transfer, I.M.E. London 1951
- 3) F.P. Bowden and T. Tabor - The friction and lubrication of solids.  
Oxford at the Clarendon Press, 1954.
- 4) L.C. Laming - Thermal conductance of Machined Metal Contacts. 1961 International Heat Transfer Conference, University of Colorado.
- 5) L.C. Roess - Theory of spreading conductance, an Appendix to : N.D. Weills and E.A. Ryder.- Thermal resistance measurements of joints formed between stationary metal surfaces.  
Trans. A.S.M.E., 1949
- 6) A.M. Ross and R.L. Stoute - Heat Transfer Coefficient between  $UO_2$  and Zircaloy-2.  
CRFD-1075, 1962
- 7) F. Boeschoten and E.F.M. Van der Held - The Thermal Conductance of Contacts between Aluminium and other Metals.  
Physica XXIII, 1957.
- 8) A. Ascoli and E. Germagnoli - On the Thermal Resistance between Metal Surfaces in Contact.  
Energia Nucleare, 3, 1956.
- 9) H. Fenech and W.M. Rohsenow - Thermal Conductance of Metallic Surfaces in Contact.  
A.E.C. Report NYO-2136.

- 10) I.V. Kragel'skii and N.B. Demkin - Determination of the true Contact Area.  
Friction and wear in machinery, 14, 1960.
- 11) S. Giuliani and C. Mustacchi - Thermal and Mechanical Studies of Solid-Solid Contacts.  
EUR 2486.e(1965)
- 12) S. Giuliani and C. Mustacchi - Heat Transfer in a Fuel Element Gas Gap.  
EUR 521.e (1964)
- 13) UC data sheet.  
Nuclear Engineering (August 1960)
- 14) High Duty alloys Ltd. (private communication)
- 15) C.A. Parsons (private communication)
- 16) S. Giuliani (private communication)
- 17) Stiel and Thodos - Research on Thermodynamic and Transport Properties - pag. 359 - A.S.M.E.  
Academic Press - 1962
- 18) Vickers-Armstrongs Ltd. (private communication)
- 19) F.A. Rough - Effects of Irradiation upon Uranium Carbide.  
BMI-1441(1960)
- 20) G.A.Cook - Argon, Helium and the rare gases.  
Interscience Publishers - 1961
- 21) R.J. Roark - Formulas for Stress and Strain  
McGraw-Hill Book Company, Inc., 1954.

## Appendix I

### Measurement of S.A.P. hardness

Hardness is generally understood as the resistance of a body to plastic deformation under a pressure applied to a portion of its surface.

The deformation which determines the load bearing area (sum of all small contact areas), is however, elastic up to certain pressure limits. Hardness will therefore be barely definable as the average pressure in a ball indentation test.

It would be incorrect to assume a definite upper pressure limit for the elastic deformation, beyond which plastic yielding takes place, because the cause of deformation is a non-isotropic stress and not a hydrostatic pressure.

The average pressure for plastic flow to start will depend on the initial shape of the contacting surfaces of the two bodies.

Materials in contact will be deformed both elastically and plastically since the local pressure will vary from point to point, generating elastic deformations in some regions and plastic deformation in others.

A relation has been shown to exist between hardness  $H$  and yield strength  $Y$

$$H = 3 Y \text{ to } 4 Y$$

However, this relation is valid when all the contact region has yielded plastically. Up to  $p = 1.1 Y$  the Hertz law can be assumed to hold (elastic region) and for

$$1.1 Y < p < 3 Y$$

some interpolated pressure-deformation law can be used to predict the deformed area (Ref.3).

Vickers microhardness tests were used in our investigation, using a projection microscope tester having a pyramid diamond indenter. Identations were made with loads of 25, 50, 100, 200, 300 and 500 grams, at various temperatures between 21 and 330°C for S.A.P. (4% and 7% Al<sub>2</sub>O<sub>3</sub>). Vickers hardness was given by the expression

$$H = \frac{1,854 P}{d^2}$$

where

P is the test weight (grams)

d is the diagonal length of the pyramidal indentation (microns)

and was plotted in fig. 38 and 39 as a function of the temperatures. Experimental measurements are tabulated below.

S.A.P. 4 ½

| Test weights (gm)               | 25    | 50    | 100   | 200    | 300    | 500    |
|---------------------------------|-------|-------|-------|--------|--------|--------|
| Temperature 25°C                |       |       |       |        |        |        |
| Diagonal length d(μ)            | 24.6  | 35.1  | 49.6  | 69.2   | 86.27  | 115.4  |
| Hardness H(kg/cm <sup>2</sup> ) | 7080  | 7510  | 7550  | 7750   | 7470   | 6950   |
| 147°C                           |       |       |       |        |        |        |
| d                               | 32.17 | 44.7  | 61.42 | 86.44  | 106.35 | 137.1  |
| H                               | 4475  | 4635  | 4925  | 4970   | 4900   | 4940   |
| 191°C                           |       |       |       |        |        |        |
| d                               | 33.28 | 47.22 | 64.90 | 91.77  | 110.75 | 144.57 |
| H                               | 4170  | 4160  | 4400  | 4410   | 4540   | 4440   |
| 203°C                           |       |       |       |        |        |        |
| d                               | 34.60 | 49.47 | 65.52 | 94.50  | 117.20 | 151.35 |
| H                               | 3865  | 3785  | 4330  | 4140   | 3770   | 4050   |
| 259°C                           |       |       |       |        |        |        |
| d                               | 35.60 | 51.72 | 70.87 | 98.95  | 127.55 | 161.57 |
| H                               | 3645  | 3470  | 3690  | 3795   | 3425   | 3550   |
| 321°C                           |       |       |       |        |        |        |
| d                               | 40.55 | 56.50 | 78.00 | 108.35 | 135.65 | 171.10 |
| H                               | 2145  | 2900  | 3050  | 3155   | 3025   | 3160   |

S.A.P. 7 %

| Test weights(gm)                |  | 25    | 50    | 100   | 200    | 300    | 500    |
|---------------------------------|--|-------|-------|-------|--------|--------|--------|
| Temperature 21°C                |  |       |       |       |        |        |        |
| Diagonal length d( $\mu$ )      |  | 26.82 | 37.32 | 52.38 | 74.35  | 90.48  | 120.70 |
| Hardness H(kg/cm <sup>2</sup> ) |  | 6440  | 6650  | 6770  | 6710   | 6800   | 6360   |
| 69°C                            |  |       |       |       |        |        |        |
| d                               |  | 27.55 | 38.45 | 59.62 | 78.48  | 93.80  | 124.50 |
| H                               |  | 6100  | 6270  | 5210  | 6020   | 6330   | 5980   |
| 108°C                           |  |       |       |       |        |        |        |
| d                               |  | 29.85 | 39.08 | 55.85 | 79.52  | 96.15  | 134.50 |
| H                               |  | 5200  | 6070  | 5940  | 5870   | 6020   | 5120   |
| 150°C                           |  |       |       |       |        |        |        |
| d                               |  | 29.72 | 43.38 | 6190  | 86.32  | 105.05 | 137.40 |
| H                               |  | 5240  | 4930  | 4840  | 4970   | 5040   | 4910   |
| 200                             |  |       |       |       |        |        |        |
| d                               |  | 31.92 | 41.52 | 61.12 | 88.35  | 108.48 | 137.80 |
| H                               |  | 4540  | 5370  | 4960  | 4750   | 4740   | 4880   |
| 255°C                           |  |       |       |       |        |        |        |
| d                               |  | 32.92 | 47.00 | 65.60 | 94.28  | 115.02 | 149.58 |
| H                               |  | 4270  | 4200  | 4310  | 4170   | 4210   | 4140   |
| 330°C                           |  |       |       |       |        |        |        |
| d                               |  | 35.80 | 53.30 | 75.88 | 104.90 | 130.68 | 169.48 |
| H                               |  | 3610  | 3260  | 3220  | 3370   | 3260   | 3230   |

Appendix II

Number of contact points

A graphical method along the lines suggested by ref. (9) was used to determine the probable number of the contact points. It consisted in an analysis of recorded surface profiles supposing that a rough surface was pressed against a flat plane.

Experimental work was done with four SAP 7% specimens A,B,C,D. Their surfaces were roughened stochastically and their profiles were recorded with the surface analyzer. Surface finishes were as follows:

|                          | A   | B   | C   | D                    |
|--------------------------|-----|-----|-----|----------------------|
| Ra ( $\mu$ )             | 1.2 | 0.8 | 1.1 | 0.4 1st measurement  |
| R <sub>t</sub> ( $\mu$ ) | 8   | 6.5 | 8   | 3                    |
| Ra ( $\mu$ )             | 1   | 1.3 | 0.9 | 0.35 2nd measurement |
| R <sub>t</sub> ( $\mu$ ) | 10  | 7.5 | 6   | 2.8                  |
| Ra ( $\mu$ )             | 1.4 | 1.4 | 1.2 | 0.45 3rd measurement |
| R <sub>t</sub> ( $\mu$ ) | 8.5 | 7.5 | 6.5 | 3.1                  |

Our analysis was carried out along 1 m. of profile record, corresponding to a real length of 0.5 cm along the specimen surface.

The initial position was established by a "datum line" which joined the two highest points of the profile. The pressure increase was simulated by a parallel translation of the datum line towards the bottom of the profile. The number of the contact points were counted for each position and the width of the actual contacts was measured and summed.

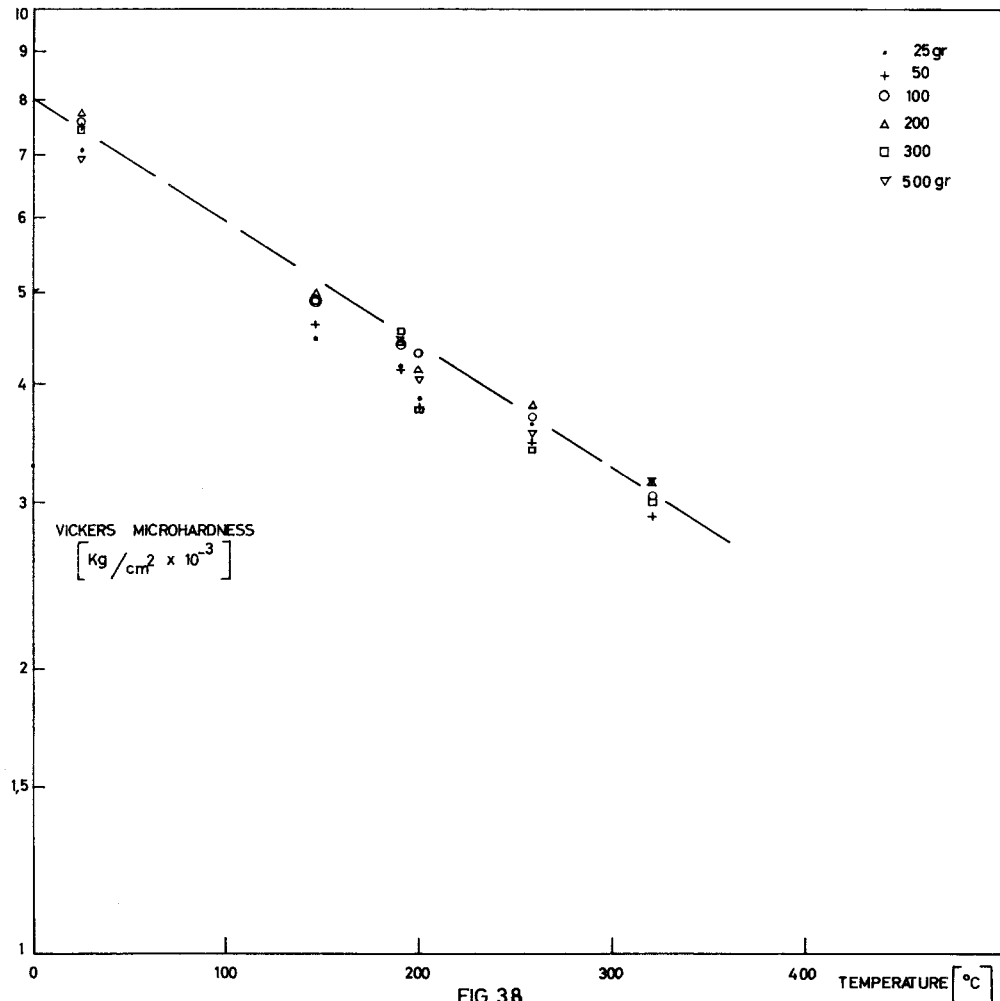


FIG. 38  
4% SAP HARDNESS VS TEMPERATURE

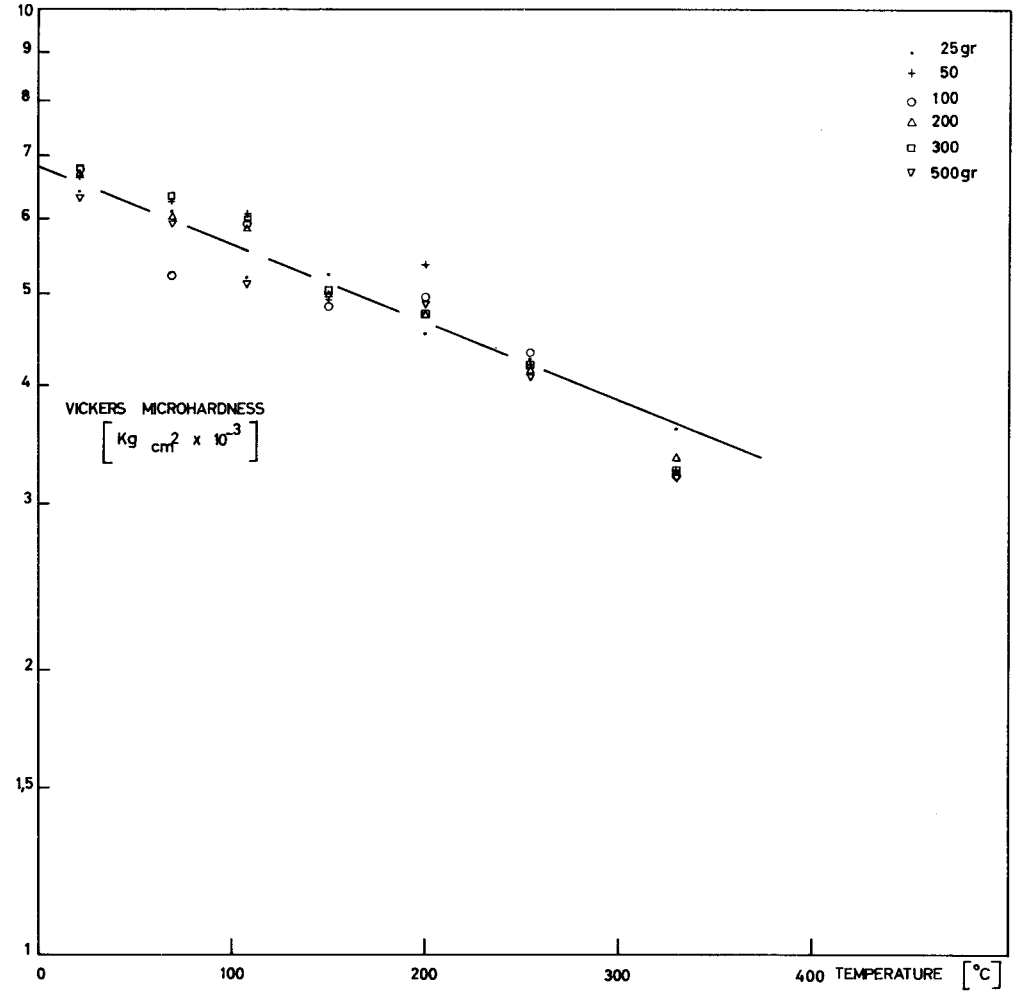


FIG. 39  
7% SAP HARDNESS VS TEMPERATURE

To a first approximation, the square of this sum yielded a value for the real contact area, which, multiplied by the hardness, would give the apparent pressure.

In our case the hardness of SAP 7% determined experimentally was  $2800 \text{ kg/cm}^2$  at  $420 \text{ }^\circ\text{C}$ .

The number of the contact points per unit area are plotted in fig. 40 versus pressure. The slope of the experimental points is about  $2/3$  in line with results from ref. (9) and ref. (11).

Another graphical determination was based on ref. (11) to determine the number of the contact points versus pressure for the case of two rough surfaces in contact.

- 1) A recorded surface profile made on a transparent paper was approached to the record of the other surface profile till first contact was attained. A mean "datum line" was drawn through the contacts.
- 2) The areas  $A_1$  and  $A_2$  of all empty spaces were measured by a planimeter above and below the datum line.
- 3) The mean height of the empty space was calculated as

$$\bar{f}_1 = \frac{A_1}{a} \quad \text{and} \quad \bar{f}_2 = \frac{A_2}{a}$$

where  $a$  is the total record length.

- 4) A parallel to the "datum line" was drawn at a distance  $2/3$  of the smaller  $\bar{f}$ , on the side of the datum line pertaining to the larger of the two  $\bar{f}$ .
- 5) Along this line, the width of the voids was determined and the quantities

$$\alpha_1 = \frac{\sum l_1 \text{ void}}{a} \quad \alpha_2 = \frac{\sum l_2 \text{ void}}{a}$$

were calculated.

The total volume of the voids on the 3-dimensional surface is

$$V_{\text{void}} = 2a \times A - \text{overlap}$$

The amount of overlapping is determined from the profile by

$$\text{overlap} = \alpha \times a^2 \times \psi$$

where the smaller  $\psi$  is chosen.

Substituting

$$V_{\text{void}} = aA (2 - \alpha)$$

The mean height of the voids is calculated as

$$\psi'_1 = \frac{V_{\text{void}}}{a^2} = \frac{A_1}{a} (2 - \alpha_1) \quad \text{and} \quad \psi'_2 = \frac{A_2}{a} (2 - \alpha_2)$$

6) The relation  $\delta = f(\psi')$

The distance  $\delta$  from the base to the contact point is given by

$$\delta = \frac{\psi'_i}{1 - \frac{K_f}{K_i}}$$

where  $K_f$  and  $K_i$  are fluid and solid thermal conductivity. Since the ratio  $K_f/K_i$  is small, one can consider that

$$\psi'_1 \cong \delta_1 \quad \text{and} \quad \psi'_2 \cong \delta_2$$

7) To fluid thermal conductance can be calculated for  $\epsilon = 0$  by

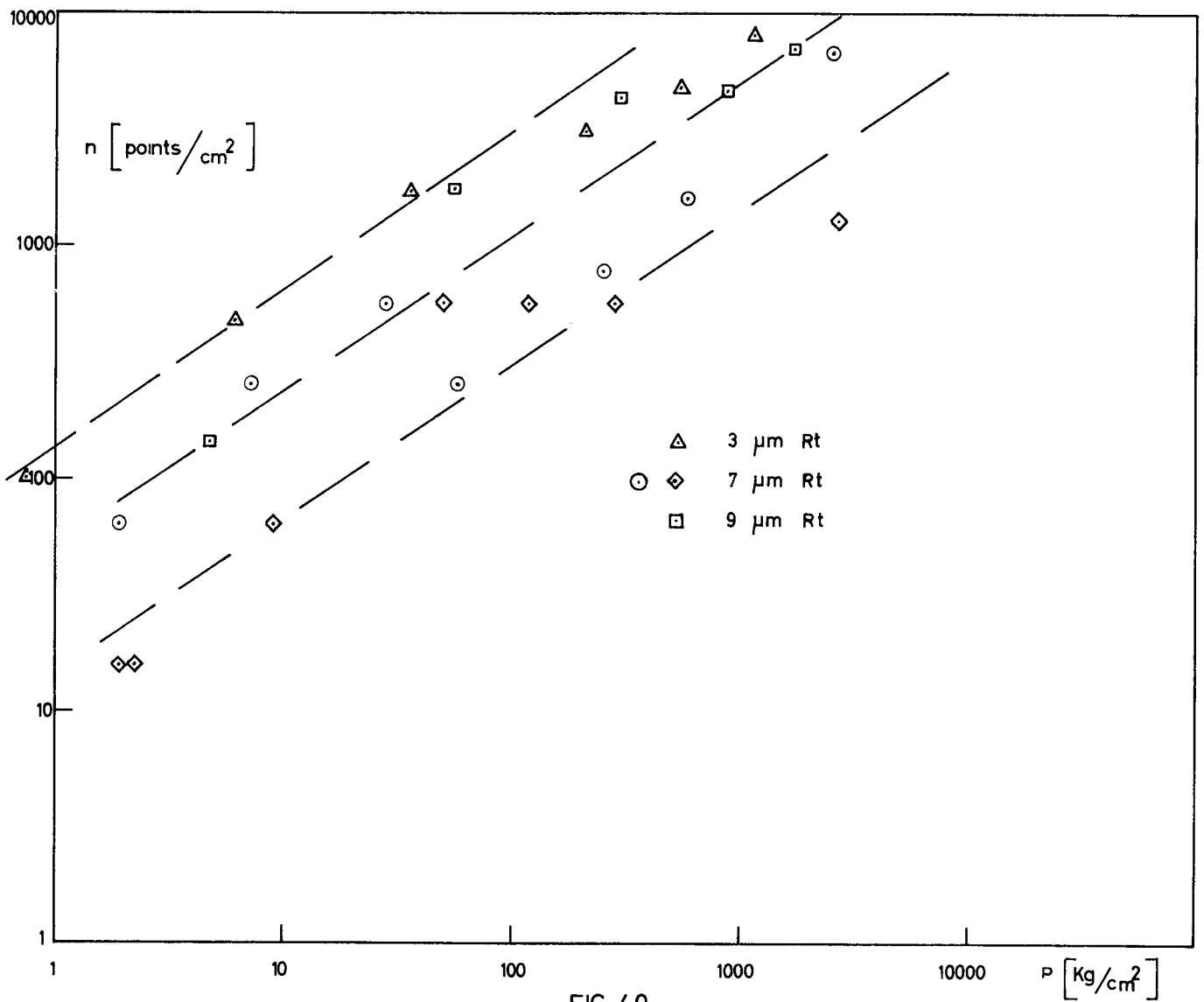


FIG. 40  
DENSITY OF CONTACT SPOTS VS PRESSURE

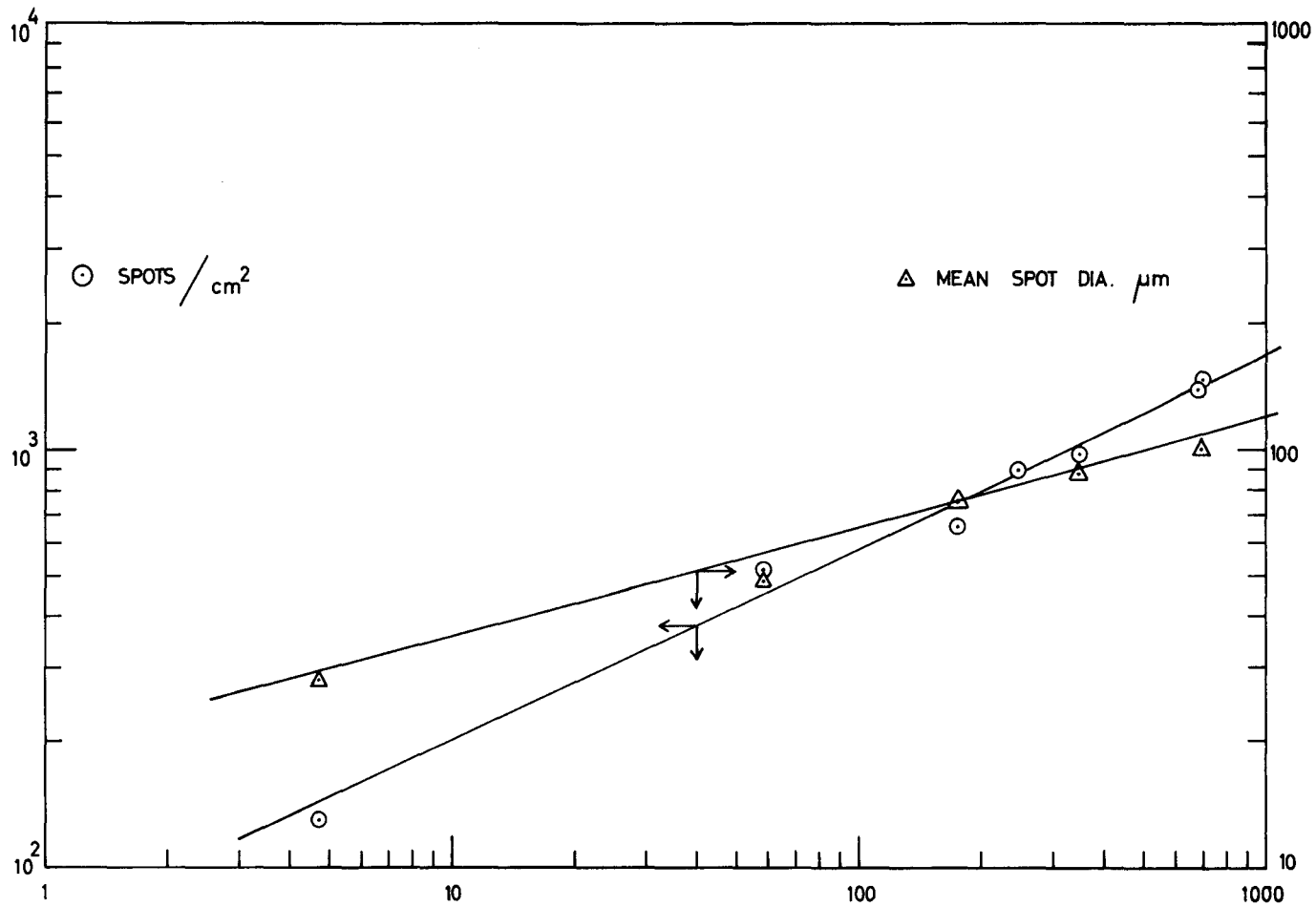


FIG. 41  
DENSITY OF CONTACT SPOTS VS PRESSURE

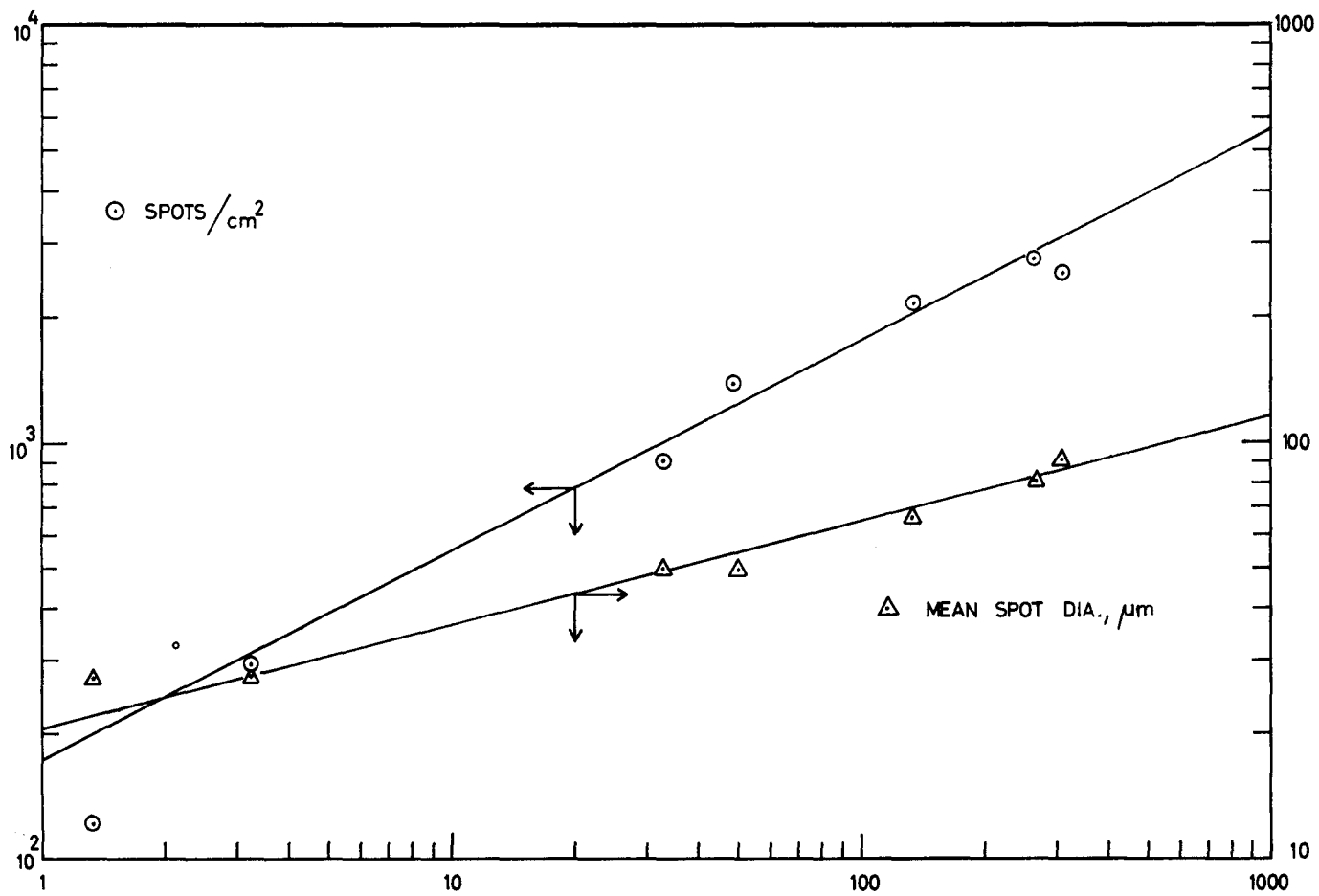


FIG. 42  
DENSITY OF CONTACT SPOTS VS PRESSURE

$$h = \frac{\frac{K_f}{\delta_1 + \delta_2}}{1 - \frac{K_f}{\delta_1 + \delta_2} \left( \frac{\delta_1}{K_1} + \frac{\delta_2}{K_2} \right)} \quad (\text{Watt/cm}^2 \text{ } ^\circ\text{C}) \quad (\text{T})$$

where  $K_1$  and  $K_2$  are the thermal conductivity of the two solids.

- 8) An increase of contact pressure is simulated by approaching the profile records to each other. To increase the randomness of contacts at each approaching step, a relative translation of the two profiles is operated; parallel to the datum line.

At each position of the datum line, the following were determined

- a) Number of contact points  $N$
  - b) Width of contacts along the datum line ( $\sum 1$ )
- The number of contact points per unit was given by

$$n = \frac{N^2}{a^2} = \frac{N^2 \times (\text{horizontal amplification})^2}{a^2}$$

The ratio  $\epsilon^2$  between the contact and the total area was

$$\epsilon^2 = \frac{(\sum 1)^2}{a^2}$$

The applied pressure was

$$P = \epsilon^2 H$$

where  $H$  is the hardness of the softer solid.

The method just described was applied to the profiles of test 32 (upper contact).

The surface finish was:

|       |                          |                        |
|-------|--------------------------|------------------------|
| Armco | $R_a = 5.42 \mu\text{m}$ | $R_t = 24 \mu\text{m}$ |
| SAP   | $R_a = 6.42 \mu\text{m}$ | $R_t = 25 \mu\text{m}$ |

Assuming

Thermal conductivity of air  $4 \times 10^{-4}$  Watt/cm°C at 200°C  
 " " " Armco 0.55 Watt/cm°C at 300°C  
 " " " SAP 2 Watt/cm°C at 200°C  
 SAP hardness 4600 Kg/cm<sup>2</sup> at 200°C

The thermal conductance of the fluid calculated by Eq. (T) is  $h = 0.085$  Watt/cm<sup>2</sup> °C. The number of contact points per unit area and the mean diameter of the points are plotted vs. the applied pressure in fig. 41.

This graphical method was applied to a UC-SAP surface as well using the recorded profile of a UC pellet and a fuel clad of the Metallurgy Dep't.

With

Thermal conductivity of UC = 0.2 W/cm°C  
 " " SAP = 2 W/cm°C  
 " " fluid(fission gases 5 Xe+1 Kr)

$$K = \left[ \left( \frac{\sqrt{5}}{\sqrt{5} + \sqrt{1}} + 1.94 \right) + \left( \frac{\sqrt{1}}{\sqrt{1} + \sqrt{5}} \times 3.17 \right) \right] 4.18 =$$

$$= 0.97 \times 10^{-4} \text{ Watt/cm}^2 \text{ °C}$$

SAP HARDNESS = 2900 kg/cm<sup>2</sup> at 400°C

The thermal conductance of the fluid calculated by Eq. (T) is  $h = 0.0745$  W/cm<sup>2</sup> °C.

The number of the contact points per unit area and the mean diameter of the points are plotted vs. the applied pressure in fig. 42.

From fig. 41 and 42 it appears that the number of the contact points for unit area increases with a power of the applied pressure close to 0.5.

### Appendix III

Data on the in-pile experiments

#### Description of the test assembly

The rig consisted of three assemblies (see in Fig. 43 the rig sketch)

- A stainless steel shield plug tube and a cement shielding.
- The second containment consists of a stainless steel tube attached to the shield plug which carries the specimen can assemblies and a water jacket. Two heater type leak detectors are put at the bottom of the second containment to detect any inward water leak from the water jacket. The water jacket is a water annulus formed by the second containment and the water guide tube.

The water guide aluminium tube is attached to the second containment and the reactor heavy water enters the annulus at the bottom.

- The specimen can assembly consists in three SS capsules joined end to end by connecting posts and located into the second containment.

As shown in Fig. 44 to obtain a total fuel length of 3.81 cm, each can contains two UC pellets (1.906 cm nominal diameter) fitted into a SAP hollow cylinder walls 1.916 cm of inner and 4.93 cm outer nominal diameter contained into a 0.088 cm thick SS can.

The fuel was arc-fused natural uranium carbide with a carbon content  $5\% \pm 0.1$  weight.

Fuel pellets were produced by centreless grinding and care was taken to check that they conform as nearly as possible to a perfectly circular cross-section.

SKETCH OF IRRADIATION RIG.

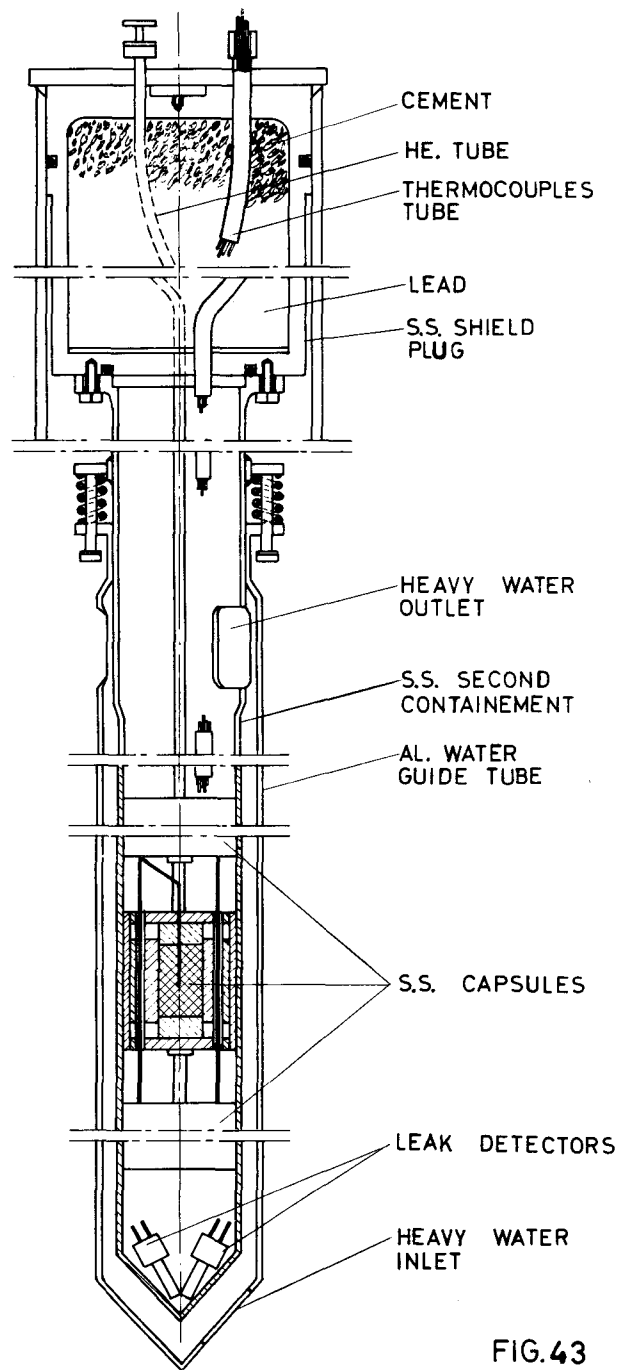


FIG. 43

ARRANGEMENT OF THE SPECIMEN CAN

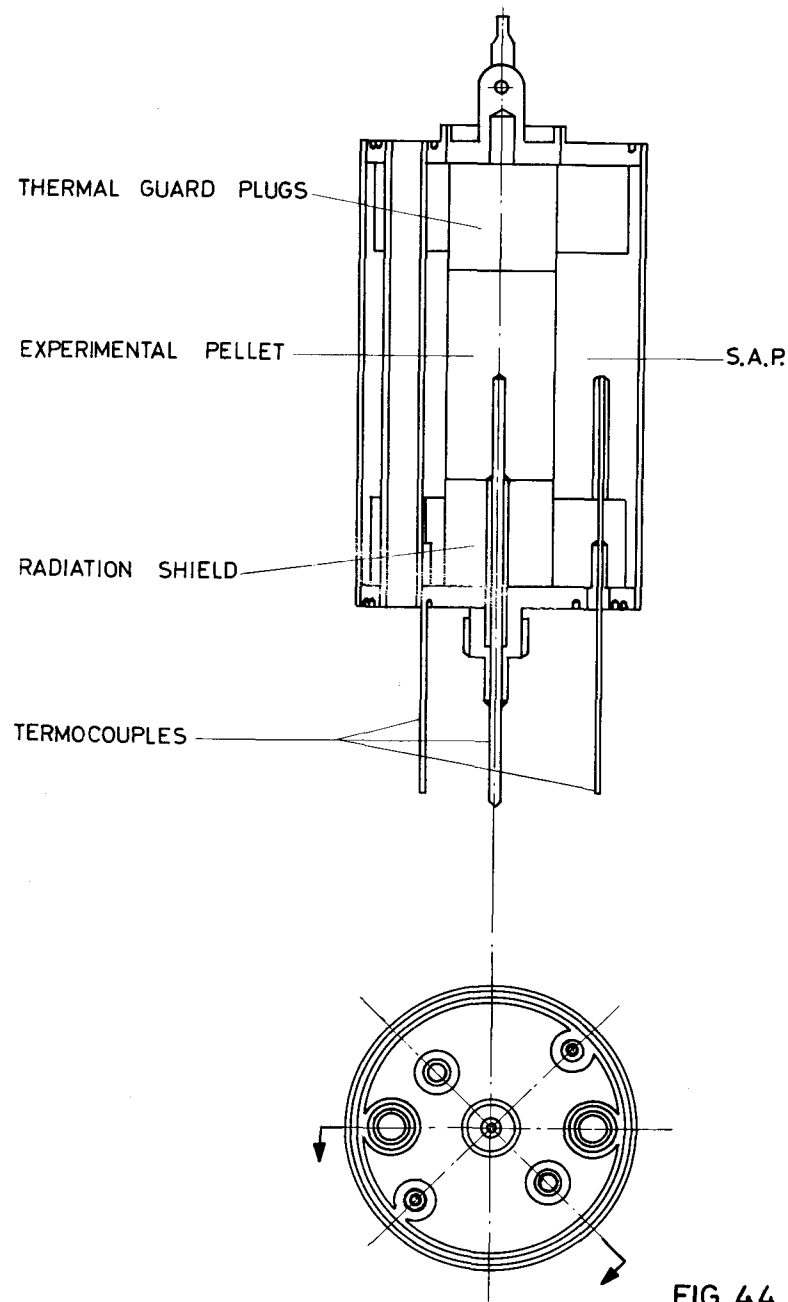


FIG. 44

The finished diameter of each pellet was adjusted to satisfy the fuel-sheath clearances required.

Pellets of 98% MgO are located between each end cap of UC pellet to prevent heat losses.

The SS capsule is evacuated and filled with Xenon gas at atmospheric pressure.

Five thermocouples are located in each capsule to determine the radial heat flow through the specimen can.

The centre  $P_t - 10\% Rh - P_t$  and four chromel-alumel thermocouples which are located in two pairs of holes at different radii, measure respectively the UC and SAP temperature.

Rig. 1

The experiment was irradiated in fuel channel N° 9 during a given reactor cycle (2weeks) and operated throughout the period without incident.

Expected values from previous calculations of the facility showed that under normal operating conditions the UC temperature would attain 1000°C and the SAP, 400°C approximatively. Infact, the temperature values were about 600°C in the UC and 150°C in the SAP width a maximum unperturbed thermal neutron flux of  $4.5 \times 10^{13}$  n/cm<sup>2</sup> sec.

The low UC temperatures did not permit an expansion of the UC pellets sufficient to obtain a contact between UC and SAP. For this reason the rig was later re-irradiated in the central channel to double the thermal neutron flux.

During a second reactor cycle higher center temperatures were achieved, but some thermocouples were apparently damaged when the assembly was moved.

Infact, the only difficulty encountered was that the central thermocouple of the can A and C became erratic after 340 hours. The can A thermocouple was reconnected by pulling a vacuum in the outer container but for a short time only.

During a third and fourth reactor cycle the experiment yielded temperatures for a capsule only.

The total irradiation time was 1012 hours with a thermal neutron flux of  $6.9 \times 10^{13}$  n/cm<sup>2</sup> sec.

Rig. 2

The experiment operated during two reactor cycles. Total irradiation time was 816 hours with a thermal neutron flux of  $6.9 \times 10^{13}$  n/cm<sup>2</sup>sec.

The radial heat flow calculation method utilized the temperature difference in the gap and the heat thermal flux on the pellet surface to determine the gap conductance.

The heat generation in UC was known from the values of the thermal neutron flux and the gamma heating rate.

The thermal neutron flux has been estimated under the assumption that the heat transfer coefficient between SAP sheath and the cooling heavy water is constant.

The differences between the mean SAP temperature and the inlet heavy water temperature during the raising and falling steps of reactor power are plotted in Fig. 45 as a function of the thermal power.

Assuming a maximum unperturbed thermal flux at the center of the reactor of  $10 \times 10^{13}$  n/cm<sup>2</sup> sec, its variation law has been obtained by fitting the experimental points with a parabolic expression of flux versus temperature difference:

$$\phi = 0.74 \beta + 0.1 \beta^2$$

where

$$\beta = \sigma + 0.04 T_r - 0.04 T_w \text{ (mV) is temperature drop sheath - heavy water and } \sigma = \frac{A+B+C+D}{4}$$

The arithmetic mean readings for each can of the SAP thermocouples mV.

DIFFERENCE BETWEEN SAP TEMPERATURE  
AND HEAVY WATER TEMPERATURE VS.  
THERMAL POWER

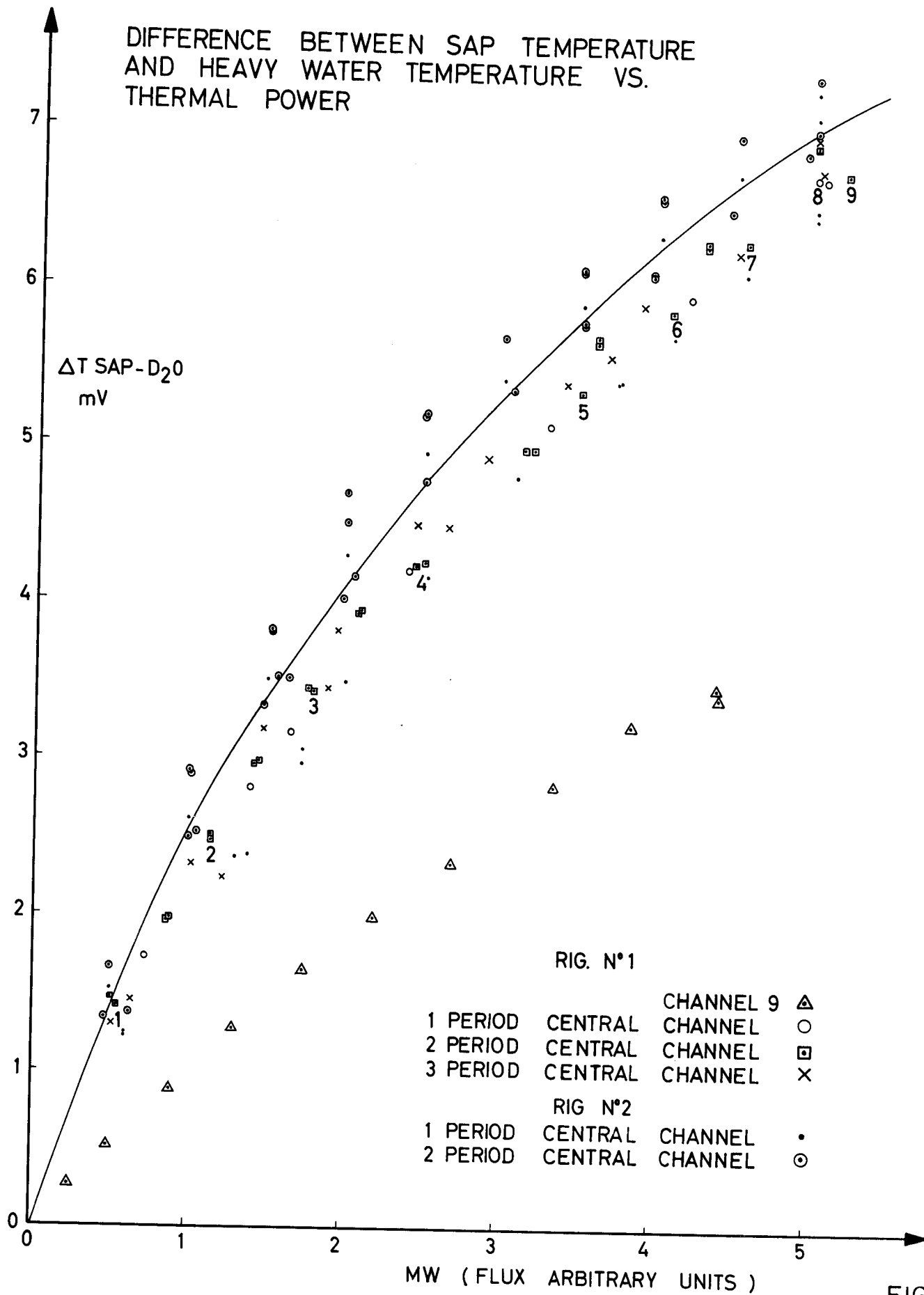


FIG.45

The gamma heating value used in the calculations has been determined experimentally by means of the leak detector thermocouple readings. However the leak detector position was about 20 cm below the last capsule in the rig. The gamma heating in the assemblies was estimated to be about 10 percent higher.

The method was the following:

The electrical supply of the leak detector was switched off and the temperature increase due to the gamma heating alone was measured as difference between the leak detector and the heavy water temperatures.

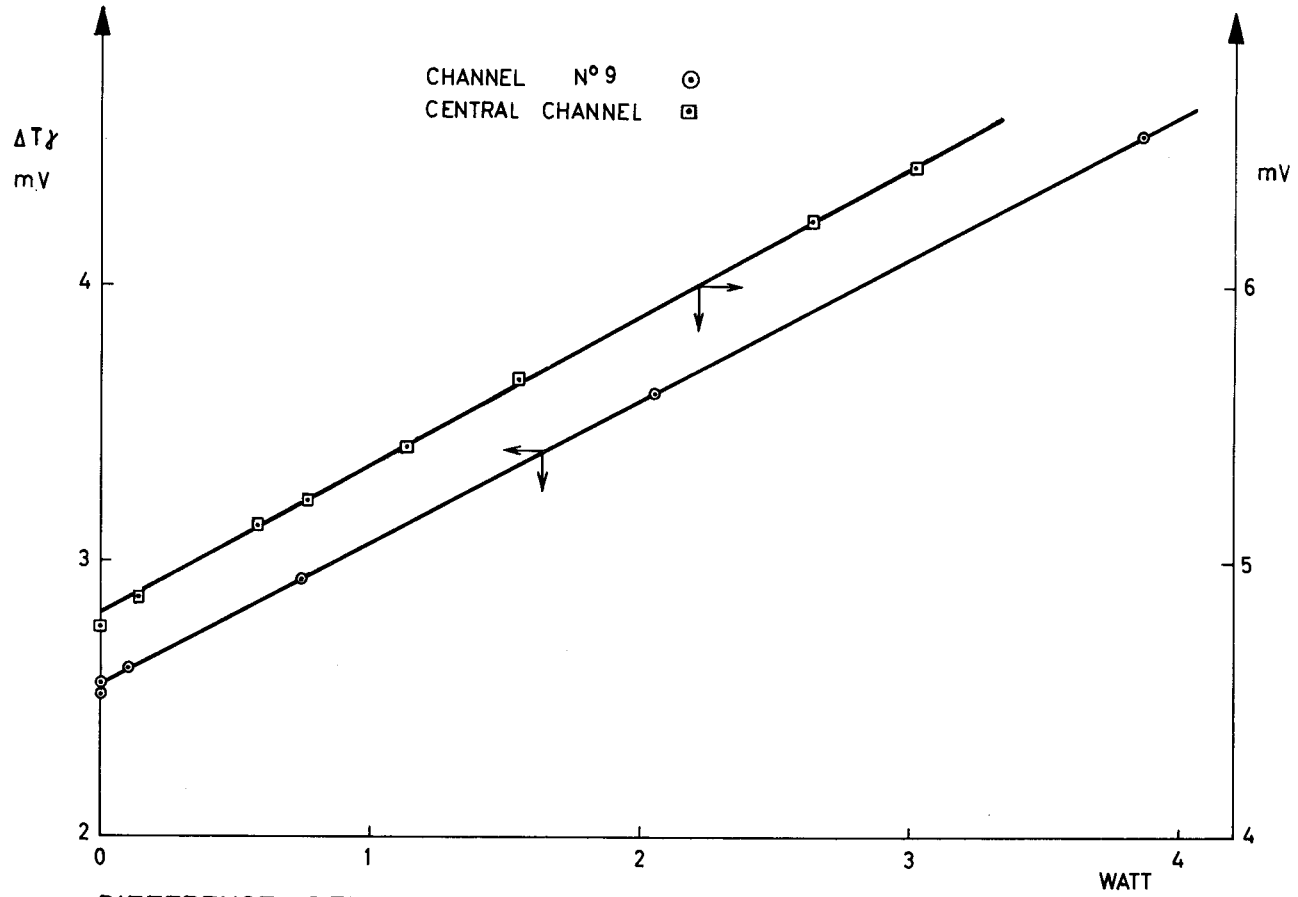
The temperature rise  $\Delta T_{\gamma}$  is plotted in Fig. 46 versus leak detector electrical power.

In reactor channel No 9 with a perturbed neutron flux of  $3.66 \times 10^{13}$  n/cm<sup>2</sup>sec. the gamma heating was 0.52 Watt/gr and in the central channel with a perturbed neutron flux of  $8.2 \times 10^{13}$  n/cm<sup>2</sup>sec, the gamma heating was twice as much.

Gamma heating in all materials is assumed to vary linearly with flux.

In reactor channel No 9 with a perturbed neutron flux  $3.66 \times 10^{13}$  n/cm<sup>2</sup>sec, gamma heating is found from Fig. 46 to be  $\gamma = 0.5$  Watt/gr - Gamma heating rate as a function of neutron flux is:

$$\gamma = \frac{0.5}{3.66} \phi = 0.1367 \phi$$



DIFFERENCE BETWEEN LEAK DETECTOR AND HEAVY WATER TEMPERATURE VS. LEAK DETECTOR POWER

FIG.46

Temperature difference between surface and centre  
of the UC pellet

As noted previously, the UC centre temperature was measured with a Pt - 10% Rh - Pt thermocouple for each capsule.

The temperature difference between UC surface and centre is given by

$$\Delta T_o = \frac{Pr_o^2}{4K_o}$$

Heat generation rate as a function of the neutron flux is:

$$\frac{\phi \times 2.7 \times 238 \times \delta_o}{250} + \text{Pot} \gamma \times \delta_o = 36.23 \phi \text{ Watt/cm}^3$$

Taking  $K_o = 0.2 \text{ Watt/cm}^\circ\text{C}$  Ref.(13)  
and  $r_o = 0.953 \text{ cm}$

$$\Delta T_o = \frac{36.23 \times (0.953)^2}{4 \times 0.2} \phi = 41 \phi \text{ }^\circ\text{C}$$

UC surface temperature is:

$$T_o = T_c - \Delta T_o = T_c - 41 \phi \text{ }^\circ\text{C}$$

Temperature drops across SAP

As noted previously, the SAP temperature is measured with two pairs of Chromel/Alumel thermocouples at different radii. Temperature drop across SAP is given by:

$$-\frac{K_2 dT_2}{dr} \times 2\pi r = Q + \pi (r^2 - r_1^2) \times \delta_2 \times \text{Pot} \gamma$$

The total heat generated is:

$$Q = 36.23 \phi s_1 s_2 \bar{n} r_0^2 \text{ Watt/cm}$$

where:

$s_1=0.9$  a factor accounting for the axial heat loss.

$s_2 = \frac{1.5}{1.75}$  a factor accounting for the ratio of the UC length to the SAP length.

Taking  $K_2 = 1.45 \text{ Watt/cm}^\circ\text{C}$  Ref. (16) and substituting:

$$\frac{-K_2 dT_2}{d\rho} 2\bar{n}\rho = \left[ 36.23 \times 0.9 \times \frac{1.5}{1.75} \times \bar{n} \times \overline{0.953^2} + \bar{n} (\rho^2 - r_1^2) \times 2.8 \times 0.1367 \right] \phi$$

$$dT_2 = - \frac{d\rho}{\rho} (8.76 \phi + 0.1329 \phi \rho^2)$$

integrating

$$\Delta T_2 = - 8.76 \phi \int_{r_1}^{r_2} \frac{d\rho}{\rho} - 0.1329 \phi \int_{r_1}^{r_2} \rho d\rho =$$

$$= - 8.76 \phi \ln \frac{r_2}{r_1} - \frac{0.1239\phi}{2} (r_2^2 - r_1^2) =$$

$$= 8.6 \phi \text{ }^\circ\text{C}$$

SAP inner surface temperature

$$T_1 = \bar{T} + 4.3 \phi \text{ }^\circ\text{C}$$

SAP outer surface temperature

$$T_2 = \bar{T} - 4.3 \phi \text{ } ^\circ\text{C}$$

Temperature drop across the gap

Temperature drops across the UC/SAP interface is:

$$\begin{aligned} \Delta T_1 &= (T_c - 41 \phi) - (\bar{T} + 4.3 \phi) = \\ &= T_c - \bar{T} - 45.3 \phi \end{aligned}$$

In our case  $\Delta T_1 \gg 0$ . This condition must be always verified.

Heat flux at the gap

The heat flux at the UC outer surface:

$$F = \frac{36.23 \phi \times \tilde{\pi} r_o^2}{2 \tilde{\pi} r_o} = 17.23 \phi \text{ Watt/cm}^2$$

Multiplying by  $s = 0.9$  (axial conduction)

$$F = 15.5 \phi$$

Gap conductance

It is given by the ratio of the gap heat flux and the temperature drops across the gap.

$$U = \frac{F}{\Delta T_1} = \frac{15.5 \phi}{T_c - \bar{T} - 45.3 \phi} \text{ Watt/cm}^2 \text{ } ^\circ\text{C}$$

Fuel-sheath gaps caused by differential thermal expansion  
and contraction

In the case of a sheathed fuel, thermal cycling produces internal stresses which can cause cracking if the linear heat rating is not limited to a value below which cracking occurs.

The calculation of the operating gaps at each temperature is made by estimating the thermal expansion of the sheath and fuel material and by assuming that the fuel remains centered within the metal sheathing.

The hot gaps are:

$$G_1 = G_0 + \text{thermal expansion of SAP} - \text{thermal expansion of UC.}$$

UC pellet deformation

In a solid cylinder, radial and tangential stress are given by the expression Ref. (21)

$$\sigma_{\text{rad}} = \frac{\alpha E}{1-\nu} \left( \frac{1}{R^2} \int_0^R T r \, dr - \frac{1}{r^2} \int_0^r T r \, dr \right)$$

$$\sigma_{\text{tang}} = \frac{\alpha E}{1-\nu} \left( -T + \frac{1}{R^2} \int_0^R T r \, dr + \frac{1}{r^2} \int_0^r T r \, dr \right)$$

where R and r is the cylinder and generical radius respectively

T is the difference between a local and the surface temperature

E is Young's modulus

ν is Poisson's ratio

α is thermal expansion coefficient.

Temperature difference between centre and surface or at a generical position is respectively:

$$T_c - T_o = \frac{PR^2}{4K} \quad \text{or} \quad T_c - t = \frac{Pr^2}{4K}$$

substituting

$$T = t - T_o = \frac{P}{4K} (R^2 - r^2)$$

where P = heat generation rate

K = thermal conductivity

By substitution

$$\sigma_{\text{tang}} = \frac{\alpha E}{1-\nu} \left[ -\frac{P}{4K} (R^2 - r^2) + \frac{1}{R^2} \int_0^R \frac{P}{4K} (R^2 - r^2) r \, dr + \right]$$

$$+ \frac{1}{r^2} \int_0^r \frac{P}{4K} (R^2 - r^2) r dr \Bigg]$$

Integrating

$$\tau_{\text{tang}} = \frac{P E \alpha}{(1-\nu) 4K} \left( \frac{3}{4} r^2 - \frac{1}{4} R^2 \right)$$

At the surfaces for  $R = r$

$$\tau_{\text{tang}} = \frac{P \alpha E R^2}{8K(1-\nu)}$$

The elongation to the stress distribution

$$\epsilon = \frac{\tau(1-\nu)^2}{E} = \frac{P \alpha R^2 (1+\nu)}{8K} = \frac{\alpha \Delta T (1+\nu)}{2}$$

In the case of UC pellet the total elongation is the sum of the thermal and the stress elongation

$$\epsilon_0 = \alpha_0 (T_0 - 20) + \frac{\alpha_0 \Delta T_0}{2} (1+\nu)$$

taking  $\alpha_0 = 10^{-5} \text{ } ^\circ\text{C}^{-1}$  and  $\nu = 0.3$

$$\epsilon_0 = 10^{-5} (T_0 + 0.65 \Delta T_0 - 20)$$

Substituting a temperature values as a function of thermal neutron flux  $\Delta T_0 = 41 \text{ } \emptyset$  and  $T_0 = T_c - 41 \text{ } \emptyset$

$$\epsilon_0 = 10^{-15} T_c - 14.3 \times 10^{-5} \emptyset - 2 \times 10^{-4}$$

Stainless steel container deformation

Thermal expansion of the SAP cylinder pressing against the container gives a stress Ref. (21)

$$\sigma = \frac{p r_3}{s}$$

The strain due to this stress is:

$$\epsilon_3 = \frac{\sigma}{E_3} = \frac{p r_3}{E_3 s}$$

The total strain is the sum of the thermal and the stress expansion:

$$\epsilon_3 = \frac{p r_3}{E_3 s} + \alpha_3 (T_3 - 20)$$

Sheath cylinder deformation

Stresses in a thick cylinder pressed by an external pressure are given by the expression Ref. (21)

$$\sigma_{\text{tang}} = p \frac{b^2(a^2 + r^2)}{r^2(b^2 - a^2)} \quad (\text{compression})$$

$$\sigma_{\text{rad}} = p \frac{b^2(r^2 + a^2)}{r^2(b^2 - a^2)} \quad (\text{compression})$$

$$\sigma_{\text{long}} = 0$$

where b, a, r are outer, inner and generical radius, respectively.

Stress due to the thermal gradient  $\Delta T$  in the same cylinder are given by the expression Ref.(21)

$$\sigma_{\text{tang.out.}} = \frac{\alpha E \Delta T}{2(1-\nu) \ln \frac{b}{a}} \left( 1 - \frac{2a^2}{b^2 - a^2} \ln \frac{b}{a} \right) \quad (\text{traction})$$

$$\sigma_{\text{tang.inn.}} = \frac{\alpha E \Delta T}{2(1-\nu) \ln \frac{b}{a}} \left( 1 - \frac{2b^2}{b^2 - a^2} \ln \frac{b}{a} \right) \quad (\text{compression})$$

$$\sigma_{\text{long}} = \sigma_{\text{tang}}$$

$$\sigma_{\text{rad}} = 0$$

Composition of strains due to the external pressure and the thermal gradient are given by

$$\epsilon_x = \frac{\sigma_x}{E} - \frac{\nu \sigma_y}{E} - \frac{\nu \sigma_z}{E}$$

The total elongation of the cylinder outer and inner radii is the sum of the thermal and the composed expansions:

$$\begin{aligned} \epsilon_{\text{tot.out.}} = & \alpha (T_{\text{out}} - 20) + \frac{\Delta T \alpha}{2 \ln \frac{b}{a}} \left( 1 - \frac{2a^2}{b^2 - a^2} \ln \frac{b}{a} \right) - \\ & - \frac{p}{E} \frac{a^2 + b^2}{b^2 - a^2} + \frac{\nu P}{E} \end{aligned}$$

$$\epsilon_{\text{tot. inner.}} = \alpha(T_{\text{inn.}} - 20) - \frac{\alpha \Delta T}{2 \ln \frac{b}{a}} \left(1 - \frac{2b^2}{b^2 - a^2} \ln \frac{b}{a}\right) - \frac{p}{E} \frac{2b^2}{b^2 - a^2}$$

From the ratio

$$\frac{\text{SAP radius}}{\text{SS radius}} = \frac{1 + \epsilon_{\text{tot. SS}}}{1 + \epsilon_{\text{tot. out. SAP}}}$$

Substituting

$$\frac{r_2}{r_3} = \frac{1 + \alpha_3(T_3 - 20) + \frac{p r_3}{E_3 S}}{1 + \alpha_2(T_2 - 20) + \frac{\alpha_2 \Delta T}{2 \ln \frac{r_2}{r_1}} \left(1 - \frac{2r_1^2}{r_2^2 - r_1^2} \ln \frac{r_2}{r_1}\right) + \frac{p}{E_2} \left(1 - \frac{r_1^2 + r_2^2}{r_2^2 - r_1^2}\right)}$$

Solving for the contact pressure

$$p = 1.38 T_2 + 0.488 \Delta T_2 - 0.934 T_3 + 30.7$$

Substituting  $T_2$ ,  $\Delta T_2$ ,  $T_3$  as a function of neutron flux

$$p = 0.466 \bar{T} + 7.46 \phi + 30.7$$

Combining and solving

$$\epsilon_1 = 1.975 \times 10^{-5} \bar{T} + 18.37 \times 10^{-5} \phi - 5.5 \times 10^{-4}$$

The radial hot gap is given by

$$G_1 = G_0 + r_0(\epsilon_1 - \epsilon_0) = G_0 + 1.89 \times 10^{-5} \bar{T} - 3.4 \times 10^{-4} + 3.02 \times 10^{-4} \phi - 9.53 \times 10^{-6} T_c$$

UC swelling

Permanent swelling measurements were not possible till the capsules were dismantled. Swelling of the UC pellets was then estimated as a function of the gap thermal resistance, the gas thermal conductivity and the thermal expansions.

The hot clearance can be calculated by the expression.

$$\text{Hot clearance} = R \times K_3$$

where

$$R = \text{gap thermal resistance cm}^2\text{/Watt}$$
$$K_3 = \text{gas thermal conductivity Watt/cm}^2\text{C.}$$

Assuming that the fuel remains centered within the metal sheathing, the hot clearance can be calculated by the difference between the residual clearance due to thermal expansion and the fuel swelling.

The expression

$$\text{hot clearance} = G_1 - \Delta r_0$$

where

$$G_1 \text{ is due to the thermal expansion}$$
$$\Delta r_0 \text{ is the fuel radial swelling.}$$

Then

$$RK_3 = G_1 - \Delta r_0$$

and the fractional radial swelling is given by

$$\frac{\Delta r_0}{r_0} = \frac{G_1 - RK_3}{r_0}$$

Gas thermal conductivity

Since the capsules were filled with Xenon gas at atmospheric pressure, the thermal conductivity of Xenon is calculated as a function of the operating temperatures from

$$K_3 = 5.35 \times 10^{-7} (t + 273)^{.824} \quad \text{Ref. (17)}$$

Experimental data analysis

The elaboration of the experimental data was made with a 7090 IBM computer code using equations of appendix III. Symbols used are explained hereafter.

Input data were

|            |   |                         |
|------------|---|-------------------------|
| TT         | = SAP thermocouple readings   | mV                      |
| GAP        | = nominal gap values  | cm                      |
| TAMB       | = room temperatures   | °C                      |
| TUC        | = UC thermocouple readings  | °C                      |
| TAQ        | = inlet heavy water temperature   | °C                      |
| TEMP       | = irradiation time values as referred to a maximum flux of $6.9 \times 10^{13}$ n/cm <sup>2</sup> sec.(hours) |                         |
| M          | = Test readings number  |                         |
| N          | = specimen can number   |                         |
| VT(N,M)    | = SAP arithmetic mean temperature   | mV                      |
| T(N,M)     | = SAP true mean temperature   | °C                      |
| DELT(N,M)  | = Temperature drop sheath-heavy water   | mV                      |
| FI(N,M)    | = thermal neutron flux  |                         |
| GAMMA(N,M) | = Gamma heating as a function of the neutron flux   |                         |
| TUCS(N,M)  | = UC pellet surface temperature as a function of the neutron flux   |                         |
| TS(N,M)    | = SAP sheath inner surface temperature as a function of the neutron flux                                      |                         |
| POT(N,M)   | = Gap heat flux as a function of neutron flux   |                         |
| COND(N,M)  | = thermal gap conductance   | Watt/cm <sup>2</sup> °C |
| A(N,M)     | = thermal gap resistance  | cm <sup>2</sup> °C/Watt |
| GAC(N,M)   | = hot gap due to the thermal expansion and the thermal stress   | cm                      |
| TX         | = arithmetic mean temperature between UC and SAP inner surface  |                         |
| XKX        | = Xenon gas thermal conductivity as a function of the operating temperatures                                  | Watt/cm°C               |
| SW(N,M)    | = UC pellet radial percent swelling   |                         |

The output data included

|  |                         |
|--|-------------------------|
| - thermal neutron flux                   | n/cm <sup>2</sup> sec.  |
| - gap heat flux                          | Watt/cm <sup>2</sup>    |
| - thermal gap conductance                | Watt/cm <sup>2</sup> °C |
| - hot gap due to thermal expansions      | cm                      |
| - UC pellet centre temperature           | °C                      |
| - SAP sheath arithmetic mean temperature | °C                      |
| - thermal gap resistance                 | cm <sup>2</sup> °C/Watt |
| - UC pellet radial percent swelling      |                         |
| - irradiation times                      | hours                   |

Results are printed as follows

|                              |   |
|------------------------------|---|
| In the first line            | = Test number and corresponding irradiation time. |
| In the following three lines | = Output data for can A, B and C respectively.    |
| In the last three lines      | = Input experimental data in the same order       |

The same code was used to elaborate the data of the second irradiated rig. However the following symbols were changed:

- 1) TSAP (N,M) = TS (N,M)
- 2) FLGAP (N,M) = POT (N,M)
- 3) RES (N,M) = A (N,M)

Comparing the two programs listed hereafter one can see that the gap value is omitted in the input data of the second rig because the three capsules were built with an equal nominal clearance.



SECONDO RIG

C  
C  
C  
C  
1 LE PROVE DA 1 A 19 SONO LA SALITA, DA 19 A 63 IL PLATEAU, DA 63 A 72  
2 LA DISCESA DEL PRIMO PERIODO LE PROVE DA 73 A 76 SONO LA PRIMA SA  
3 LITA, DA 77 A 94 LA SECONDA SALITA, DA 94 A 123 IL PLATEAU, DA 123 A  
4 142 LA DISCESA DEL SECONDO PERIODO

DIMENSION TT(4,3,142), TAMB(144), TUC(3,142), TAQ(144), VT(3,144), T(3,  
1144), FI(3,144), GAMMA(3,144), TUCS(3,144), TSAP(3,144), FLGAP(3,144), C  
2 OND(3,144), RES(3,144), GAC(3,144), SW(3,144), TEMP(144), DELT(3,144), G  
3 ACVE(3,144)  
10 READ INPUT TAPE 5,10,TT  
FORMAT (4E12.4)  
20 READ INPUT TAPE 5,20,TAMB  
FORMAT (6E12.4)  
30 READ INPUT TAPE 5,30,TUC  
FORMAT (6E12.4)  
40 READ INPUT TAPE 5,40,TAQ  
FORMAT (6E12.4)  
41 READ INPUT TAPE 5,41,TEMP  
FORMAT (6F10.2)  
DO 50 M=1,142  
DO 60 N=1,3  
VT(N,M)=(TT(1,N,M)+TT(2,N,M)+TT(3,N,M)+TT(4,N,M))/4.  
44 T(N,M)=24.4\*VT(N,M)+0.976\*TAMB(M)  
DELT(N,M)=VT(N,M)-4.E-2\*TAQ(M)+4.E-2\*TAMB(M)  
FI(N,M)=0.74\*DELT(N,M)+0.1\*DELT(N,M)\*\*2.  
45 FI(N,M)=0.5\*FI(N,M)  
60 CONTINUE  
50 CONTINUE  
DO 70 M=1,142  
DO 80 N=1,3  
GAMMA(N,M)=1.367E-1\*FI(N,M)  
64 TUCS(N,M)=TUC(N,M)-41.\*FI(N,M)  
TSAP(N,M)=T(N,M)+4.3\*FI(N,M)  
66 FLGAP(N,M)=15.5\*FI(N,M)  
COND(N,M)=FLGAP(N,M)/(TUCS(N,M)-TSAP(N,M))  
68 RES(N,M)=1./COND(N,M)  
GAC(N,M)=1.5E-3+1.89E-5\*T(N,M)-3.4E-4+3.02E-4\*FI(N,M)-9.53E-6\*TUC(  
1 N,M)  
77 TX=(TUCS(N,M)+TSAP(N,M))\*0.5  
78 XKX=5.35E-7\*(TX+2.73E2)\*\*0.824  
778 GACVE(N,M)=RES(N,M)\*XKX  
79 SW(N,M)=(GACVE(N,M)-GAC(N,M))\*1.05  
795 SW(N,M)=(-SW(N,M))  
80 CONTINUE  
WRITE OUTPUT TAPE 6,85,M,TEMP(M)  
85 FORMAT (1H0,37X,14HPROVA NUMERO ,13,5X,7HTEMPO ,F8.2,///)  
WRITE OUTPUT TAPE 6,90  
90 FORMAT (1H ,11X,96HFLUSSO NEUTR FLUSSO TER CONDUIT GAP  
1 TEMP CARB TEMP SAP RESIS TERM SWELLING,///)  
WRITE OUTPUT TAPE 6,100,(FI(N,M),FLGAP(N,M),COND(N,M),GAC(N,M),TUC  
1(N,M),T(N,M),RES(N,M),SW(N,M),GACVE(N,M),N=1,3)  
100 FORMAT (1H ,11X,9E12.4)  
WRITE OUTPUT TAPE 6,200  
200 FORMAT (1H ,6X,6HMV SAP,14X,3HTUC,6X,4HTAMB,7X,3HTAQ,6X,4HTEMP///)  
WRITE OUTPUT TAPE 6,101,((TT(I,N,M),I=1,4),TUC(N,M),TAMB(M),TAQ(M)  
1,TEMP(N),N=1,3)  
101 FORMAT (1H ,4F5.2,4F10.2)  
70 CONTINUE  
CALL EXIT  
END(1,0,0,0,0,0,0,0,0,0,0,0,0,0,0)

Notation for Appendix III

|              |  |  |
|--------------|--|--|
| $r_0$        | - UC pellet radius   | - 0.953 cm   |
| $r_1$        | - SAP inner radius   | - 0.958 cm   |
| $r_2$        | - SAP outer radius   | - 2.465 cm   |
| $r_3$        | - SS container inner radius                                      | - 2.464 cm   |
| $\rho$       | - Generical radius   |  |
| $S$          | - SS container thickness   | - 0.088 cm   |
| $\alpha_0$   | - UC thermal expansion coefficient                               | - $10 \times 10^{-6} / ^\circ\text{C}$ ref. (13)   |
| $\alpha_2$   | - SAP " " "  | - $21.5 \times 10^{-6} / ^\circ\text{C}$ ref. (14) |
| $\alpha_3$   | - SS " " "   | - $14.5 \times 10^{-6} / ^\circ\text{C}$           |
| $E_0$        | - UC Young's modulus   | - $2.2 \times 10^6 \text{ kg/cm}^2$ ref. (13)      |
| $E_2$        | - SAP " "  | - $0.6 \times 10^6 \text{ kg/cm}^2$ ref. (14)      |
| $E_3$        | - SS " "   | - $2 \times 10^6 \text{ kg/cm}^2$                  |
| $\nu$        | - Poisson's ratio  | - 0.3  |
| $\nu_1$      | - SAP " "  | - 0.4 ref. (15)                                    |
| $\delta_0$   | - UC density   | - $13.4 \text{ gr/cm}^3$ ref. (13)                 |
| $\delta_2$   | - SAP "  | - $2.8 \text{ gr/cm}^3$ ref. (14)                  |
| $T_c$        | - UC centre temperature  | - $^\circ\text{C}$                                 |
| $T_0$        | - UC surface "   | - $^\circ\text{C}$                                 |
| $T_1$        | - SAP inner surface temperature                                  | - $^\circ\text{C}$                                 |
| $T_2$        | - SAP outer " "  | - $^\circ\text{C}$                                 |
| $T_3$        | - SS inner " "   | - $^\circ\text{C}$                                 |
| $\bar{T}$    | - SAP mean temperature   | - $^\circ\text{C}$                                 |
| $t$          | - $U_{CT_0}$ -SAP, mean surface temperature                      | - $^\circ\text{C}$                                 |
| $T_r$        | - room temperature   | - $^\circ\text{C}$                                 |
| $T_w$        | - inlet temperature of heavy water                               | - $^\circ\text{C}$                                 |
| $\Delta T_0$ | - temperature difference between centre and surface of UC pellet | - $^\circ\text{C}$                                 |

- $\Delta T_2$  - temperature drop across SAP - °C  
 $\Delta T_1$  - temperature drop across UC-SAP interface - °C  
 $G_0$  - nominal radial clearance UC-SAP- cm  
 $G_1$  - hot radial clearance UC-SAP - cm  
 $\epsilon_0$  - radial deformation of UC pellet-surface  
 $\epsilon_1$  - " " of SAP inner surface  
 $\epsilon_2$  - " " of SAP outer surface  
 $\epsilon_3$  - " " of SS inner surface  
 $p$  - pressure to SAP-SS container interface - kg/cm<sup>2</sup>  
 $\phi$  - neutron flux - n/cm<sup>2</sup>sec  
 $P$  - power generation in the UC - Watt/cm<sup>3</sup>  
 $Q$  - linear heat rating for UC - Watt/cm  
 $Pot \gamma$  - gamma heating - Watt/gr  
 $F$  - heat flux at UC surface - Watt/cm<sup>2</sup>  
 $U$  - contact or gap thermal conductance - Watt/cm<sup>2</sup>°C  
 $R$  - contact or gap thermal resistance - cm<sup>2</sup>°C/Watt  
 $K_0$  - UC thermal conductivity - Watt/cm°C ref. (13)  
 $K_2$  - SAP thermal conductivity - Watt/cm°C ref. (16)  
 $K_3$  - Xenon gas thermal conductivity - Watt/cm°C ref. (17)  
 $\frac{\Delta r_0}{r_0}$  - swelling of UC pellet  
 $\sigma$  - arithmetic mean of SAP readings defined by  $\sigma = \frac{A+B+C+D}{4}$  mV  
 $\beta$  - sheath-heavy temperature drop water defined by  
 $\beta = \sigma + 0.04 T_r - 0.04 T_w$

Appendix IV

Physical constants in the sample computations

= Gas Thermal conductivity

|    |                      |                      |        |
|----|----------------------|----------------------|--------|
|    | Fission gases        | Helium               |        |
| Kf | $9.7 \times 10^{-5}$ | $2.5 \times 10^{-3}$ | W/cm°C |

= Sum of max. microroughnesses

|            |                    |    |
|------------|--------------------|----|
| $\sum R_t$ | $2 \times 10^{-3}$ | cm |
|------------|--------------------|----|

= Maximum microroughness

|       |                      |    |
|-------|----------------------|----|
| $R_t$ | $1.8 \times 10^{-3}$ | cm |
|-------|----------------------|----|

= Pellet radius

|       |     |                 |    |
|-------|-----|-----------------|----|
|       | UC  | UO <sub>2</sub> |    |
| $r_o$ | 1.5 | 0.5             | cm |

= Fuel Density

|   |      |                 |                   |
|---|------|-----------------|-------------------|
|   | UC   | UO <sub>2</sub> |                   |
| d | 13.4 | 10.2            | g/cm <sup>3</sup> |

= Average fuel Thermal conductivity

|    |      |                 |        |
|----|------|-----------------|--------|
|    | UC   | UO <sub>2</sub> |        |
| Kp | 0.15 | 0.03            | W/cm°C |

= Fuel Thermal expansion coefficient

|            |           |                 |                  |
|------------|-----------|-----------------|------------------|
|            | UC        | UO <sub>2</sub> |                  |
| $\alpha_p$ | $10^{-5}$ | $10^{-5}$       | °C <sup>-1</sup> |

= Poisson's ratio

$$\nu_p = \nu_c = 0.3$$

= Fuel Young's modulus

|                |                   |                   |                    |
|----------------|-------------------|-------------------|--------------------|
|                | UC                | UO <sub>2</sub>   |                    |
| E <sub>p</sub> | 2x10 <sup>6</sup> | 2x10 <sup>6</sup> | Kg/cm <sup>2</sup> |

= Clad operating Temperature

$$\bar{T} = 400^{\circ}\text{C}$$

= Microhardness at operating temperature

|   |       |        |       |                          |
|---|-------|--------|-------|--------------------------|
|   | SAP   | MAGNOX | ZRY2  | S.S.                     |
| H | 3,200 | 1,050  | 2,900 | 5,400 Kg/cm <sup>2</sup> |

= Clad Thermal conductivity

|                |     |        |      |                          |
|----------------|-----|--------|------|--------------------------|
|                | SAP | MAGNOX | ZRY2 | S.S.                     |
| K <sub>c</sub> | 1.7 | 1.25   | 0.17 | 0.16 W/cm <sup>o</sup> C |

= Clad Thermal expansion coefficient

|            |                    |                      |                       |                                       |
|------------|--------------------|----------------------|-----------------------|---------------------------------------|
|            | SAP                | MAGNOX               | ZRY2                  | S.S.                                  |
| $\alpha_c$ | 2x10 <sup>-5</sup> | 2.6x10 <sup>-5</sup> | 1.17x10 <sup>-5</sup> | 1.5x10 <sup>-5</sup> oC <sup>-1</sup> |

= Clad Young's modulus

|                |                   |                     |                      |   |
|----------------|-------------------|---------------------|----------------------|---|
|                | SAP               | MAGNOX              | ZRY2                 | S.S.                                    |
| E <sub>c</sub> | 5x10 <sup>5</sup> | 1.4x10 <sup>5</sup> | 6.44x10 <sup>5</sup> | 1.45x10 <sup>6</sup> kg/cm <sup>2</sup> |

#### Acknowledgement

We acknowledge the valuable collaboration of Messrs. F. Daniele, S. Giuliani and L. Kestemont in carrying out this investigation, especially concerning microhardness measurements, assistance during irradiation and post-irradiation examinations.